2009

Biochemical and functional characterization of a tetra-phosphorylation motif

Catherine Sykes
University of Windsor

BIOCHEMICAL AND FUNCTIONAL CHARACTERIZATION OF A TETRA-PHOSPHORYLATION MOTIF

by

Catherine Sykes

A Thesis
Submitted to the Faculty of Graduate Studies
through Chemistry and Biochemistry
in Partial Fulfillment of the Requirements for
the Degree of Master of Science at the
University of Windsor

Windsor, Ontario, Canada

2009

Your file Votre référence
ISBN: 978-0-494-57589-5
Our file Notre référence
ISBN: 978-0-494-57589-5

Author's Declaration of Originality

I hereby certify that I am the sole author of this thesis and that no part of this thesis has been published or submitted for publication.

I certify that, to the best of my knowledge, my thesis does not infringe upon anyone's copyright nor violate any proprietary rights and that any ideas, techniques, quotations, or any other material from the work of other people included in my thesis, published or otherwise, are fully acknowledged in accordance with the standard referencing practices. Furthermore, to the extent that I have included copyrighted material that surpasses the bounds of fair dealing within the meaning of the Canada Copyright Act, I certify that I have obtained a written permission from the copyright owner(s) to include such material(s) in my thesis and have included copies of such copyright clearances to my appendix.

I declare that this is a true copy of my thesis, including any final revisions, as approved by my thesis committee and the Graduate Studies office, and that this thesis has not been submitted for a higher degree to any other University or Institution.

Abstract

Hierarchical phosphorylation of four Ser/Thr residues orchestrates the ubiquitination and proteasomal degradation of the transcriptional co-activator, β-catenin [16]. To the best of our knowledge, β-catenin is the only known protein with this tetra-phosphorylation motif (TPM). However, the sophistication of this scheme prompted our hypothesis that there are other proteins regulated by this TPM.

Herein, we identified two novel TPM-containing proteins, TAZ and KLF7. Characterization of the TAZ and KLF7 TPMs revealed significant similarities and differences with respect to the biochemical role of the β-catenin TPM and demonstrated a functional consequence of their TPMs within the TAZ- and KLF7-mediated inhibition of adipogenesis.

We also provide the first direct evidence that TAZ is highly phosphorylated. Using mass spectrometry, we identified ten TAZ phosphorylation sites, of which three mapped to the TPM. Additionally, we present preliminary functional analyses of phosphorylation sites adjacent to the 14-3-3 binding site and WW domain of TAZ.

This work is dedicated to my most loving and supportive family and to the memory of my beautiful grandma, Dorothy Sykes

Acknowledgements

Firstly, I would like to express my most sincere appreciation to my supervisor, Dr. Otis Vacratsis, for welcoming me into his research group as a second year undergraduate and providing me with hours of invaluable training and endless guidance in the past six years. His passion for science is infectious and as a result I have found myself pursuing things I never would have imagined (i.e. this Master's Degree). I want to thank Dr. Vacratsis for believing in this project, especially when I no longer did, without his dedication to the TPM, I am sure I would have delved into the equally scary world of hYVH1 research. Most of all, I want to extend my deepest gratitude to Dr. Vacratsis for being so understanding over the past years — your words of wisdom and pep talks have always been appreciated.

I am greatly indebted to all of the Vacratsis lab members, past and present: Zareen Butt, Khaled El Mosrati, Anna Kozarova, Priya Sharda, John Mucaki, Catherine Cheng, Chris Bonham, Tony Nakhle, Roberto Amato, Colleen Mailloux, Steve Malone, Danish Hassan, Justin Renaud, and Norah Franklin. Working long hours in the lab never really felt like a chore because I have always had the good fortune of being surrounded by such good friends. Without the constant support and friendship of all of my lab mates, I would not have enjoyed this work as much as I have — our lunches, birthday celebrations, conferences, and everyday shenanigans made me extend my stay longer than I had planned!

I would like to thank my committee members, Dr. L. Porter, Dr. B. Mutus, and Dr. O. Vacratsis for reading and evaluating this work. I also appreciated the helpful discussion and advice that was offered at my mid-term committee meeting. A thank-you is also due to Dr. P. Dutton for chairing my defense.

A considerable thank-you goes out to all of the faculty members of the Biochemistry department: Dr. S. Ananvoranich, Dr. S. Pandey, Dr. L. Lee, Dr. B. Mutus,

and Dr. J. Gauld for so generously allowing me access to all of their equipment and for always being willing to help whenever it was required. I would also like to thank the staff of the Chemistry and Biochemistry Department, most notably Beth Kickham, Kim Kickham, and Marlene Bezaire. A special thanks goes out to Marlene for always having all of the answers. Her hard work and dedication is so greatly appreciated and without her I would probably still be pondering my defense date! I would also like to acknowledge all of my fellow chemistry and biochemistry graduate students, past and present, who have made this department feel like one big extended family.

I want to thank a number of people who have contributed to this work by generously providing much needed constructs or allowing me access to equipment that was needed: Dr. L. Porter (University of Windsor), for providing the HA-ubiquitin construct; Dr. L. Lei (Arizona State University), for providing the Myc-KLF7 construct; Dr. K. L. Guan (University of Michigan), for the HA-GSK3β (S9A) construct; Dr. A. Ali, for the Myc-β-catenin TPM mutant; Bob Hodge (University of Windsor), for allowing me to use equipment in the Biology Department Core Facility; and the University of Michigan Mass Spectrometry Facility, for allowing me to utilize their machines. I am also very grateful to the Natural Sciences and Engineering Research Council of Canada (NSERC) and to the University of Windsor for the funding that I have received for both my undergraduate and graduate studies.

Finally, I would like to extend my most heartfelt gratitude to my parents and my brothers for putting up with me throughout my university career (I think I am almost done!). I would like to thank my parents for driving me to and from school, without their constant love and support I would not be here today. A special thank-you goes out to Jesse Robinet for his endless patience and for always being there for me when I needed help (especially when my hard drive crashed mid-thesis!). I owe you!

Table of Contents

List of Tables

List of Figures

Chapter I) ***Introduction***

Chapter III) ***Results***

PART I) Identification and Characterization of TPM-Containing Proteins

Chapter IV) Discussion and Future Work

List of Appendices

List of Abbreviations

ADP	adenosine diphosphate
AMP	adenosine monophosphate
AMSCs	adipose-derived mesenchymal stem cells
APC	adenomatous polyposis coli
ARF	alternate reading frame
AS47	Akt Substrate of 47 kDa
AS160	Akt Substrate of 160 kDa
AS250	Akt Substrate of 250 kDa
ATM	ataxia telangiectasia-mutated
ATP	adenosine triphosphate
ATR	ATM-Rad3-related
BCS	bovine calf serum
BSA	bovine serum albumin
β-TrCP	Beta-Transducin Repeat-Containing Protein
C^t	carboxy-terminal
ΔC^t	carboxy-terminal mutant
CAF	chemically assisted fragmentation
CD4	cluster of differentiation 4
Cdc2	cell division cycle 2
Cdc25C	cell division cycle 25 homolog C
cDNA	complementary deoxyribonucleic acid
C/EBP	CCAAT/enhancer-binding protein
CHX	cycloheximide
CIAP	calf intestinal alkaline phosphatase
CID	collision-induced dissociation

CK1α	casein kinase 1α
CMV	cytolomegalovirus
CRM1	chromosomal region maintenance protein 1
Cul1	cullin1
Da	daltons
DB	dot blot
DMEM	Dulbecco's Modified Eagle's Medium/Nutrient F-12 Ham
DMSO	dimethyl sulfoxide
DNA	deoxyribonucleic acid
DTT	dithiothreitol
E1	ubiquitin-activating enzyme
E2	ubiquitin-conjugating enzyme
E3	ubiquitin ligase
EDTA	ethylenediaminetetraacetic acid
ER	endoplasmic reticulum
FBS	fetal bovine serum
FOXO	forkhead box O
GSK3β	glycogen synthase kinase 3β
HA	haemagglutinin
HEK	human embryonic kidney
HIV-1	human immunodeficiency virus 1
HPLC	high performance liquid chromatography
IB	immunoblot
IBMX	3-isobutyl-1-methyl xanthine
IgG	immunoglobulin G
IL-6	interleukin-6
IMAC	immobilized metal affinity chromatography

IP	immunoprecipitation
kDa	kilodaltons
KLF7	Krüppel-like factor 7
LB	Luria's Broth
LC	liquid chromatography
MALDI	matrix-assisted laser desorption/ionization
MS	mass spectrometry
MSCs	mesenchymal stem cells
MS/MS	tandem mass spectrometry
m/z	mass-to-charge ratio
N^t	amino-terminal
ORO	Oil Red O
P_i	inorganic phosphate
PBS	phosphate buffered saline
PC2	polycystin 2
PCR	polymerase chain reaction
PKA	Protein Kinase A
PKB	Protein Kinase B
PMSF	phenylmethylsulphonyl fluoride
PPARγ	peroxisome proliferator-activated receptor γ
PSD	post-source decay
PVDF	polyvinylidene difluoride
Rbx1	Ring-box 1
Runx2	Runt related transcription factor 2
SCF	Skp1/Cul1/F-box protein
SDM	serine double mutant
SDS-PAGE	sodium dodecyl sulfate-polyacrylamide gel electrophoresis

SILAC	stable isotope labeling with amino acids in cell culture
Skp1	S-phase kinase-associated protein
STDM	serine/threonine double mutant
SUMO	Small Ubiquitin-like Modifier
TAZ	Transcriptional co-activator with PDZ-binding motif
TBS	tris-buffered saline
TCF/LEF	T cell factor/lymphocyte enhancer factor
TIS	timed ion selector
TOF	time-of-flight
TPM	Tetra-Phosphorylation Motif
ΔTPM	tetra-phosphorylation motif mutant
UKLF	Ubiquitous Krüppel-like factor
UV	ultraviolet
Vpu	Virus protein U
WWTR1	WW domain-containing transcriptional regulator-1
YAP	Yes-associated protein

Chapter 1

Introduction

1.1 Post-Translational Modifications

The final stage in the biosynthetic pathway of numerous proteins involves their exposure to various forms of further processing, collectively referred to as post-translational modifications [1]. The functional significance of the numerous post-translational modifications varies from one protein to the next. However, in general, post-translational modifications have been shown to influence the regulation of various biological properties of proteins, such as activity, stability, localization, or ligand binding [1,2]. The key to understanding the consequence of protein modification lies within the fact that the majority of post-translational modifications involve the covalent addition of a functional group, such as a carboxyl group, an alkyl group, a glycosyl group, or a phosphoryl group, to a specific amino acid residue; the covalent linkage of another protein or peptide to the protein of interest, as is the case in the ubiquitination and SUMOylation of proteins; or the alteration of the protein structure, which can occur in response to disulfide bridge formation or proteolytic cleavage [1,2]. Thus, post-translational modifications exert their influences through the introduction or removal of chemically reactive groups. Overall, post-translational modifications enhance the diversity and versatility of the structure and functions of proteins, explaining their prevalence in higher eukaryotic organisms [2,3].

1.2 Phosphorylation: A Reversible Regulatory Modification

One of the most prevalent forms of post-translational modification is the reversible phosphorylation of proteins, which involves the addition of a phosphoryl group to an amino acid side chain. The reversible nature of protein phosphorylation is afforded by the opposing activities of two enzyme superfamilies, the protein kinases and protein phosphatases. Protein kinases catalyze the transfer of the γ-phosphoryl group of adenosine triphosphate (ATP) to an amino acid side chain of the recipient protein, while protein phosphatases oversee the dephosphorylation reaction, catalyzing the hydrolysis of the high energy phosphoester bond between the phosphoryl group and the implicated amino acid side chain (Figure 1.1) [3]. Within eukaryotic cells, the most common form of phosphorylation is O-phosphorylation, which involves the addition of a phosphoryl group to the hydroxyl side chains of serine, threonine, and tyrosine residues (Figure 1.2) [3]. Serine and threonine phosphorylation have been documented to be far more abundant than the phosphorylation of tyrosine residues at a ratio of 1800:200:1 [4]. Studies of prokaryotic phosphorylation have also revealed the occurrence of N-phosphorylation (arginine, histidine, lysine), S-phosphorylation (cysteine), and acyl-phosphorylation (aspartate, glutamate), albeit still to a lesser degree than O-phosphorylation [5]. It has been reported that approximately 30 – 50% of proteins present within a eukaryotic cell are phosphorylated at any given time and that genes encoding protein kinases and protein phosphatases constitute approximately 2% of the entire human genome, facts that attest to the prevalence and significance of protein phosphorylation as a regulatory mechanism [6,7].

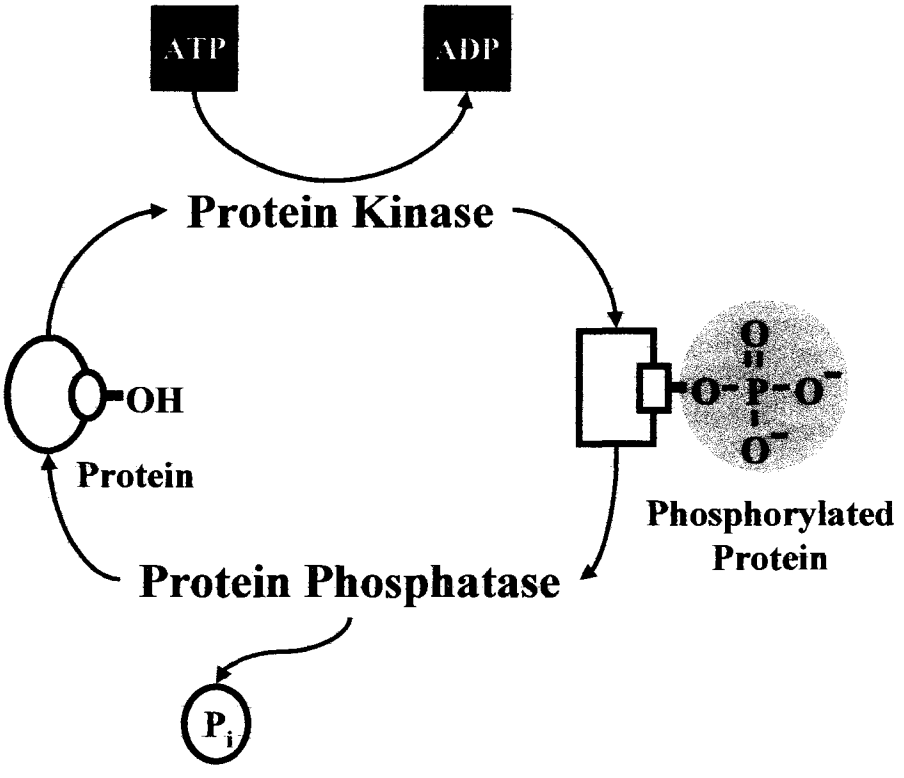

Figure 1.1- Reversible Protein Phosphorylation. Protein phosphorylation involves the addition of a phosphoryl group to an amino acid side chain. The reversible nature of phosphorylation is afforded by the opposing activities of two enzyme superfamilies, the protein kinases and protein phosphatases. Protein kinases catalyze the transfer of the γ-phosphoryl group of ATP to an amino acid side chain of the recipient protein. The addition of a negatively charged phosphoryl group can shift a protein from one state (○) to another (□) by influencing many aspects of protein behavior, including structure, subcellular localization, activity, stability, and substrate specificity. Protein phosphatases catalyze the dephosphorylation reaction by facilitating the hydrolysis of the phosphoester bond between the protein and the phosphoryl group, liberating inorganic phosphate (P_i) that is used to form ATP from ADP.

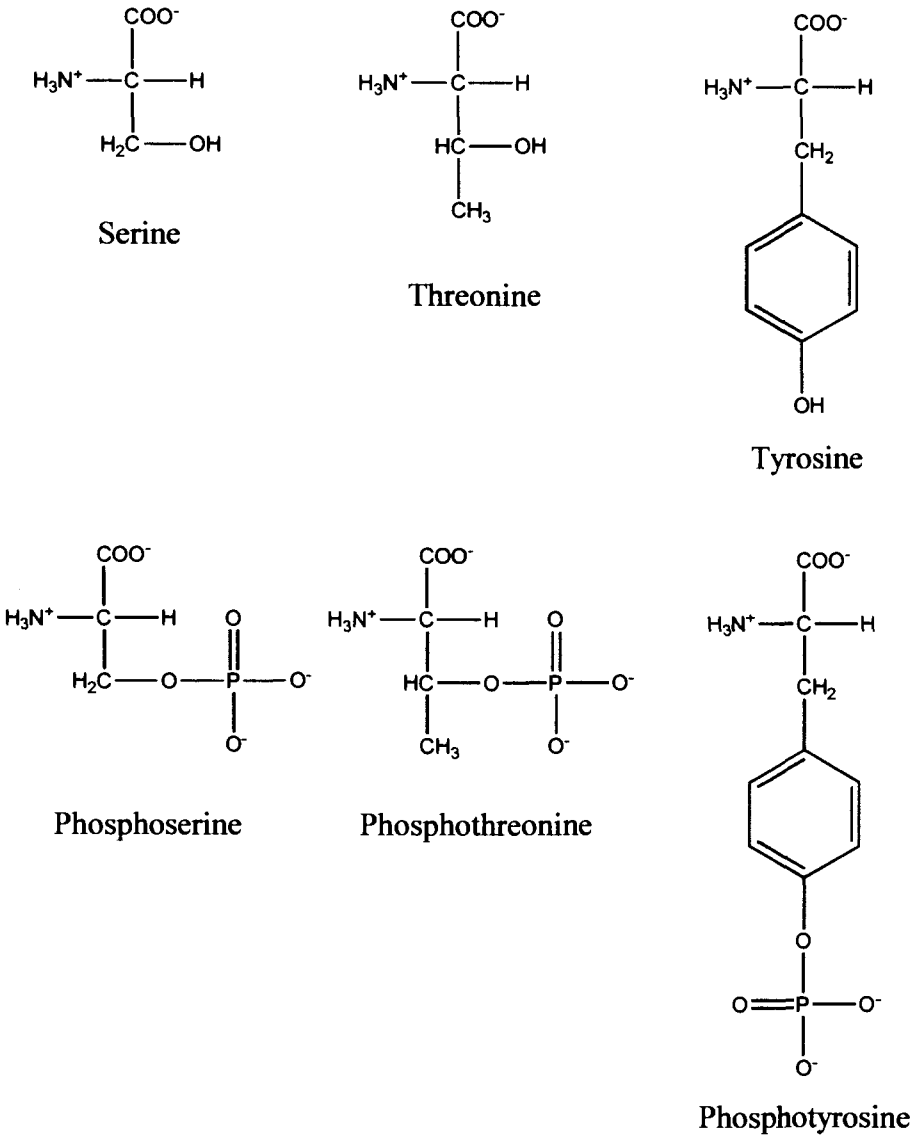

Figure 1.2- O-Phosphorylation of Serine, Threonine, and Tyrosine [1]. Within eukaryotic cells, the most common form of protein phosphorylation is O-phosphorylation, which involves the addition of a phosphoryl group to the hydroxyl functional group of a serine, threonine, or tyrosine residue.

1.2.1 Phosphorylation Regulates Numerous Cellular Processes

The regulatory capacity of protein phosphorylation is often likened to a light switch, as phosphorylation or dephosphorylation can trigger the shift of the target protein between a modified and an unmodified state [2]. Essential to understanding the mechanism by which phosphorylation mediates protein behavior is the knowledge that the addition of a phosphoryl group to a serine, threonine, or tyrosine residue replaces a neutral functional group with that which is negatively charged. Protein phosphorylation can lead to an alteration in protein structure, as a result of a change in the electrostatic interactions, hydrogen bonding network, and/or hydrophobic interactions in the vicinity of the newly incorporated phosphoryl group [2]. Induced changes in protein conformation can have a number of consequences, including alterations in enzymatic activity, substrate specificity, subcellular localization, stability, and complex formation [8]. It is variations in protein behaviors such as these that assist in the relay of information from an initial extracellular stimulus to the internal cellular machinery: the central dogma of signal transduction.

Protein phosphorylation has long been identified as a critical regulator in a vast number of cellular processes. Today, it is believed that phosphorylation plays some role in practically every eukaryotic biological pathway [3]. Most notably, it has been implicated in the inner-workings of signal transduction cascades regulating cell cycle progression, transcription, translation, cell differentiation, cytoskeletal rearrangement, apoptosis, and cellular metabolism [3]. Since phosphorylation is at the core of the cellular signal transduction cascade, the activities of the protein kinases and protein phosphatases that mediate this post-translational modification must be tightly maintained. Aberrant control of the aforementioned enzymes can result in abnormal levels of phosphorylation and dephosphorylation, which have both been associated with various

pathological conditions, such as cancer, diabetes, neurodegeneration, and cardiovascular disease [3,9].

1.3 Multisite Phosphorylation

Research focused on the elucidation of the human phosphoproteome, the complete collection of phosphorylated proteins within the cell, yielded the estimation that the sum of potential phosphorylation sites likely exceeds 100,000 [7]. In 2002, it was reported that fewer than 2,000 phosphorylation sites had been identified with the majority of the unidentified phosphorylation sites predicted to map to proteins containing multiple phosphorylation sites [10]. Multisite phosphorylation, which refers to the phosphorylation of a protein on multiple amino acid residues, continues to emerge as a widespread cellular mechanism. Not only does the requisition for multiple phosphorylation events heighten the potential for the regulation of all aspects of protein behavior, but it also enables several regulatory strategies to operate within the same protein, as the phosphorylation of each site can result in a unique set of consequences [11]. The phosphorylation of several sites within a protein can transpire in a number of ways. For instance, a single protein kinase may be responsible for phosphorylating a multitude of sites in a protein, a feat shown to afford strict control over the strength and duration of a specific cellular response, as the termination of the signal is dependent upon multiple dephosphorylation events [11]. Multisite phosphorylation of a protein can also be achieved through the activities of two or more distinct protein kinases, allowing the potential for the integration of various signaling pathways [11].

1.3.1 Hierarchical Phosphorylation Generates Critical Thresholds for Cellular Activities

The interactions between phosphorylation sites within a multiply phosphorylated protein enhance the means by which phosphorylation can exert its regulatory capacity. It has been shown that phosphorylation sites may be mutually exclusive, meaning that the initial phosphorylation of an amino acid residue prevents subsequent phosphorylation events on other residues [11]. Phosphorylation sites may also interact in a positive manner, such that the phosphorylation of one site serves to favor the phosphorylation of others [11]. Numerous proteins have been identified that undergo multisite phosphorylation in a sequential manner, which is in accordance with this latter form of phosphorylation site interdependency [12]. This pattern of phosphorylation, termed ordered phosphorylation, sequential phosphorylation, or hierarchical phosphorylation, is characterized by the phosphorylation of amino acid residues in a defined order; hence, phosphorylation at a specific site is a requirement for successive phosphorylation events.

Traditionally, it was believed that hierarchical phosphorylation provided redundant control of protein behavior. However, it now appears that this intriguing phosphorylation mechanism affords ultrasensitive regulation of cellular activities through the generation of temporal and enzyme activation thresholds [13]. The ability of hierarchical phosphorylation to impart a temporal threshold on its regulatory activities stems from the presence of a lag period following the onset of phosphorylation, as a critical level of protein kinase activity must be attained to ensure successful multisite phosphorylation before the final regulatory goal can be achieved [13]. A single phosphorylation event, even one where the catalysis of its phosphorylation has been slowed to match the time required for multiple phosphorylation events, is unable to produce a similar temporal threshold; thus, hierarchical phosphorylation provides a

means by which the cell can assess the necessity for the execution of various cellular processes, given that the proper conditions are met [13].

It has also been stated that the requirement for multiple phosphorylation events sets a threshold for kinase activity, such that at low levels of kinase activation, the target protein will exist in lowly phosphorylated forms, but as the activity of the implicated kinase(s) increases, the amount of multiply phosphorylated protein will also increase [13]. The presence of such a threshold allows the target protein to ignore low, or perhaps basal, levels of kinase activity that exist during periods where its regulation is not required, ensuring that a response is not elicited until the activity of the kinase has exceeded the threshold level [13].

1.4 Ordered Multisite Phosphorylation Regulates β-catenin Degradation

The extensively studied, multifunctional protein, β-catenin, provides an interesting example of hierarchical phosphorylation coupled to ubiquitin-mediated proteasomal degradation. Initial studies focused on elucidating the function of β-catenin revealed its involvement in the cadherin-based cell adhesion system, where it serves to tether transmembrane cadherin receptors to α-catenin, which in turn associates with actin filaments of the cytoskeleton [14]. However, it was the discovery of its transcriptional co-activation capabilities within a highly conserved Wnt signaling pathway that intrigued researchers and spurred enormous research efforts towards understanding the regulation of β-catenin [14]. The canonical Wnt/β-catenin pathway has been implicated in the regulation of critical cellular processes, such as proliferation, cell fate determination, and differentiation, in both the developing embryo and in adult tissues [14,15].

A critical output of the canonical Wnt/β-catenin signaling cascade is the regulation of cytosolic β-catenin protein levels [16]. In accordance with the current model of the pathway, the engagement of the Wnt co-receptors by specific Wnt ligands is

believed to initiate a series of events, which ultimately disrupt the function of a multi-protein β-catenin degradation complex that assembles along the scaffold protein, Axin, and contains β-catenin, as well as the tumor suppressor protein, adenomatous polyposis coli (APC), and two serine/threonine kinases (glycogen synthase kinase 3β (GSK3β) and casein kinase Iα (CKIα)) [14,16]. Consequently, β-catenin escapes its degradation and accumulates within the cytoplasm, with high levels of transcriptionally active β-catenin undergoing translocation into the nucleus, where it associates with T cell factor/lymphocyte enhancer factor (TCF/LEF) transcription factors to co-activate the expression of Wnt-responsive genes [14].

The absence of extracellular Wnt stimulation is met by the constitutive degradation of β-catenin, which preserves low levels of this transcriptional mediator for the purpose of maintaining Wnt target genes in a transcriptionally inactive form. It is the inclusion of β-catenin within the aforementioned multi-protein complex that promotes its phosphorylation-dependent degradation [14]. Studies have shown that β-catenin degradation is tightly regulated by the ordered multisite phosphorylation of four Ser/Thr residues located within its highly conserved amino (N)-terminal region by the kinases present within the destruction complex (Figure 1.3). The initial phosphorylation of β-catenin, which occurs on Ser45, is catalyzed by CKIα [16,17]. In the context of β-catenin phosphorylation, CKIα is said to function as a "priming" kinase, since its phosphorylation of Ser45 is both necessary and sufficient for the ensuing phosphorylation of β-catenin by GSK3β [16,17]. The introduction of a phosphate group at Ser45 generates a GSK3β consensus site, which consists of a phosphorylated residue separated from a second putative phosphorylation site by three arbitrary residues (S/TXXXpS/pT), enabling GSK3β to catalyze the phosphorylation of Thr41, followed by that of Ser37, and finally Ser33, as each of these sites also constitutes a GSK3β consensus site [16,17]. The hierarchical phosphorylation of β-catenin at these four sites generates an intriguing phosphorylation motif that we have termed the tetra-phosphorylation motif (TPM).

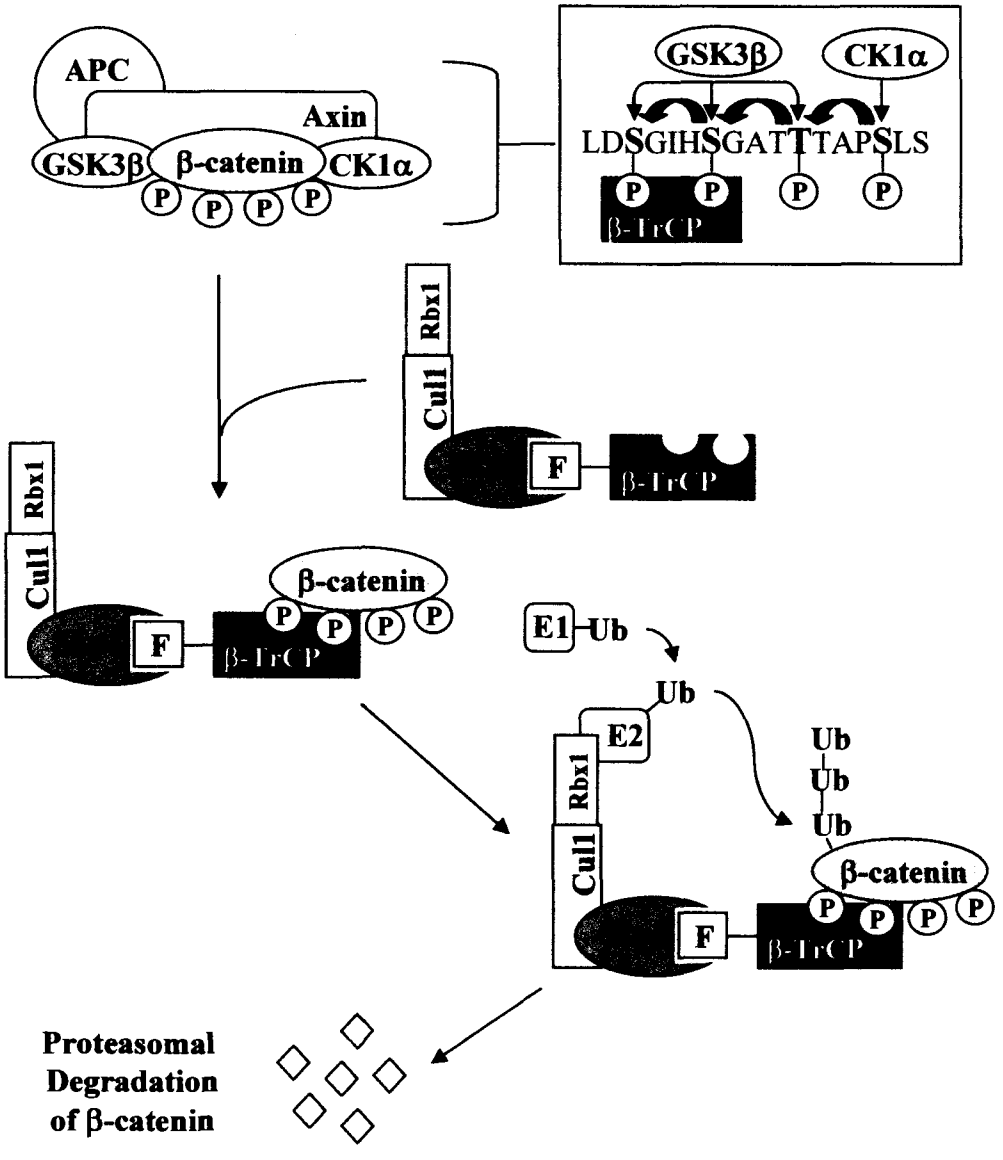

Figure 1.3- Phosphorylation-Dependent Degradation of β-catenin [15,19]. In the absence of Wnt signaling, Axin binds simultaneously to APC, β-catenin, GSK3β, and CKIα, forming the β-catenin destruction complex. Consequently, β-catenin is phosphorylated on Ser45 by CKIα, which allows the phosphorylation of Thr41, Ser37, and Ser33 by GSK3β in an ordered fashion (shown in box). Phosphorylation at Ser33 and Ser37 creates a docking site for β-TrCP, present within an SCF (Skp1/Cul1/F-box) complex, facilitating the poly-ubiquitination of β-catenin. (E1, ubiquitin (Ub)-activating enzyme; E2, ubiquitin (Ub)-conjugating enzyme). Subsequent to its ubiquitination, β-catenin is targeted to the proteasome for degradation.

Studies focused on deducing the degradation mechanism of β-catenin revealed that it proceeded via the ubiquitin-proteasome pathway, which involves its ubiquitination and subsequent degradation by the proteasome [18]. The presence of the hyperphosphorylated TPM within the N-terminal region of β-catenin generates a docking site for β-TrCP, the specificity component of the ubiquitination apparatus, whose phosphorylation-dependent recognition of β-catenin invokes its ubiquitination [18,19]. The ligation of a multimeric ubiquitin chain to β-catenin, primarily at Lys19, marks β-catenin for recognition and, ultimately, destruction by the 26S proteasome [20,21].

1.4.1 Ubiquitin-Mediated Proteolysis

Protein degradation via the ubiquitin-proteasome pathway involves two distinct systems: the ubiquitin conjugation cascade and the 26S proteasome complex [22]. The initial stage of this bipartite pathway involves the enzymatic ligation of ubiquitin, a highly conserved 76 amino acid protein, to the target protein, in a process referred to as ubiquitination. Ubiquitination is afforded by the concerted actions of three unique enzymes, denoted E1, E2, and E3 (Figure 1.4) [22]. Firstly, the E1, or ubiquitin-activating enzyme, catalyzes the adenylation of ubiquitin at the expense of ATP, serving to activate ubiquitin, which then engages in a thioester bond with an active site cysteine residue of E1. E1 then transfers the bound ubiquitin to a cysteine residue located within the active site of an E2, also known as the ubiquitin-carrier protein or ubiquitin-conjugating enzyme [22]. Lastly, the E2 seeks out and binds to a member of the ubiquitin-protein ligase family, or E3, which is responsible for the recognition and binding of specific substrates. The binding of E2 to an E3 brings the E3-bound substrate into the vicinity of the ubiquitin-bound E2, enabling the ligation of the ubiquitin monomer to an internal lysine residue of the protein substrate. Following mono-ubiquitination, a poly-ubiquitin chain may be synthesized through the actions of the same

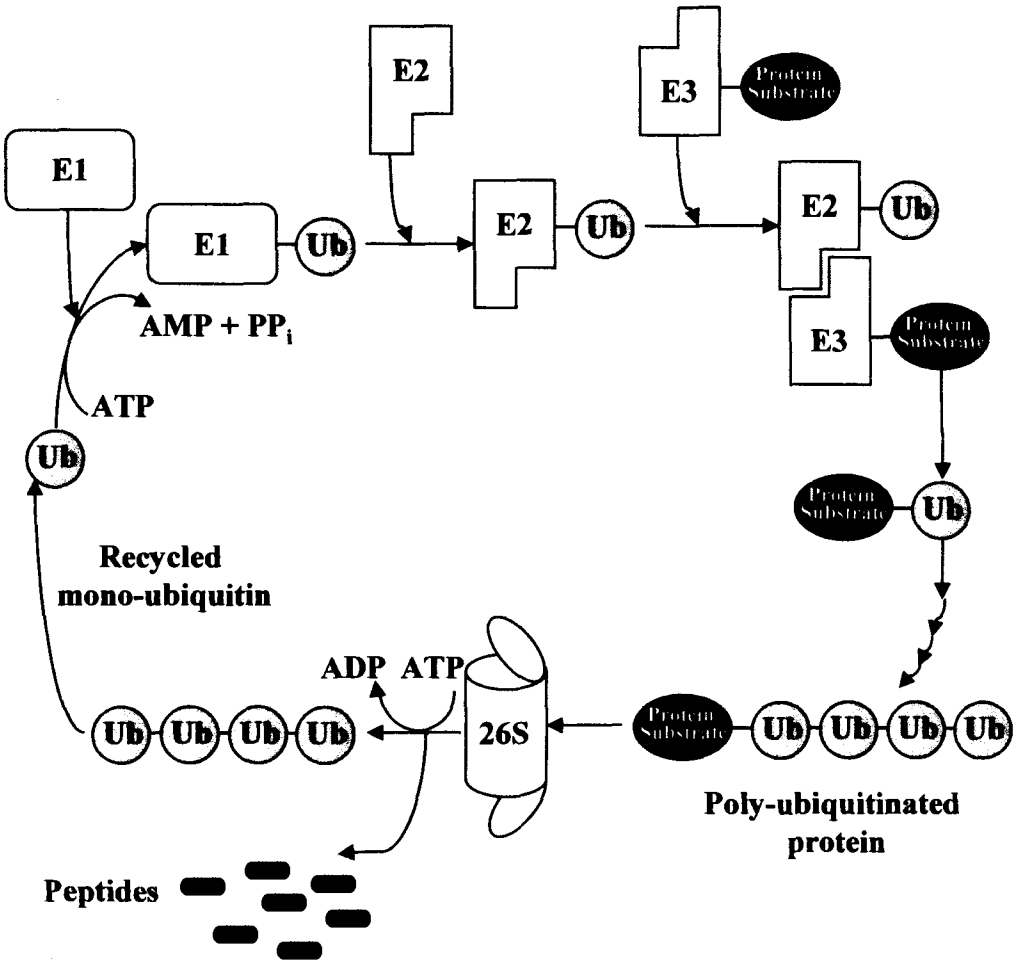

Figure 1.4- Ubiquitin-Proteasome Pathway [22,23]. E1 (ubiquitin-activating enzyme) catalyzes the adenylation of ubiquitin (Ub) at the expense of ATP, which serves to activate ubiquitin. Activated ubiquitin then forms a thioester bond with a Cys residue within the E1 active site. The activated ubiquitin is then transferred to an active site Cys residue of an E2 (ubiquitin-conjugating enzyme). E2 complexes with an E3 (ubiquitin ligase), which associates with the target protein substrate. The activated ubiquitin moiety is then transferred to the side chain of a Lys residue within the protein substrate, yielding a mono-ubiquitinated protein. After multiple rounds of ubiquitin transfer, a poly-ubiquitin chain is formed. Poly-ubiquitinated proteins are recognized and hydrolyzed into small peptides by the 26S proteasome. In a manner that remains to be determined, the ubiquitin polymer is cleaved from the substrate and the ubiquitin monomers are recycled.

enzymatic cascade; however, the activated ubiquitin moiety is not ligated to the substrate, but is conjugated to a specific lysine residue within the previously bound ubiquitin molecule [22,23].

Since a diverse array of critical regulatory proteins undergoes ubiquitin-mediated proteolysis, it is important that the degradation machinery explicitly recognizes target proteins, so as to ensure specific control of their degradation [22]. The specificity of the ubiquitin-proteasome pathway is conferred mainly through the identity of the participatory E3 ligase. There exist a number of different ubiquitin ligase families, with each family exhibiting unique substrate binding preferences afforded through their recognition of a specific motif within the substrate(s) [24]. In the case of the ubiquitin-mediated degradation of β-catenin, hierarchical phosphorylation of its TPM results in the generation of a degradation signal, or phosphodegron, constituting phosphorylated Ser37 and phosphorylated Ser33, as well as neighboring residues, namely Asp32 and Gly34 [19]. A phosphodegron akin to this form, DpSGϕXpS, where ϕ and X represent hydrophobic and arbitrary amino acids, respectively, has been identified in all known substrates of the E3 ligase complex, $SCF^{\beta\text{-}TrCP}$ [20]. This E3 ligase, which has been shown to facilitate the ubiquitination of β-catenin, consists of four subunits: the scaffold protein, Cullin1 (Cul1); the RING-domain protein, Rbx1, which is anchored by Cul1, allowing it to bridge the E2-E3 interaction; and the adaptor protein, Skp1, which tethers the fourth subunit, the F-box protein, β-TrCP, to Cul1 [19,20]. The F-box protein is the component of the SCF (Skp1/Cul1/F-box) ligase that directly interacts with the specific protein substrate; thus, the presence of protein-protein interaction domains within the F-box proteins dictates their substrate specificities [20]. For example, β-Transducin repeat containing protein (β-TrCP), the F-box protein of the SCF ligase responsible for the ubiquitination of β-catenin, directly associates with the β-catenin phosphodegron via its WD40-repeat domains [20].

Consequent of their poly-ubiquitination, proteins fated for degradation are subject to the second branch of the ubiquitin-proteasome pathway. The presence of a covalently linked ubiquitin polymer along the length of a protein acts as a recognition signal for the eukaryotic 26S proteasome, which is composed of three major subunits: the core 20S protein and two 19S regulatory complexes [25]. The 19S complexes are positioned at either end of the 20S proteasome forming a pseudo lid and base, which function in the binding and unfolding of the poly-ubiquitinated protein substrate, as well as in the threading of the unfolded substrate protein into the 20S proteolytic chamber [25]. Studies of the 20S proteasome have revealed that it is of a multi-enzymatic nature, in that it is capable of at least three different protease activities, akin to chymotrypsin, trypsin, among others [24,25]. This array of protease activity ensures that virtually all of the peptide bonds within a protein substrate are susceptible to cleavage, enabling the generation and release of relatively small peptides from the ubiquitinated protein. It is interesting to note that, in a manner which remains to be established, the poly-ubiquitin chain is stripped from the target protein and the individual ubiquitin monomers are recycled [25]. The involvement of the 26S proteasome provides direction to this degradation scheme, for it is not until this final step that the fate of the targeted protein is ultimately decided, as its proteolytic degradation poses the first non-reversible step [24].

1.4.2 Aberrant Control of β-catenin Protein Levels Leads to Malignant Tumor Formation

The significance of the β-catenin TPM in the regulation of its phosphorylation-dependent degradation is underscored by the identification of β-catenin variants that harbor mutations at the TPM phosphorylation sites and at surrounding residues in various human malignant tumors [26]. Mutations at Ser33 and Ser37, as well as other residues imperative to the formation of the β-catenin phosphodegron, such as Asp32, Gly34, and

Ile35, have been shown to abolish β-TrCP binding. Mutations at Thr41 and Ser45 eradicate the potential for subsequent phosphorylation events at Ser37 and Ser33; thereby, also impeding the phosphorylation-dependent recognition of β-catenin by β-TrCP. Studies have shown that, due to all such mutations, β-catenin is able to escape ubiquitination and as a result is stabilized [16,19]. The failure to promote the proteasomal degradation of β-catenin enables irregular cytoplasmic accumulation and its subsequent localization into the nucleus, resulting in prolonged transcriptional co-activation of TCF/LEF target genes, which include a number of known oncogenes, namely *c-myc*, *cyclin D1*, and *matrilysin* [26]. Therefore, excessive transcription driven by the co-activation of β-catenin can lead to abnormal cell proliferation and ultimately, tumor formation.

To our knowledge, β-catenin remains the only protein reported, thus far, as having this specific tetra-phosphorylation motif (TPM). However, the level of inborn sophistication within the regulation of β-catenin degradation leads one to speculate that there likely exist other TPM-containing proteins regulated in a manner similar to β-catenin.

1.5 Valuable Tools in the Analysis of Phosphoproteins

A systems biology approach to studying signal transduction cascades involves a comprehensive identification of all of the factors that function in the relay of information from an extracellular stimulus to the intracellular machinery. As the reversible phosphorylation of proteins is known to be the foremost event in the transmission of cellular signals, a thorough understanding of the inner-workings of the various signaling cascades is heavily reliant on the detection and characterization of all of the proteins regulated by this post-translational modification [27]. The analysis of phosphorylated proteins can be a formidable challenge, owing to the highly dynamic nature of

phosphorylation. It can be difficult to capture proteins in their phosphorylated form, especially already lowly abundant signaling proteins, as only a small fraction of the available pool of a protein is likely phosphorylated at any given time [28]. Hence, large-scale phosphoproteomic studies have been hampered, due to the inability to effectively utilize traditional proteomic techniques, for, when used alone, the sensitivity and specificity of these conventional tools often permit the detection of only the most abundant phosphoproteins and phosphopeptides [10]. The last decade has seen a dramatic advancement in the field of phosphoproteomics; a feat attributed to the development of efficient phosphopeptide and phosphoprotein enrichment methods. The employment of such methods to isolate phosphorylated proteins and peptides from the gamut of unphosphorylated moieties, prior to further analytical processing, namely through biological mass spectrometry, has become the mainstay of phosphoproteomic investigations [28].

1.5.1 Application of Phosphorylation-Specific Antibodies

Antibodies with specificities directed against phosphorylated residues have been commercially available for years, although, only recently have they enjoyed application to the study of the phosphoproteome. Phosphoantibodies provide a simple, specific, and sensitive method of phosphoprotein isolation and detection, as, in theory, they can be utilized in both immunoprecipitation and immunoblotting experiments [10]. The employment of phosphotyrosine-specific antibodies has proven the most fruitful, as their successful application in the aforementioned methodologies, in conjunction with mass spectrometry, has made possible the identification of a vast number of novel phosphotyrosine-containing proteins, enhancing the knowledge of this phosphorylation event during both physiological and pathophysiological circumstances [29,30].

Historically, phosphoserine and phosphothreonine antibodies have not been met with the same enthusiasm as their phosphotyrosine counterparts, as their reputations have been plagued by poor conduct in immunoprecipitation procedures [31]. However, optimizations in the field of phosphoserine and phosphothreonine antibody development have yielded promising results. For example, using a variety of phosphoserine and/or phosphothreonine antibodies, Grønborg *et al.* were able to enrich for proteins phosphorylated on these residues via immunoprecipitation, enabling the mass spectrometric identification of Frigg, a novel substrate of protein kinase A (PKA) [27]. Perhaps the most significant development with respect to phosphoserine- and phosphothreonine-specific antibodies has come in the production of antibodies against specific phosphorylated sequences (phosphomotifs), most notably, consensus kinase phosphorylation sites [7]. The utilization of a phosphoantibody reactive to a sequence optimally phosphorylated by a given kinase subfamily has the potential for more focused and biologically informative phosphoproteomic investigations, as it enables the capture of only subsets of the phosphoproteome.

In the first study of its kind with phosphoserine/phosphothreonine motif antibodies, Kane *et al.* successfully enriched putative substrates of protein kinase Akt, also termed protein kinase B (PKB), through immunoprecipitation with a phosphomotif antibody raised against the Akt consensus sequence, RXRXXpS/pT (X, arbitrary amino acid; pS/pT, phosphoserine/phosphothreonine) from insulin-stimulated, mouse 3T3-L1 preadipocyte cells. Their efforts, which also relied on immunoblotting with the phosphomotif antibody and mass spectrometry, led to the identification of a novel Akt substrate, shown to be doubly phosphorylated by Akt, which they designated Akt substrate of 160 kDa, or AS160 [32]. At least four other promising Akt substrate candidates were pending further characterization at the time of this investigation. In recent years, it appears that at least two of these putative substrates, AS47 and AS250, were revealed as novel Akt substrates [33,34]. The simplicity and productivity of this

phosphomotif antibody-based method proved its value in experiments of this type, spawning numerous studies focused on elucidating the signaling networks of specific protein kinases.

Following many years dedicated to improving the quality of phosphomotif antibodies, their utility in immunoprecipitation experiments was expanded to include phosphopeptide enrichment. As has been the case with all phosphorylation-state antibodies, antibodies specific to phosphotyrosine-containing motifs were the first to be successfully employed in the isolation of phosphopeptides from a complex mixture of enzymatically-digested peptides [30]. However, in a recent phosphoproteomic undertaking, Matsuoka *et al.* successfully immunoprecipitated phosphopeptides with phosphoserine/phosphothreonine-specific motif antibodies in an attempt to identify putative substrates of the protein kinases, ATM (ataxia telangiectasia-mutated) and ATR (ATM-Rad3-related), key components of the cellular DNA damage response [35]. An array of phosphomotif antibodies, specific for the consensus sequences of a variety of well known ATM and ATR substrates, were used to enrich for phosphopeptides belonging to potential ATM and ATR substrates. Studies have shown that these highly related kinases, which share substrate specificity, optimally phosphorylate serine (S) or threonine (T) residues immediately followed by a glutamine (Q) residue, generating fairly limited consensus sequences of SQ and TQ [35].

This study also illustrates the application of phosphomotif antibodies to a specific biological process. In order to delineate the signaling pathways involved in the cellular response to DNA damage, Matsuoka *et al.* compared the phosphorylation state of peptides isolated from untreated cells to that of peptides isolated from irradiated cells using a mass spectrometric-based technique, referred to as SILAC (stable isotope labeling with amino acids in cell culture), which involves differential *in vivo* labeling of proteins [35]. Distinctive labeling was afforded by the incorporation of heavy or light isotope-laden arginine and lysine residues into the proteins of the two cell populations during

normal protein synthesis. Subsequent to the irradiation, the heavy and light cell lysates were mixed in a 1:1 ratio, digested with trypsin, and the resultant tryptic peptides were subjected to immunoprecipitation with phospho-SQ- and phospho-TQ-specific antibodies [35]. Separation and analysis of the bound phosphopeptides by liquid chromatography (LC) coupled to tandem mass spectrometry (MS/MS) revealed some 900 phosphorylation sites, all of which contained an ATM/ATR consensus site, exhibiting phosphorylation-induction upon DNA damage as indicated by a comparison of the intensities of the differentially labeled SILAC pairs, which represent the phosphorylated peptide in the presence or absence of irradiation. Interestingly, functional characterization of a limited number of the candidate ATM/ATR substrates revealed a high concentration of proteins involved in the regulation of the DNA damage response and DNA repair [35]. The identification of such a vast number of proteins containing phosphorylated S/T motifs analogous to those found within known ATM and ATR substrates, clearly demonstrates the advantage of phosphopeptide enrichment prior to further analysis.

1.5.2 Unambiguous Identification of Phosphopeptides and Phosphorylation Sites Using MALDI-TOF Mass Spectrometry

A thorough characterization of protein phosphorylation and the regulatory mechanisms it imparts on the modified protein must involve an identification of the site(s) targeted for phosphorylation. Nowadays, the detection of phosphoproteins and phosphopeptides, as well as the localization of specific phosphorylation sites, are usually accomplished with mass spectrometry. This powerful analytical tool has become the mainstay for the analyses of amino acid sequencing and post-translational modifications, namely phosphorylation, as its sensitivity, mass accuracy, analytical speed, and information output are unparalleled [36]. Although a variety of mass spectrometric instrumentation is available, all mass spectrometers are comprised of four major

components: a sample inlet, an ionization source, a mass analyzer, and a detection system [36]. It is the nature of these former three components that is often used to define the class of instrument, with different combinations of the various forms of these elements providing a diverse array of mass spectrometric technologies [36]. For the purpose of this study, only MALDI-TOF and MALDI-TOF/TOF mass spectrometry will be described.

Mass spectrometry can be described as the study of gas-phase ions; hence, analytes must be converted to gaseous ions prior to their analysis. Historically, the production of gas-phase ions of high molecular weight biomolecules, such as proteins and peptides, was viewed as an abominable challenge; however, the advent of 'soft' ionization techniques, such as matrix-assisted laser desorption/ionization (MALDI), have made this feat a fairly routine process [36]. MALDI involves dissolving the analyte material, usually enzymatically-digested peptides, in a solution containing a UV-absorbing matrix [36]. Upon evaporation of the solvent, the matrix crystallizes, with the peptide molecules being incorporated into the crystals. The processes of dissolution and crystallization are conducted on the surface of a MALDI probe, which ultimately enters the spectrometer at the sample inlet. Pulses of UV laser light are concentrated on the probe, facilitating the vaporization of the matrix, which serves to promote the co-vaporization of the integrated peptides. Peptide ionization is afforded by the inherent acidity of the matrix, as well as by the addition of dilute acids to the peptides during sample preparation [36].

The nature of MALDI to generate ions in a pulsed fashion was ideal for its being coupled to the method of mass analysis referred to as time-of-flight (TOF) [36]. TOF mass analysis bases the measurement of the mass-to-charge (m/z) ratio of a peptide upon the time it takes to travel through a field-free region to the detector. Following ionization, peptide ions are given a fixed amount of kinetic energy through their acceleration within an electric field, generated through the application of a high voltage

(Figure 1.5A). The peptides then enter the field-free flight tube, where they travel at a velocity inversely related to their m/z ratio; thus, peptides with relatively low m/z ratios travel more rapidly, reaching the detector first, while those with larger m/z ratios lag behind and are detected later [36]. This provides a peptide mass fingerprint of the analyte material, which not only depicts the m/z ratios of the peptide ions present, but also the intensity at which they were detected. In order to facilitate the putative identification of an unknown protein, the experimental m/z ratios can be assessed by mass mapping software, such as MS-Fit, which attempts to identify the protein in question by comparing these query ratios to theoretical and/or experimental ratios stored within sequence databases [36].

MALDI-TOF mass spectrometry (MALDI-TOF-MS) is one of the most commonly used mass spectrometric strategies, owing to its sensitivity and relative simplicity; however, conventional MALDI-TOF analysis cannot provide the protein/peptide sequence information obtained through tandem mass spectrometry (MS/MS) [36,37]. An extension of TOF mass analyzers are configured such that they are capable of studying post-source decay (PSD) reactions, which can provide primary sequence information of a selected peptide ion. PSD describes the process whereby a peptide ion, often referred to as the precursor ion in the context of PSD, fragments in the flight tube as a result of its instability, which is due to excess internal energy gained directly from the laser or through high-energy collisions with other peptide ions [37]. Within the flight tube, the precursor ion and its fragment ions travel at the same velocity and are therefore, not differentiated by the detector when operating in linear mode [36]. MALDI-TOF-PSD, which is performed in reflector mode, takes advantage of the fact that the kinetic energy of the fragment ions is much lower than that of the original precursor ion, due to their mass difference (Figure 1.5B). The precursor and fragment ions are deflected toward a second detector using an electrically charged reflectron mirror located at the end of the flight tube. Once again, the ions are discriminated by flight time

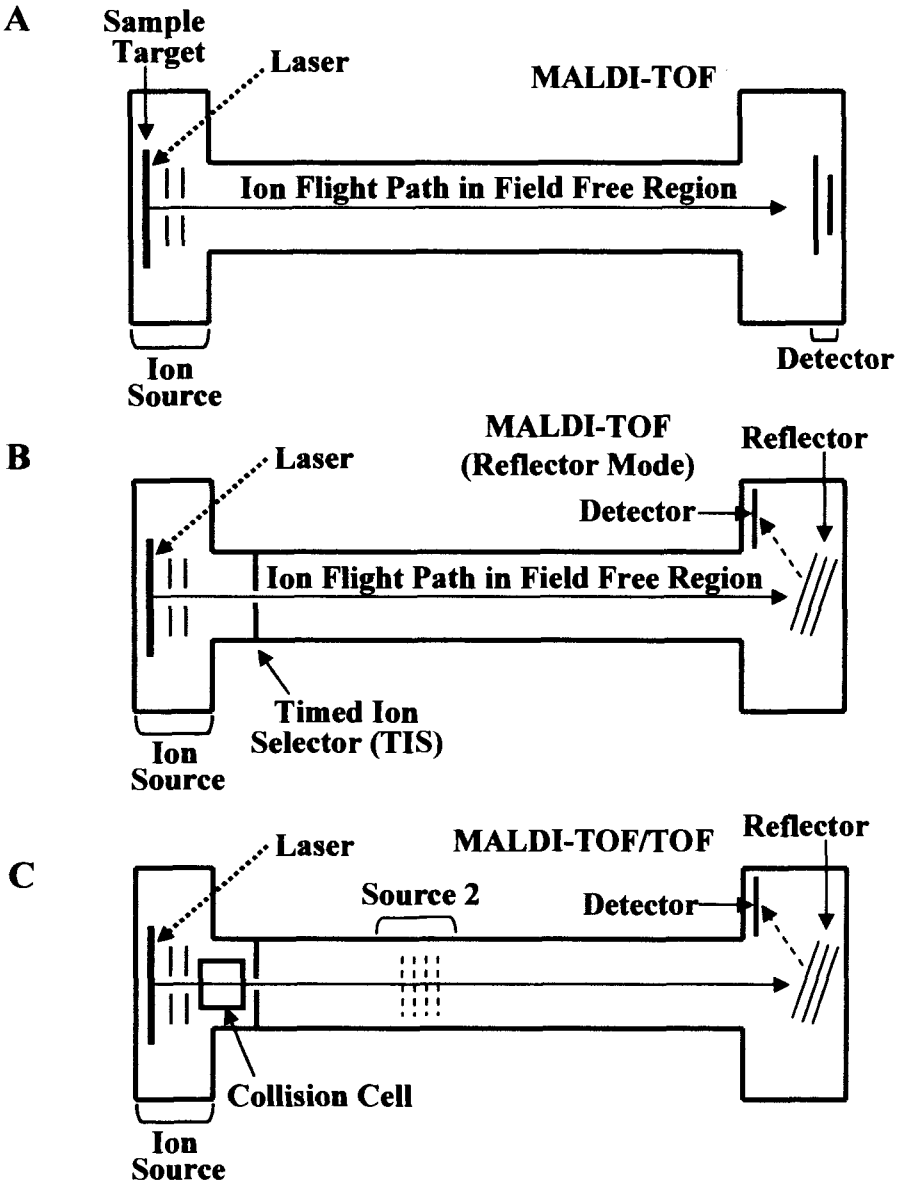

Figure 1.5- Schematic Diagrams of MALDI-TOF and MALDI-TOF/TOF Mass Spectrometers [36,38]. Laser pulses vaporize the matrix crystals, carrying the peptide ions into the gas phase. Gaseous ions are accelerated through the ion source into the flight tube to the detector. **(A)** MALDI-TOF mass spectrometer. **(B)** MALDI-TOF mass spectrometer operating in reflector mode. The reflector redirects the flight path of a precursor ion and its fragments to a second detector. **(C)** MALDI-TOF/TOF mass spectrometer operating in reflector mode. TOF1 ranges from the ion source to Source 2, whereas TOF2 comprises the area spanning Source 2 to the reflector.

dispersion with the fragment ions reaching the final detector at different times depending on their m/z ratios [36]. The presence of an electrostatic ion gate, often referred to as a timed ion-selector (TIS), allows PSD analysis of a precursor ion with a specific m/z ratio, by deflecting non-selected m/z ions away from the entrance of the flight tube [36]. The resulting spectrum displays the precursor ion, as well as its fragment ions, whose detection provides amino acid sequencing information whether through *de novo* sequencing or through the use of information maintained within protein sequencing databases.

The classical method of PSD analysis can be time-consuming, as the acquisition of PSD data involves the detection of fragment ions in multiple mass ranges using different mirror voltages with a final stitching of these segments to produce the complete fragment ion spectra [36,38]. In an effort to overcome the shortcomings of PSD analysis, MALDI is often coupled to a TOF/TOF mass analyzer, which is capable of true tandem mass spectrometric (MS/MS) experimentation [38]. As the name suggests, TOF/TOF mass analyzers differ from their TOF counterparts in that they house two TOF mass analyzers in a linear arrangement (Figure 1.5C). The first TOF region, functions in a manner similar to a singular TOF mass analyzer, as it is responsible for the acceleration and focusing of the analyte ions [38]. Following precursor ion selection, a precursor ion and its fragment ions move into a second ion source contained within the second TOF region, where they are reaccelerated and forced to travel at velocities inversely related to their own m/z ratios, allowing the acquisition of a complete fragmentation spectra in one step at a fixed mirror voltage [38]. MALDI-TOF/TOF mass spectrometers are also most often equipped with a collision cell, which enables the collision-induced dissociation (CID) of a selected precursor ion through high-energy collisions with inert gas molecules. This allows TOF/TOF mass analyzers to provide MS/MS data from the analysis of both PSD and CID products, which enhances the quality of the fragment ion spectra, as PSD is

often limited to the formation of large fragment ions, whereas CID can promote the generation of smaller fragments [38].

The interpretation of an MS/MS spectrum, whether generated through PSD and/or CID, relies on a common nomenclature to characterize the various types of fragment ions that may occur. A majority of the fragmentation events of a precursor ion involves the breakage of the peptide bond, resulting in the formation of two fragments, one containing the N-terminus and the other the C-terminus [39]. The classification of these ions depends upon the location of the proton on the precursor ion. If the proton is retained on the N-terminal fragment, a b-ion will be observed, whereas, if the proton is present on the fragment containing the C-terminal, a y-ion is detected (Figure 1.6A). Although relatively less abundant in CID, other forms of fragmentation do exist, namely those resulting in immonium ions, which are characteristic of individual amino acids, or internal fragment ions, produced by a double cleavage of the peptide backbone [39].

The post-translational modification of a protein commonly involves the addition of a functional group to a particular amino acid side chain. Thus, the identification of modified peptides by mass spectrometry is made possible through the detection of characteristic mass differences between the modified and unmodified versions of a given peptide. In the case of phosphorylation, mass spectrometric analysis reveals a net mass increase of 80 daltons (Da) from the unphosphorylated peptide to its phosphorylated form, owing to the addition of a phosphate group and the concerted loss of a water molecule [37]. Provided that the amino acid sequence of the protein in question is known, phosphopeptides can be putatively identified using peptide mass calculator programs, such as MS-Digest, which enable the comparison of experimental m/z data to theoretical data determined by *in silico* digestion.

Unambiguous identification of a phosphopeptide and precise determination of its phosphorylation site(s) can be achieved through PSD or MS/MS analysis. Putative phosphopeptides, detected through initial mass spectrometric analysis, can be selectively

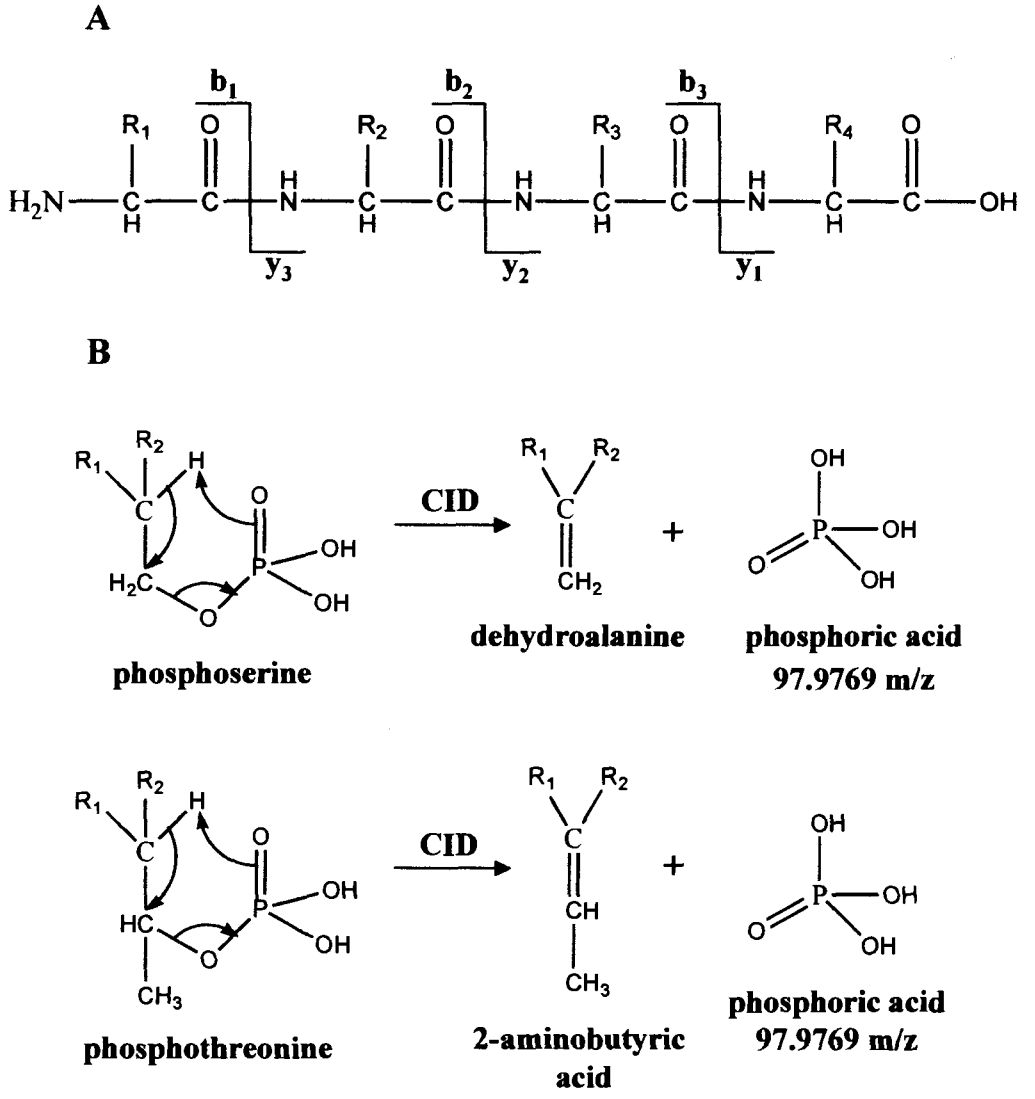

Figure 1.6- Peptide Ion Fragmentation [39]. **(A)** The predominant fragmentation of a precursor ion involves the breakage of the peptide bond. If the charge is retained on the N-terminal fragment, a b-ion is detected; whereas, if the charge is retained on the C-terminal fragment, a y-ion is observed. **(B)** Fragmentation of phosphoserine- and phosphothreonine-containing peptides is often accompanied by a neutral loss of phosphoric acid (H_3PO_4), which results in their conversion to dehydroalanine and 2-aminobutyric acid, respectively. The loss of ~98 m/z from the precursor ion is diagnostic of the loss of H_3PO_4.

fragmented and the fragment ions analyzed for the presence of a phosphate group. Phosphopeptide ions can be identified by their tendency to lose meta-phosphoric acid (HPO_3) and phosphoric acid (H_3PO_4) during fragmentation, which are diagnostically represented as losses of 80 Da and 98 Da, respectively. While serine- or threonine-phosphorylated peptide ions predominantly exhibit the loss of 98 Da (Figure 1.6B), peptide ions containing phosphotyrosine residues generally show only a loss of 80 Da, enabling the differentiation between tyrosine and serine/threonine phosphorylation [28]. Examination of the set of fragment ions generated through PSD and/or CID can provide the information required to map the phosphate group to a specific residue along the precursor ion. As mentioned previously, the highly reversible nature of phosphorylation poses a challenge to the study of phosphoproteins. Phosphopeptide detection and phosphorylation site identification is further confounded by the suppression of signals elicited by phosphoproteins, which can be attributed to the sheer abundance of unphosphorylated peptides within complex peptide mixtures [28]. The prevalence of phosphopeptide signal suppression makes the enrichment of phosphorylated peptides prior to mass spectrometric analysis a very critical task.

1.6 Project Objectives

The overall purpose of this study is to identify proteins containing a novel phosphorylation motif, first discovered within the N-terminal region of β-catenin [16]. This phosphomotif is comprised of four phosphorylated serine or threonine residues with each phosphorylation site separated from the last by three amino acid residues: pS/pTXXXpS/pTXXXpS/pTXXXpS/pT, where pS, pT represent phosphoserine and phosphothreonine residues, respectively, and X represents arbitrary amino acid residues. We have termed this specific phosphorylated sequence the tetra-phosphorylation motif (TPM). The remarkable level of regulation imparted by the β-catenin TPM in the control of its degradation leads us to hypothesize that the TPM exists within other proteins.

Specifically, our objectives are as follows:

1.) Characterize a purified, polyclonal phosphospecific antibody raised against a TPM phosphopeptide library.

2.) Identify novel TPM-containing proteins using bioinformatic, immunological, and mass spectrometric methods.

3.) Characterize the functional consequence of the TPM in novel proteins containing this phosphomotif, in terms of its role in protein stability and cellular regulation.

Chapter 2

Materials and Methods

2.1 Antibodies

The chicken TPM phosphoantibody was developed by Aves Labs Inc. (Tigard, OR) against a synthetic phosphopeptide antigen library (CZ[pS] XXX [pS]XX X[pS]X XX[pS]), which consists of phosphopeptides with phosphoserine (pS) residues at every fourth position and all possible combinations of amino acids at the X positions. Polyclonal, TPM phosphoantibodies were purified by double subtractive affinity chromatography. Mouse ANTI-FLAG® M2 Monoclonal, rabbit anti-actin, and rabbit β-catenin antibodies were purchased from Sigma-Aldrich, Inc. (Saint Louis, MO). The monoclonal, mouse haemagglutinin (HA) antibody was obtained from Berkeley Antibody Company (BAbCO; Richmond, CA), whereas the mouse KLF7 polyclonal antibody was from Abnova Corp. (Taipei, Taiwan). Mouse c-Myc (clone 9E10) antibody was purchased from Santa Cruz Biotechnology, Inc. (Santa Cruz, CA). Rabbit anti-TAZ and mouse anti-ubiquitin (clone P4D1) antibodies were purchased from Cell Signaling Technology, Inc. (Beverly, MA). The rabbit 14-3-3 antibody was from Abcam Inc. (Cambridge, MA). Horseradish peroxidase-conjugated, donkey anti-chicken IgY (H+L) antibody was purchased from Gallus Immunotech, Inc. (Fergus, ON). Horseradish peroxidase-conjugated, goat anti-rabbit IgG (H+L) antibody was from Bio-Rad Laboratories, Inc. (Hercules, CA) and the horseradish peroxidase-conjugated, goat anti-mouse IgG (H+L) antibody was from Promega Corp. (Madison, WI).

2.2 Plasmids

Wild-type TAZ cDNA (MGC-19891; ATCC) was subcloned into the pFLAG-CMV-2 eukaryotic expression vector (Sigma-Aldrich, Inc.) to generate FLAG-TAZ. Briefly, full-length, human, placental TAZ cDNA, cloned within the prokaryotic expression vector, pOTB7, was obtained as an *E. coli* stab. The bacteria were cultured in Luria's Broth (LB) with 25 μg/mL chloramphenicol. The plasmid DNA was then isolated using the GenElute® Plasmid Miniprep Kit (Sigma-Aldrich, Inc.), according to the manufacturer's instructions. The TAZ cDNA was amplified via PCR with the Platinum® *Pfx* DNA Polymerase (Invitrogen Corp.; Burlington, ON), using the following primers: Sense, 5'-CGGAATTCGATGAATCCGGCCTCG-3' and Antisense, 5'-CGTTAAGGATCCTTACAGCCAGGTTAG-3', which contain the *Eco*R I and *Bam*H I restriction enzyme recognition sites, respectively. The resulting PCR product was verified on a 1% agarose gel with 0.02% ethidium bromide and subsequently purified using the QIAquick® PCR Purification Kit (Qiagen, Inc.; Mississauga, ON), according to the manufacturer's instructions. The verified product was then subcloned into the *Eco*R I and *Bam*H I sites of the pFLAG-CMV2 expression vector, which incorporates a FLAG tag at the N-terminus of all constructs, via in-gel ligation. Briefly, pFLAG-CMV-2 and the purified TAZ PCR product were digested with *Eco*R I (Promega Corp.) and *Bam*H I (Promega Corp.) at 37°C for 2 h, and run on a 1% low-melt agarose gel with 0.02% ethidium bromide. The corresponding bands were excised from the gel and melted at 65°C for 10 - 15 min.. Ligation was then performed overnight at 4°C with T4 DNA Ligase (Promega Corp.). DH5α *E. coli* competent cells were transformed with the ligated pFLAG-CMV-2-TAZ expression vector and grown on LB/Agar medium with 100 μg/mL ampicillin. Wild-type KLF7, encoded within the pCS2+MT eukaryotic expression vector, which incorporates 6 Myc tags at the N-terminal of the encoded protein, was kindly provided by Dr. L. Lei (Arizona State University).

Mutant constructs were generated via site-directed mutagenesis with cloned *Pfu* DNA Polymerase from Stratagene (Cedar Creek, TX). The PCR products, verified by 1% agarose gel with 0.02% ethidium bromide and digested with *Dpn* I (New England Biolabs, Ltd.; Pickering, ON) to degrade the methylated template DNA, were then transformed in DH5α *E. coli* competent cells and grown on LB/Agar medium with 100 μg/mL ampicillin. The plasmid DNA was isolated as previously mentioned. The FLAG-tagged TAZ S58A/S62A double mutant construct (FLAG-TAZ SDM) was generated by subsequent site-directed mutagenesis events. Initially, FLAG-TAZ S58A was created with the following primers: Sense, 5'-GAGCCTGATGCGGGCTCGCACTCG-3' and Antisense, 5'-CGAGTGCGAGCCCGCATCAGGCTC-3', using FLAG-TAZ as the template DNA. The FLAG-TAZ SDM construct was then generated by mutating Ser62 to an alanine using FLAG-TAZ S58A as the template DNA, along with the following primers: Sense, 5'-GCTCGCACGCGCGCCAGTCCAG-3' and Antisense, 5'-CTGGACTGGCGCGCGTGCGAGC-3'. The Myc-tagged, double mutant of KLF7 (Myc-KLF7 STDM), which harbours alanine substitutions at Thr19 and Ser23, was created in the same manner as mentioned above for FLAG-TAZ SDM. The initial mutation was made at Thr19 with the following primers: Sense, 5'-CAACTTGTCCACGACGCCGGCTACTTCTC-3' and Antisense, 5'-GAGAAGTAGCCGGCGTCGTGGACAAGTTG-3' using Myc-KLF7 as the template DNA. The S23A mutation was then made on the Myc-KLF7 T19A template DNA, with the following primers: Sense, 5'-GGCTACTTCGCAGCTTTACCATCCCTGGAG-3' and Antisense, 5'-CTCCAGGGATGGTAAAGCTGCGAAGTAGCC-3'. The FLAG-tagged TAZ tetra-mutant construct (FLAG-TAZ ΔTPM), which contains alanine mutations at Ser58, Ser62, Ser66, and Ser70, was also generated by subsequent site-directed mutagenesis experiments. Firstly, Ser66 was mutated to an alanine, using the following primers and FLAG-TAZ SDM as the template DNA: Sense, 5'-GCGCCAGTCCGCCACCGACTCGTCG-3' and Antisense, 5'-

CGACGAGTCGGTGGCGGACTGGCGC-3', followed by the mutation of Ser70 to an alanine, using the following primers and FLAG-TAZ S58A/S62A/S66A as the template DNA: Sense, 5'-CACCGACTCGGCGGGCGGCC-3' and Antisense, 5'-GGCCGCCCGCCGAGTCGGTG-3'.

FLAG-TAZ S117A was created by introducing an alanine mutation at Ser117 on the FLAG-TAZ template DNA with the following primers: Sense, 5'-CCGCCAGCAGGCCTACGACGTGAC-3' and Antisense, 5'-GTCACGTCGTAGGCCTGCTGGCG-3'. The FLAG-TAZ S117D mutant was also produced from the FLAG-TAZ template DNA by substituting Ser117 with an aspartic acid residue using the following primers: Sense, 5' CCTCCGCCAGCAGGACTACGACGTGACC-3' and Antisense, 5'-GGTCACGTCGTAGTCCTGCTGGCGGAGG-3'. FLAG-TAZ S93A was generated by substituting Ser93 of FLAG-TAZ with an alanine residue using the primers listed here: Sense, 5'-GTCGCCCGCGGCCCTGCAGCTG-3' and Antisense, 5'-CAGCTGCAGGGCCGCGGGCGAC-3'. The FLAG-TAZ S93D mutant was also produced on FLAG-TAZ by replacing Ser93 with an aspartic acid residue using the following primers: Sense, 5'-GTCGCCCGCGGACCTGCAGCTGGG-3' and Antisense, 5'-CCCAGCTGCAGGTCCGCGGGCGAC-3'. The 14-3-3 binding mutant of TAZ, FLAG-TAZ S89A, was produced by mutating Ser89 to an alanine on FLAG-TAZ using the following primers: Sense, 5'-CTCGCACGCGTCGCCCGCGTC-3' and Antisense, 5'-GACGCGGGCGACGCGTGCGAG-3'.

The FLAG-TAZ ΔC^tDSG and FLAG-TAZ ΔTPM/ΔC^tDSG mutants were generated by substituting Ser314, which corresponds to Ser309 of mouse TAZ, of FLAG-TAZ or FLAG-TAZ ΔTPM, respectively, with an alanine residue, using the ensuing primers: Sense, 5'-GCAGAGCACTGACGCTGGCCTGGGGTTAG-3' and Antisense, 5'-CTAACCCCAGGCCAGCGTCAGTGCTCTGC-3'. Myc-TAZ, Myc-TAZ ΔTPM, Myc-TAZ ΔC^tDSG, and Myc-TAZ ΔTPM/ΔC^tDSG were then constructed by liberating

the gene encoding KLF7 from the pCS2+MT vector and inserting the genes encoding the aforementioned TAZ variants in its place. Briefly, FLAG-TAZ, FLAG-TAZ ΔTPM, FLAG-TAZ ΔC^{t}DSG, and FLAG-TAZ ΔTPM/ΔC^{t}DSG were amplified via PCR with the Platinum® *Pfx* DNA Polymerase (Invitrogen Corp.), using the following primers: Sense, 5'-CGGAATTCGATGAATCCGGCCTCG-3', which adds an *Eco*R I site upstream of the *taz* gene, and Antisense, 5'-GGATTCTCTAGATTACAGCCAGGTTAG-3', which inserts an *Xba* I restriction site at the 3' end of the *taz* gene. The resulting PCR products were verified on a 1% agarose gel with 0.02% ethidium bromide and then purified using the QIAquick® PCR Purification Kit (Qiagen, Inc.), according to the manufacturer's instructions. The *klf7* gene was then excised from the pCS2+MT vector by digesting the vector with *Eco*R I (Promega Corp.) and *Xba* I (Promega Corp) for 2 h at 37°C. The varying forms of the *taz* gene were digested in the same manner as pCS2+MT and subsequently inserted into the *Eco*R I and *Xba* I restriction sites of the pCS2+MT expression vector via in-gel ligation, using the method described previously for the generation of pFLAG-CMV-2-TAZ.

All PCR primers were synthesized by Invitrogen Corp. and the sequences of all of the DNA constructs were verified by automated DNA sequencing (ACGT Corp.; Toronto, ON). All plasmid DNA was amplified by transforming DH5α *E. coli* competent cells and subsequently isolated using the HiSpeed® Plasmid Maxi Kit (Qiagen, Inc.), according to the manufacturer's specifications.

The HA-tagged ubiquitin construct was generously provided by Dr. L. Porter (University of Windsor). FLAG-β-TrCP, encoded within the pcDNA3 mammalian expression vector, was obtained as a bacterial stab from Addgene Inc. (Cambridge, MA). The HA-tagged GSK-3β (S9A) mutant construct was generously provided by Dr. K. L. Guan (University of Michigan). The Myc-tagged β-catenin ΔTPM mutant was a gracious gift from Dr. A. Ali (University of Windsor).

2.3 Cell Culture

Human embryonic kidney (HEK) 293 and mouse 3T3-L1 embryonic fibroblast cells were obtained from American Type Tissue Culture Collection (ATCC; Manassas, VA). HEK 293 cells were grown as a monolayer in Dulbecco's Modified Eagle's Medium/Nutrient F-12 Ham (D-MEM/F-12), supplemented with 10% fetal bovine serum (FBS), 2mM L-glutamine, and antibiotics (100 units/mL penicillin, 100 μg/mL streptomycin), at 5% CO_2 and 37°C. 3T3-L1 cells were grown as a monolayer in Dulbecco's Modified Eagle Medium (D-MEM/F-12), supplemented with 10% bovine calf serum (BCS), 2mM L-glutamine, and antibiotics (100 units/mL penicillin, 100 μg/mL streptomycin), at 5% CO_2 and 37°C. The cells were maintained at 70 - 80% confluency on 6-well plates or 100 mm tissue culture dishes (Sarstedt, Inc.; Montreal, QC). L-glutamine, antibiotics, and 10X Trypsin-EDTA were purchased from Gibco™ Life Technologies (Invitrogen Corp.). D-MEM/F-12 and FBS were from Sigma-Aldrich, Inc., while the BCS was purchased from Hyclone (Thermo Fisher Scientific, Inc.; Ottawa, ON).

2.4 Transient Transfection, Cell Treatments, and Cell Lysis

HEK 293 and 3T3-L1 cells were transfected with expression vectors encoding HA-GSK3β (S9A) (7 μg/100 mm dish), Myc-β-catenin ΔTPM (7 μg/100 mm dish), various FLAG-TAZ and Myc-TAZ constructs (1-3 μg/30 mm dish; 5 μg/100 mm dish), wild-type Myc-KLF7 and Myc-KLF7 STDM (1-3 μg/30 mm dish; 5 μg/100 mm dish), FLAG-β-TrCP (10 μg/100 mm dish), and HA-ubiquitin (10 μg/100 mm dish). These amounts of DNA were maintained within co-transfection experiments. Empty vector DNA (pFLAG-CMV-2) was transfected alongside single transfections to normalize the DNA content during co-transfections.

Briefly, approximately $5x10^5$ cells per 30 mm dish and approximately $2x10^6$ cells per 100 mm dish were seeded in D-MEM/F-12 media 24 h prior to transfection. Cells were transiently transfected at a confluency of approximately 70 - 80% with FuGENE-HD Transfection Reagent (Roche Diagnostics; Laval, QC), according to manufacturer's specifications, unless a different transfection method was specified. Four hours post-transfection, cell culture media was replaced with fresh media.

Cells were treated with MG-132 (Calbiochem; San Diego, CA), a proteasome inhibitor, and Calyculin A (LC Laboratories; Woburn, MA), a Ser/Thr phosphatase inhibitor, approximately 24 h after transfection. Cells were incubated with 10 μM MG-132 and/or 100 nM Calyculin A for 1 h at 37°C and 5% CO_2, prior to cell lysis. Cells were then lysed in lysis buffer (50 mM Tris-HCl (pH 7.4), 1% Triton X-100, 150 mM NaCl, 0.1% SDS) in the presence of protease (aprotinin, PMSF, EDTA) and phosphatase (NaF) inhibitors. Briefly, untreated cells or cells solely treated with MG-132 were washed with cold Dulbecco's Phosphate-Buffered Saline (D-PBS; Sigma-Aldrich, Inc.) and then suspended in ice cold lysis buffer. Calyculin A-treated cells lift from the tissue culture dish and become suspended in the media, consequently, they were pelleted at 2500 rpm for 5 min. at room temperature. The cells were then washed with cold PBS and resuspended in ice-cold lysis buffer. Whole cell lysates were cleared at 14,000 rpm at 4°C for 20 min., so as to pellet the cellular debris. Where indicated, protein concentration was measured using the Bradford reagent (BioRad Laboratories, Inc.), according to manufacturer's instructions. Cleared cell lysates were immediately subjected to immunoprecipitation or were maintained at –20°C until further experimentation.

2.5 Immunoprecipitation and Immunoblotting Analysis

The immunoprecipitation of FLAG-tagged and Myc-tagged proteins was enabled through the incubation of cleared cell lysates with Anti-FLAG® M2-Affinity Gel (Sigma-

Aldrich, Inc.) or Anti-c-Myc Agarose Conjugate (Sigma-Aldrich, Inc.), respectively, for 3 h at 4°C on a horizontal rotator. Following incubation, immune complexes were gently centrifuged at <6000 rpm for 1 min. and washed 2 – 4 times with cold IP wash buffer (50 mM Tris-HCl (pH 7.4), 0.1% Triton X-100, 150 mM NaCl, 0.1% SDS). The bound proteins were eluted through the addition of 2X SDS protein loading dye (0.120 M Tris-HCl (pH 6.8), 4% SDS, 0.3% β-mercaptoethanol, 10% glycerol, 0.004% bromophenol blue, 3% dithiothreitol (DTT)), boiling for 5 min. at 95 - 100°C, followed by harsh vortexing and centrifugation at >14,000 rpm. The samples were maintained at –20°C until subsequent analysis.

Cleared cell lysates, denatured in 6X SDS protein loading dye (0.350 M Tris-HCl (pH 6.8), 10% SDS, 0.3% β-mercaptoethanol, 30% glycerol, 0.012% bromophenol blue, 3% DTT) and proteins eluted from immune complexes were resolved via SDS-PAGE on 10 - 12% polyacrylamide gels. All gels were run at 150 V in 1X SDS-PAGE running buffer (0.192 M, 0.025 M Tris-base, 0.01% SDS, pH 8.3). Following SDS-PAGE, proteins were transferred to methanol-activated, Immobilon™-P polyvinylidene difluoride (PVDF) membrane (Millipore Corp.; Bedford, MA), unless otherwise specified. Protein transfer was performed for 1 h at 100 V in ice-cold 1X transfer buffer (20% methanol, 0.192 M glycine, 0.025 M Tris-base, pH 8.3). Following transfer, all membranes were blocked in 5% non-fat, dry milk in 1X Tris-Buffered Saline (1X TBS; 0.068 M NaCl, 8.3mM Tris-base, pH 7.6) containing 0.1% Tween®-20 (1X TBSt; Fisher Scientific, Inc.), with the exception of membranes to be probed with the TPM phosphoantibody, which were blocked in 5% bovine serum albumin (BSA; Sigma-Aldrich, Inc.) in 1X TBSt. Membranes probed with primary antibodies requiring 1 h incubation were blocked overnight at 4°C with gentle agitation, whereas those incubated with primary antibodies overnight were blocked for only 1 h at room temperature. Immediately following blocking, the membranes were probed with the indicated primary antibody as outlined below. Anti-TPM was used at a dilution of 1:1000 in 1X TBSt. The

β-catenin primary antibody was also used at 1:1000 in 5% BSA in 1X TBSt. Anti-TAZ was used at a dilution of 1:2500 in 1X TBSt, whereas anti-actin was utilized at 1:1000 in 1X TBSt. The pan-14-3-3 antibody was used at 1:1000 in 1X TBSt. Membranes probed with the antibodies described above were incubated overnight at 4°C with gentle agitation. Anti-FLAG was used at 1:3000 in 2.5% milk dissolved in 1X TBSt, while anti-c-Myc was used at 1:1000 in 2.5% milk in 1X TBSt. The KLF7 antibody was diluted 1:3000 in 2.5% milk in 1X TBSt. The ubiquitin antibody was used at 1:5000 in 2.5% milk in 1X TBSt. Anti-HA was utilized at a dilution of 1:1000 in 2.5% milk in 1X TBSt. The antibodies listed above were incubated for 1 h at room temperature with gentle agitation. Following primary antibody incubation, all membranes underwent three washes of 5 min. each with 1X TBSt, with the exception of those membranes probed with anti-TPM, which were subjected to three 15 min. washes. Membranes were then incubated with their species-specific, horseradish peroxidase-conjugated secondary antibody, followed by washing as indicated above. All secondary antibodies were incubated for 45 min. at room temperature at a dilution of 1:5000 in 1X TBSt. Immunoreactive bands were visualized via chemiluminescence using the SuperSignal® West Femto Maximum Sensitivity Substrate (Thermo Fisher Scientific, Inc.), according to the manufacturer's instructions.

2.6 In Vitro Dephosphorylation Assays

2.6.1 Synthetic Peptide Library Assays

The synthetic phosphopeptide (CZ[pS] XXX [pS]XX X[pS]X XX[pS]; Aves Labs, Inc.) and non-phosphopeptide libraries (CZS XXX SXX XSX XXS; Aves Labs, Inc.) were reconstituted with HPLC-grade water (Honeywell, Inc.; Muskegon, MI) to 4 mg/mL. Calf intestinal alkaline phosphatase (CIAP; Promega, Corp.), was diluted from 1

unit/μL to 0.5 units/μL with 50 mM ammonium bicarbonate, pH 8.0, to reduce the glycerol content of the CIAP storage buffer, as glycerol is incompatible with mass spectrometry. Twenty micrograms of the phosphopeptide library were incubated with 2 units of CIAP in 20 μL of 50 mM ammonium bicarbonate, pH 8, at 37°C for increasing time points to achieve dephosphorylation of approximately 1 phosphate group (5 min.), approximately 2 phosphate groups (90 min.), and approximately 3 phosphate groups (120 min.). At the indicated time points, 4 μL aliquots were taken from the reaction mixture and the dephosphorylation reaction was quenched by the addition of 5% formic acid (Sigma-Aldrich, Inc.). The reconstituted phosphopeptide and peptide libraries were subjected to the same reaction conditions described above; however the reactions were quenched immediately with 5% formic acid to generate tetra-phosphorylated and unphosphorylated peptides, respectively.

The phosphopeptide and peptide libraries were then analysed by mass spectrometry using a matrix-assisted laser desorption ionization (MALDI)-time of flight (TOF) mass spectrometer (Applied BioSystems Voyager-DE™ PRO BioSpectrometry™ Workstation; Applied BioSystems, Framingham, MA) in linear mode. The samples were crystallized on a MALDI target plate (Applied BioSystems) with a matrix of α-cyano-4-hydroxycinnamic acid (Sigma-Aldrich, Inc.) in 60% acetonitrile, 1% formic acid. The mass profiles of the phosphopeptide libraries were analysed for a loss of phosphate group(s) (-m/z 80, -m/z 160, -m/z 240, -m/z 320), so as to determine the approximate number of phosphates remaining on the phosphopeptide libraries.

The peptide libraries corresponding to 0 phosphates, approximately 1 phosphate, approximately 2 phosphates, approximately 3 phosphates, and 4 phosphate groups were diluted to a final concentration of 0.1 μg/μL in HPLC-grade water for dot blot analysis. One microlitre of each sample was directly spotted on nitrocellulose membrane (Millipore Corp.) and allowed to completely dry. Immunoblot analysis with the TPM phosphoantibody was then conducted as outlined above (2.5).

2.6.2 Immunoprecipitant and Lysate Assays

Following the final wash step of the immunoprecipitation procedure outlined earlier (2.5), the immune complexes were resuspended in 200 μL of lysis buffer. Approximately 100 μL of the resuspended immunoprecipitants were incubated with 3 units of CIAP (1 unit/μL; Promega Corp.), as was a 25 μL aliquot of cleared cell lysate, for 30 min. at 37°C, while the remaining immunoprecipitants and a second aliquot of lysate were left untreated. CIAP activity was quenched by the addition of 20 μL of 2X SDS protein loading dye to the immunoprecipitants and 10 μL of 6X SDS protein loading dye to the lysates. Proteins were then resolved by SDS-PAGE and detected through anti-FLAG immunoblotting (2.5).

2.7 Phosphorylation Site Analysis of FLAG-TAZ

2.7.1 Large-Scale Immunoprecipitation

Six 10 cm tissue culture plates were each seeded with approximately $2x10^6$ HEK 293 cells in DMEM/F12 media 24 h prior to transient transfection. The cells were given fresh DMEM/F12 media 1 h prior to transfection. Each plate was transfected with 15 μg of FLAG-TAZ DNA using the calcium phosphate ($CaPO_4$) method [40]. Briefly, 15 μg of FLAG-TAZ DNA were diluted in 50 μL of 2.5 M $CaCl_2$, which was then brought to a final volume of 500 μL with 1/10 TE buffer (1 mM Tris-HCl, 0.1 mM EDTA, pH 7.6). The mixture was then added in a drop-wise fashion to an equal volume (500 μL) of 2X HEPES buffer (140 mM NaCl, 1.5 mM Na_2HPO_4, 50 mM HEPES, pH 7.05) while mixing. In order to facilitate DNA-$CaPO_4$ co-precipitate formation, the mixture was allowed to incubate for 20 min. at room temperature. The DNA-$CaPO_4$ complexes were then added drop-wise to the cells and incubated for 4 h at 37°C, 5% CO_2, after which the

culture media was replaced with fresh DMEM/F12. Approximately 24 h post-transfection, the cells were treated with 10 μM MG-132 and 100 nM Calyculin A for 1 h at 37°C, 5% CO_2. Each plate of cells was then harvested in 300 μL of lysis buffer and lysed in the manner indicated above (2.4). The cleared cell lysates were then pooled and immunoprecipitation of FLAG-TAZ was performed using 75 μL of Anti-FLAG® M2-Affinity Gel (Sigma-Aldrich, Inc.), as outlined previously (2.5). Immune complexes were eluted from the beads by boiling at 95°C for 5 min. in 65 μL of 2X SDS protein loading dye and subsequently resolved by 10% SDS-PAGE. Proteins were visualized by Coomassie staining (40% ethanol, 10% acetic acid, 0.1% Coomassie Brilliant Blue) and subsequently destained with Destain Solution (40% ethanol, 10% acetic acid) to reduce the background stain. They were also transferred to PVDF membrane and immunoblotted with the FLAG antibody, as specified above (2.5).

2.7.2 Mass Spectrometric Analysis

The protein band corresponding to FLAG-TAZ, visualized through Coomassie staining, was carefully excised from the polyacrylamide gel using a sterile blade in a laminar flow hood. The band was then destained in destain solution (50% acetonitrile, 50 mM ammonium bicarbonate) for 35 min. at 37°C with gentle agitation. Dependent on the extent of staining, the destaining procedure may have been repeated once with fresh destain solution. Dehydration of the gel piece was then achieved with two changes of HPLC-grade acetonitrile (Honeywell, Inc.), until it appeared opaque. The gel piece was then thoroughly dried by speed vacuuming (Speedvac Plus SC110A; Sorvall) for 20 minutes. The protein was then subjected to in-gel trypsin digestion with approximately 500 - 750 ng of modified, sequencing grade trypsin (Promega Corp.) resuspended in 50 mM ammonium bicarbonate, pH 8.0, to a final concentration of 13 ng/μL. A 5 μL aliquot was taken from the in-gel digestion sample, following approximately 1 - 3 h of

digestion. Trypsin digestion was then allowed to proceed overnight at 37°C with agitation. Following digestion, the sample was harshly vortexed and centrifuged at >14,000 rpm. The supernatant (pre-extraction solution), containing digested peptides freed from the gel piece, was then collected and acidified with 5% formic acid (Sigma-Aldrich, Inc.). Remaining peptides were extracted from the gel through incubation in 200 µL of extraction solution (60% acetonitrile, 1% formic acid) for 45 min. at 37°C with shaking. The sample was then vortexed and centrifuged, and the supernatant was removed and added to 5 µL of 5% formic acid. Peptide extraction was repeated one time with 100 µL of extraction solution for 10 minutes. The collected peptide solutions were then concentrated to approximately 10 µL by speed vacuuming (Speedvac Plus SC110A; Sorvall).

If required, peptide samples were desalted using ZipTip® C18 Microtips (Millipore, Inc.), following speed vacuuming. Briefly, microtips with a volume capacity of 10 µL (1 volume) were activated with 5 volumes of 60% acetonitrile, followed by equilibration with 10 volumes of 1% formic acid. The peptides were then bound to the resin by repeated pipetting in the concentrated peptide solution and washed with 5 volumes of 1% formic acid. The bound peptides were eluted by repeated pipetting in 1 volume of 60% acetonitrile, 1% formic acid.

Tryptic peptides were spotted on a MALDI target plate (Applied BioSystems), as indicated previously (2.6.1), and were analyzed on a MALDI-TOF mass spectrometer (Applied BioSystems Voyager-DE™ PRO BioSpectrometry™ Workstation; Applied BioSystems). The mass spectra were acquired in linear mode and were internally mass-calibrated. The tryptic peptide ion masses were compared to those generated by an *in silico* tryptic digestion of the human TAZ protein (NCBI Accession #: NP_056287) using the MS-Digest program of Protein Prospector (UCSF; University of California, San Francisco, CA), which enabled the recognition of all potential phosphopeptide ions. Multiple precursor ions of interest were subjected to automated, collision-induced

dissociation (CID) to verify the identity of the phosphopeptides and to map the phosphorylation sites to specific residues, unless indicated otherwise. MS/MS analysis was conducted at the University of Michigan Mass Spectrometry Facility (Ann Arbor, MI) via MALDI-TOF/TOF (4800 MALDI-TOF/TOF^{TM} Analyzer; Applied BioSystems). The precursor ion fragment masses were analysed with the MS-Product program of Protein Prospector (UCSF).

2.8 Protein Stability Assay

Approximately $2.5x10^4$ HEK 293 cells were seeded in 30 mm tissue culture dishes 24 h prior to transient transfection. Cells were then transfected with 1 μg of FLAG-TAZ, FLAG-TAZ ΔTPM, Myc-KLF7, or Myc-KLF7 STDM using FuGENE-HD Transfection Reagent (Roche Diagnostics), according to manufacturer's instructions. Forty-eight hours post-transfection, cells were treated with 200 μg/mL of cycloheximide (Sigma-Aldrich, Inc.) resuspended in DMSO to induce the inhibition of protein translation. At the indicated time points following cycloheximide treatment, the cells were lysed in 200 μL of lysis buffer, as described previously (2.4). The concentration of extracted protein in each of the samples was measured using the Bradford reagent (BioRad Laboratories, Inc.), according to product specifications. Equal amounts of protein were then resolved by SDS/PAGE and subsequently analysed by anti-FLAG or anti-c-Myc immunoblot analysis, as outlined above (2.5). The same membranes were also probed with actin antibody to ensure equal protein loading.

2.9 Preadipocyte Differentiation and Oil Red O Staining

Mouse 3T3-L1 preadipocyte cells were seeded 24 h prior to transfection at approximately $5x10^5$ cells per 30 mm tissue culture dish in DMEM/F12 containing 10%

BCS. Cells were transiently transfected with 3 μg of the specified DNA using FuGENE-HD Transfection Reagent (Roche Diagnostics), according to manufacturer's instructions. Preadipocyte differentiation was conducted according to the specifications outlined in the Adipogenesis Assay Kit from Caymen Chemical (Ann Arbor, MI). All reagents required for the differentiation were provided within the aforementioned kit. Briefly, cells were allowed to reach confluency (approximately 24 – 30 h post-transfection), at which time differentiation was induced by the addition of induction media, which contains 1X solutions of 3-isobutyl-1-methyl xanthine (IBMX), dexamethasone, and insulin in DMEM/F12 containing 10% FBS. After 72 h of induction, the cells were weaned from the induction media by its replacement with insulin media, which contains a 1X solution of insulin in DMEM/F12 with 10% FBS. Forty-eight hours later, fresh insulin media was added to the cells to support further differentiation. The cells were then monitored until the desired degree of lipid accumulation was reached (approximately 48 h after the second change of insulin media), at which time Oil Red O (ORO) staining was commenced.

All of the reagents required for ORO staining were also provided within the Adipogenesis Assay Kit (Caymen Chemical). The staining was conducted in accordance with the kit instructions. All steps were performed at room temperature with a 2 mL solution volume. Briefly, the differentiated cells were fixed for 15 min. in 1X Fixative Solution, followed by two 5 min. wash steps in an alcohol-based solution. The fixed cells were allowed to completely dry and then stained in a working solution of ORO (60% ORO in water; filtered with a 0.45 μM syringe filter). Following the 20 min. staining period, residual dye was removed through multiple washes with distilled water and two 5 min. washes with the Wash Solution. Phase contrast images of the ORO stained cells were then taken at magnifications of 50x or 100x using a Leica Inverted Research Microscope (Leica Microsystems; Richmond Hill, ON).

Chapter 3

Results

PART I) Identification and Characterization of TPM-Containing Proteins

3.1 Characterization of the TPM Phosphoantibody

In order to identify novel tetra phosphorylation motif (TPM)-containing proteins, a polyclonal antibody was raised against a phosphopeptide library consisting of peptides with the TPM sequence (pSXXXpSXXXpSXXXpS). The antibody was purified through double subtractive affinity chromatography, using phosphorylated and non-phosphorylated (SXXXSXXXSXXXS) peptide-library-conjugated columns to obtain phosphospecific antibodies.

3.1.1 The TPM Phosphoantibody Reacts with Tetra-Phosphorylated Peptides

The specificity of the TPM phosphoantibody was tested through its reactivity with differentially phosphorylated peptide libraries by dot blot analysis. In order to achieve phosphopeptide libraries with approximately three, two, and one phosphate group(s), the synthetic TPM phosphopeptide library was subjected to dephosphorylation by alkaline phosphatase for increasing time periods. The original non-phosphopeptide library and the TPM phosphopeptide library were used to represent peptide libraries with zero and four phosphate groups, respectively.

Following alkaline phosphatase incubation, MALDI-TOF mass spectrometry was employed to determine the phosphorylation state of each of the peptide libraries. Each of the peptide libraries yielded a broad peak, representative of the fact that the libraries contain a large number of different peptides (Figure 3.1A). Comparison of the masses associated with the central most portion of the peaks with that of the tetra-phosphorylated peptide library revealed mass shifts of approximately 80 m/z (5 min.), 160 m/z (90 min.), and 240 m/z (120 min.), signifying a loss of approximately one, two, and three phosphate groups, respectively.

To evaluate the reactivity of the TPM phosphoantibody with the various peptide libraries, dot blot analysis was conducted (Figure 3.1B). It was observed that increased incubation of the TPM phosphopeptide library with alkaline phosphatase lead to a loss of recognition by the TPM phosphoantibody. Importantly, the phosphoantibody exhibited the strongest reactivity with the tetra-phosphorylated peptide library, while not reacting with the non-phosphorylated peptide library, demonstrating the phosphospecificity of the TPM phosphoantibody.

3.1.2 The TPM Phosphoantibody Does Not Recognize the TPM Mutant of β-catenin

As β-catenin is the only protein reported, thus far, to contain a TPM [16,17], the specificity of the TPM phosphoantibody was further evaluated through its ability to distinguish between wild-type β-catenin and a β-catenin TPM mutant (β-catenin ΔTPM), in which all four of the TPM phosphorylation sites have been mutated to alanine residues. HEK 293 cells were untransfected, transfected with HA-GSK-3β (S9A), a constitutively active GSK-3β mutant, or co-transfected with HA-GSK-3β (S9A) and Myc-β-catenin ΔTPM. Anti-β-catenin immunoblot analysis of the whole cell lysates, resolved by SDS/PAGE, revealed two bands at approximately 110 kDa and 115 kDa, which coincide

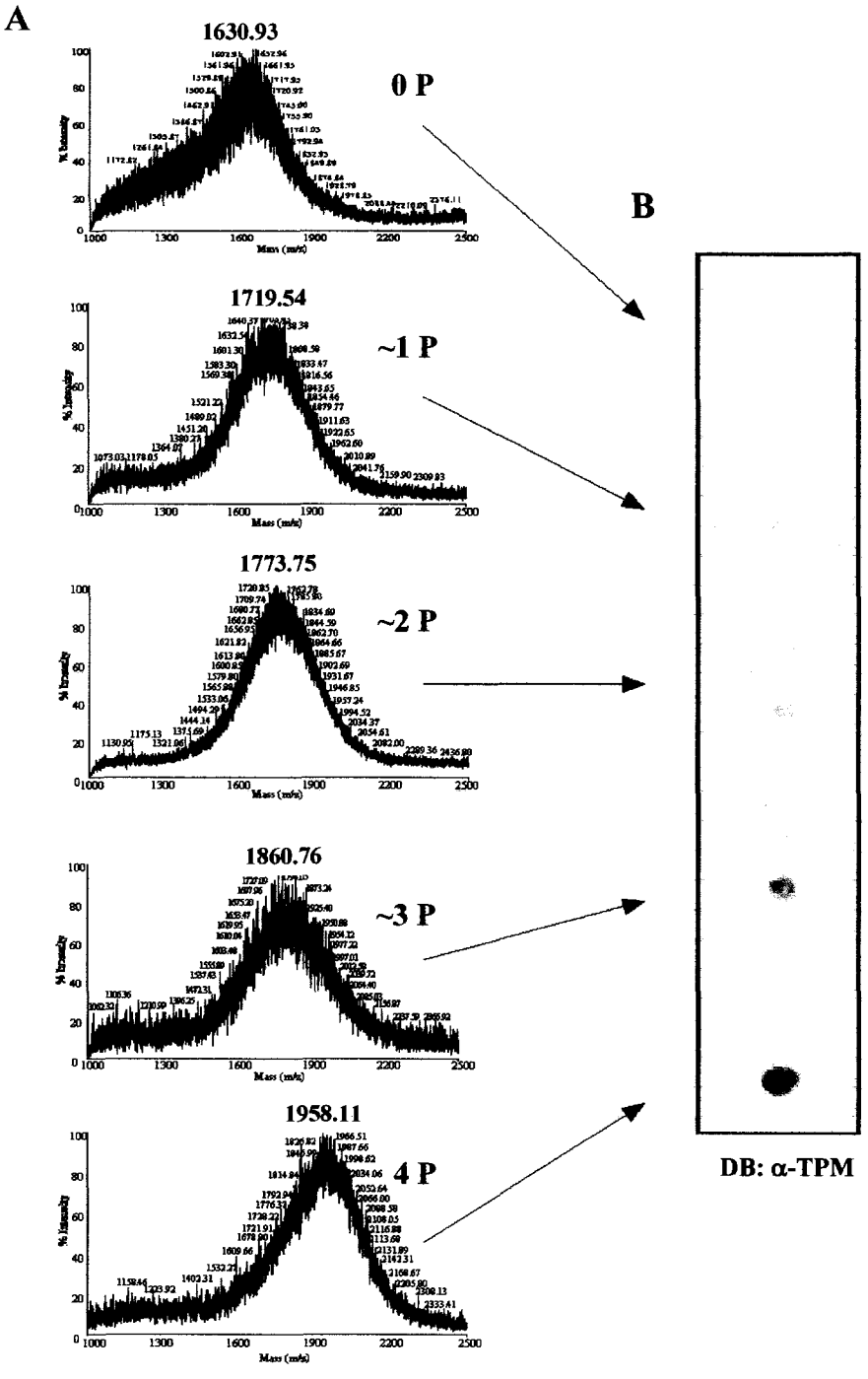

Figure 3.1- Analysis of Anti-TPM Specificity. **(A)** The reconstituted synthetic TPM phosphopeptide library was incubated with 2 units of CIAP for 5 min., 90 min., and 120 min. to generate phosphopeptide libraries with ~3, ~2, and ~1 phosphate group(s), respectively. The non-phosphopeptide library and the TPM phosphopeptide library were used to represent peptides that have 0 and 4 phosphate groups, respectively. The reactions were quenched with 5% formic acid. The libraries were all analysed by MALDI-TOF mass spectrometry for the loss of phosphate groups (~80 m/z). **(B)** Dot blot (DB) analysis of the peptide libraries was conducted with the TPM phosphoantibody. This figure is representative of three different experiments.

with endogenous, wild-type β-catenin and Myc-β-catenin ΔTPM, respectively (Figure 3.2A). The mutant form of β-catenin migrates slightly slower than does wild-type β-catenin, due to the addition of the Myc epitope tag. The anti-TPM immunoblot revealed reactivity with only wild-type β-catenin (Figure 3.2B) and not with the TPM mutant, indicating that the antibody specifically recognizes proteins phosphorylated at a TPM. This also conveyed that the TPM phosphoantibody reacted with β-catenin at the TPM and not at any other position along the protein. The TPM phosphoantibody was also reactive with an array of proteins across a wide molecular weight range, with each band representing a potential TPM-containing protein. The anti-HA immunoblot (Figure 3.2C) was performed to ensure equivalent exogenous expression of HA-GSK-3β (S9A). The results obtained also indicate the ability of the TPM phosphoantibody to function within immunoblot experiments.

3.2 Identification of Putative TPM-Containing Proteins

3.2.1 Phosphatase and Proteasome Inhibition Enables TPM Phosphoantibody Recognition of Potential TPM Proteins

In order to observe the cellular profile of TPM-containing proteins, we performed an anti-TPM immunoblot analysis of whole cell lysates isolated from HEK 293 cells. Putative TPM proteins were identified based on their reactivity with the TPM phosphoantibody and by their responsiveness to phosphatase and proteasome inhibition. Cells were pre-treated with Calyculin A, a potent Ser/Thr phosphatase inhibitor, to increase the stoichiometry of phosphorylated proteins. MG-132 (Carbobenzoxy-L-leucyl-L-leucyl-L-leucinal), a potent proteasome inhibitor, was also applied to cells to prevent the proteasome-mediated degradation of ubiquitin-conjugated, phosphorylated TPM-containing proteins. The anti-TPM immunoblot of untreated whole cell lysates

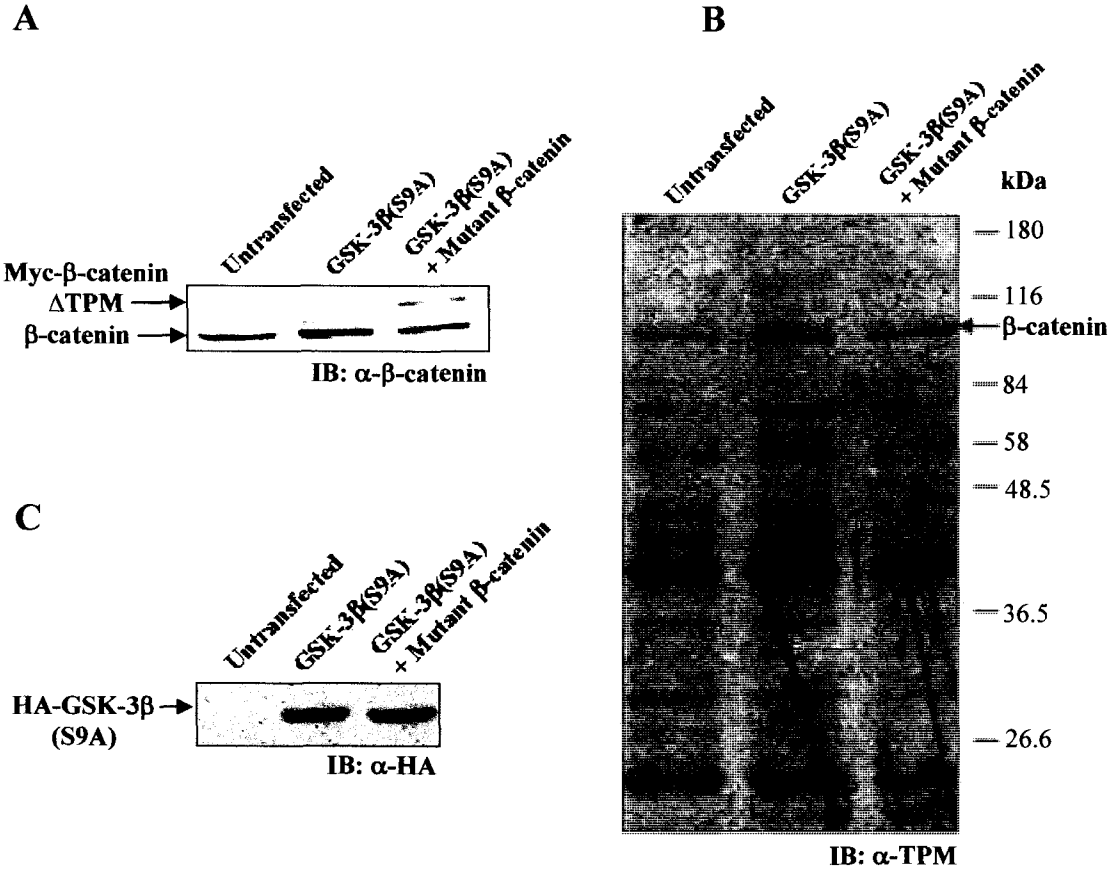

Figure 3.2- Mutation of the β-catenin TPM Abolishes Its Recognition by the TPM Phosphoantibody. HEK 293 cells were left untransfected or were transfected with HA-GSK-3β (S9A) alone or co-transfected with HA-GSK-3β (S9A) and Myc-β-catenin ΔTPM. Cell lysates were resolved by SDS/PAGE and immunoblotted (IB) with **(A)** anti-β-catenin, **(B)** anti-TPM, and **(C)** anti-HA. The positions of the molecular weight markers (in kDa) along the anti-TPM immunoblot are as indicated. These results are representative of two separate experiments.

revealed numerous immunoreactive protein bands (Figure 3.3A; *upper panel*). Importantly, a number of these anti-TPM reactive proteins (110 kDa, 100 kDa, 90 kDa, 75 kDa, 65 kDa, 60 kDa, 45 kDa, 40 kDa, and 35 kDa) exhibited increased intensity with proteasome and phosphatase inhibitor treatment. An assay of the actin levels, conducted via anti-actin immunoblot, proved that the intensity differences between the untreated and treated lysates on the anti-TPM immunoblot were not the result of unequal protein loading (Figure 3.3A; *lower panel*).

3.2.2 Immunoblot and Bioinformatic Analyses Reveal TAZ and KLF7 as Putative TPM Proteins

Bioinformatic sequence analysis of the human SwissProt database with an ambiguous form of the TPM sequence (DS/TGXXS/TXXXS/TXXXS/T) identified approximately 30 genes encoding putative TPM-containing proteins (Appendix 1). Interestingly, examination of these potential TPM proteins revealed two proteins, Transcriptional co-activator with PDZ-binding motif (TAZ) and Krüppel-like factor 7 (KLF7), with intriguing similarities to β-catenin. Since, both TAZ and KLF7, like β-catenin, function as transcriptional mediators in the regulation of processes, such as cell differentiation and development, and the TPMs of all three proteins are located in their extreme N-termini, we questioned whether endogenous TAZ and/or KLF7 could be aligned with a TPM-reactive band within Figure 3.3A. Immunoblot analyses of the same untreated and treated HEK 293 cell lysates with anti-TAZ and anti-KLF7 enabled the alignment of endogenous TAZ and KLF7 with two predominant, anti-TPM-reactive bands at 65 kDa (p65) and 40 kDa (p40), respectively (Figure 3.3B).

Alignment of the amino acid sequences of human TAZ (Accession No.: NP_056287), KLF7 (Accession No.: CAG46909), and β-catenin (Accession No.: CAA61107), presented in Figure 3.4, highlights the presence of the TPM in the N-

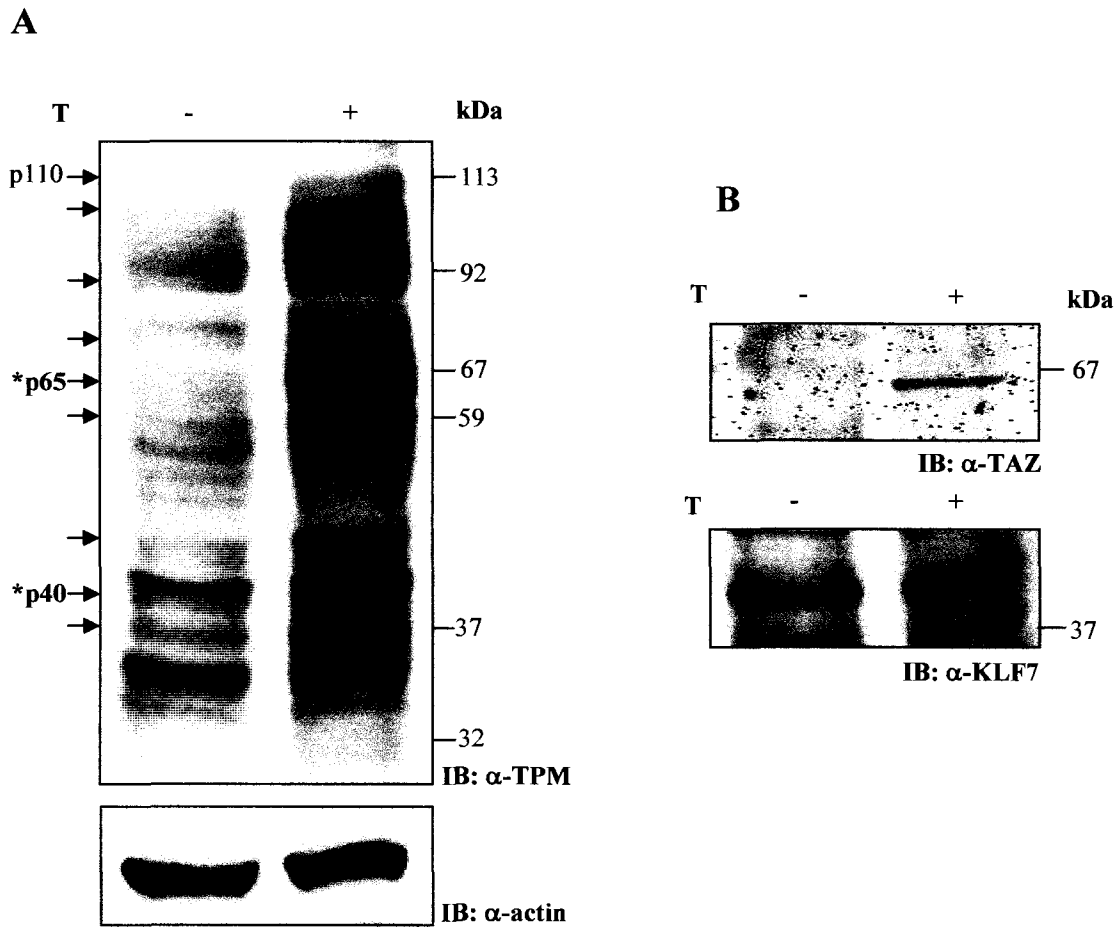

Figure 3.3- Identification of Putative TPM-Containing Proteins. HEK 293 cells were untreated (-) or treated (+) ~48 h after being seeded. Treatment (T) involved a 1 h incubation with 10 μM MG-132 and 100 nM Calyculin A. Equal amounts of protein, as measured by the Bradford method, were resolved through SDS/PAGE and immunoblotted (IB) with **(A)** anti-TPM (*upper panel*). Potential TPM proteins are indicated with arrows. β-catenin (p110) and the putative TPM proteins, TAZ (p65) and KLF7 (p40) are represented by Protein (p) followed by their approximate molecular weights. An anti-actin immunoblot (*lower panel*) was conducted to ensure equal protein loading. **(B)** Immunoblot analyses of the same lysates with anti-TAZ (*upper panel*) and anti-KLF7 (*lower panel*) were aligned with the anti-TPM immunoblot. Molecular weight markers (in kDa) are indicated. These results are representative of three experiments.

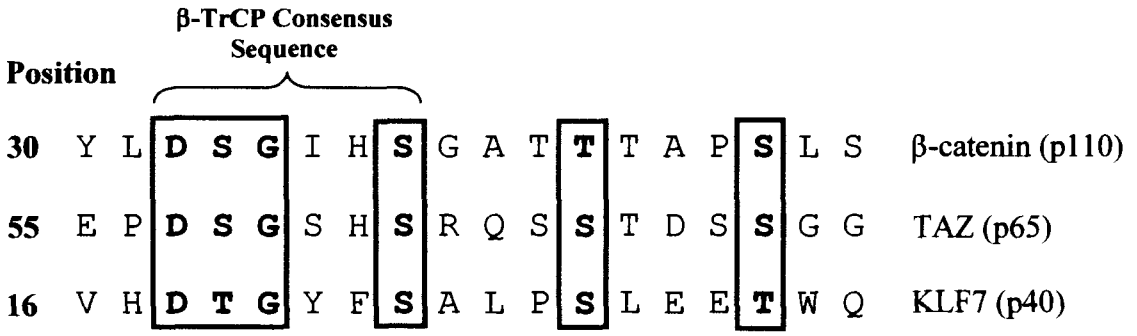

Figure 3.4- TAZ and KLF7 are Putative TPM-Containing Proteins. TAZ and KLF7, the putative TPM-containing proteins with approximate molecular weights of 65 kDa and 40 kDa, respectively, were aligned with β-catenin, the only TPM protein reported to date. The presence of the TPM is highlighted in all three proteins. The common β-TrCP recognition site (DS/TGXXS) between β-catenin, TAZ, and KLF7 is also shown. The amino acid position at which the alignment was initiated is indicated at left.

terminal region of each of these proteins. The spacing of the phosphorylation sites, constituting the β-catenin TPM, is also maintained within the putative TPM sequences of TAZ and KLF7. Moreover, both TAZ and KLF7 contain consensus β-TrCP recognition sequences (DS/TGXXS) within the context of their TPMs, similar to that observed in β-catenin, which is responsible for its ubiquitin-mediated proteasomal degradation [18,19].

3.2.3 TAZ and KLF7 React with the TPM Phosphoantibody

To facilitate further investigation of TAZ and KLF7 as putative TPM proteins, full-length human *taz* cDNA was subcloned into the pFLAG-CMV-2 vector, generating an N-terminally, FLAG-tagged *taz* construct. pCS2+MT/KLF7, which encodes N-terminally, Myc(x6) epitope-tagged KLF7, was kindly provided by Dr. L. Lei (Arizona State University). As a means of confirming our identifications of TAZ and KLF7 as TPM-containing proteins, we examined their reactivity with the TPM phosphoantibody.

Firstly, FLAG-TAZ was over-expressed in HEK 293 cells, treated with Calyculin A and/or MG-132 to enrich for TPM-modified FLAG-TAZ, and subsequently subjected to anti-FLAG immunoprecipitation. Interestingly, anti-FLAG immunoblot analysis of the cleared cell lysates revealed that, upon treatment, FLAG-TAZ undergoes a significant upward mobility shift, which indicates that TAZ is likely subject to post-translational modification (Figure 3.5; *lower panel*). This slower migrating species of FLAG-TAZ was observed with Calyculin A treatment, in the absence of MG-132, suggesting that TAZ is a heavily phosphorylated protein. Both of the differentially modified forms of FLAG-TAZ were immunoprecipitated, with the faster migrating, unmodified TAZ co-migrating with the IgG heavy chain (Figure 3.5; *middle panel*). Immunoblot analysis of the anti-FLAG immune complexes revealed that the slower migrating, post-translationally modified form of FLAG-TAZ was detected by the TPM phosphoantibody, indicating the presence of a putative TPM within TAZ (Figure 3.5; *upper panel*).

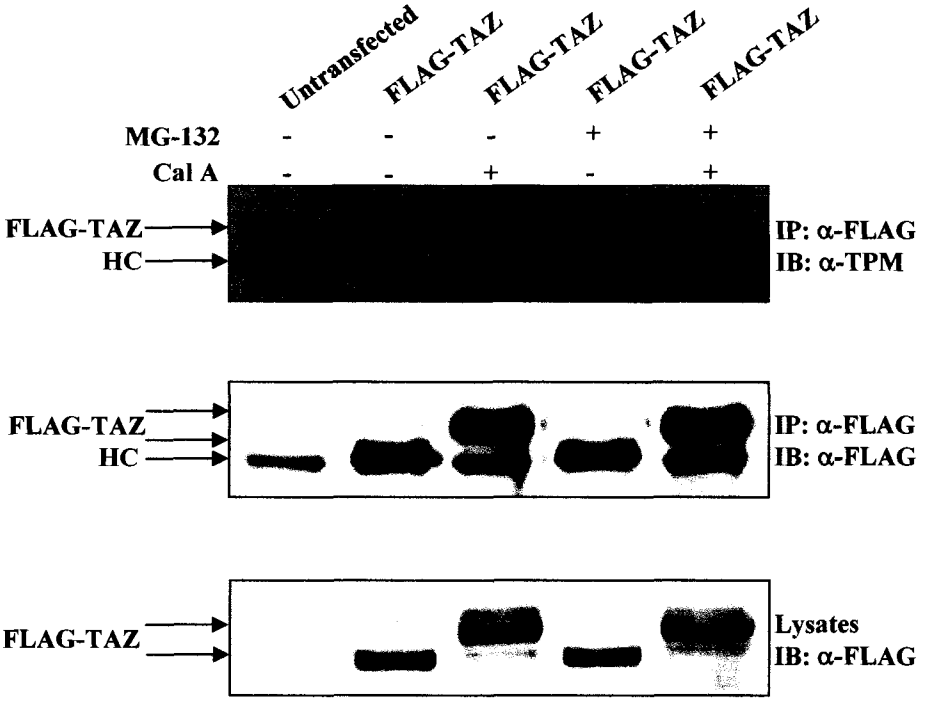

Figure 3.5- FLAG-TAZ is Recognized by the TPM Phosphoantibody. HEK 293 cells were untransfected or transiently transfected with FLAG-TAZ. Approximately 24 h post-transfection, cells were treated with (+) or without (-) MG-132 (10 μM) and/or Calyculin A (100 nM) for 1 h. Following lysis, cleared cell lysates were subjected to anti-FLAG immunoprecipitation (IP). The immune complexes were resolved by SDS/PAGE and immunoblotted (IB) with anti-TPM (*upper panel*) and anti-FLAG (*middle panel*). Cleared cell lysates were also separated by SDS/PAGE and immunoblotted with anti-FLAG (*lower panel*). In the anti-FLAG immunoblots, the two arrows from the FLAG-TAZ label indicate its differentially modified forms. Where required, the IgG heavy chain is indicated (HC).

Notably, the unmodified, faster migrating form of FLAG-TAZ did not react with the TPM phosphoantibody; thus, it is probable that the TPM is not phosphorylated in this form of TAZ.

The reactivity of KLF7 with the TPM phosphoantibody was assayed in the same manner as was that of TAZ. Myc-KLF7 was transiently transfected in HEK 293 cells, treated with Calyculin A and/or MG-132, and isolated via anti-c-Myc immunoprecipitation. Immunoblotting of the cell lysates and anti-c-Myc immune complexes with the c-Myc antibody shows that Myc-KLF7 also exhibits a mobility shift with Calyculin A treatment, indicating its potential phosphorylation (Figure 3.6; *middle and lower panels*). Unlike TAZ, treated KLF7 produces an upward smearing pattern, which is suggestive of the presence of higher molecular weight, ubiquitinated forms of KLF7. Immunoblot analysis of the immune complexes depicted the reactivity of Myc-KLF7 with the TPM phosphoantibody, indicating KLF7 as a putative TPM protein (Figure 3.6; *upper panel*). It was again observed that anti-TPM recognition was dependent upon phosphatase inhibition, as only Myc-KLF7, previously treated with Calyculin A, was detected. This indicates that TPM phosphorylation of both TAZ and KLF7 is likely to be regulated by phosphatases, whose identities remain to be determined.

3.2.4 Mass Spectrometric Analysis of TAZ Validates the Presence of its TPM

In order to unambiguously confirm that the TPM of TAZ is phosphorylated, we analysed over-expressed FLAG-TAZ via MALDI-TOF mass spectrometry. HEK 293 lysates, over-expressing FLAG-TAZ, were either untreated or treated with Calyculin A and MG-132 and then immunoprecipitated with anti-FLAG-conjugated agarose. Following extensive washing, the proteins were resolved by SDS/PAGE and subsequently visualized via Coomassie stain. A prominent Coomassie-stained band was

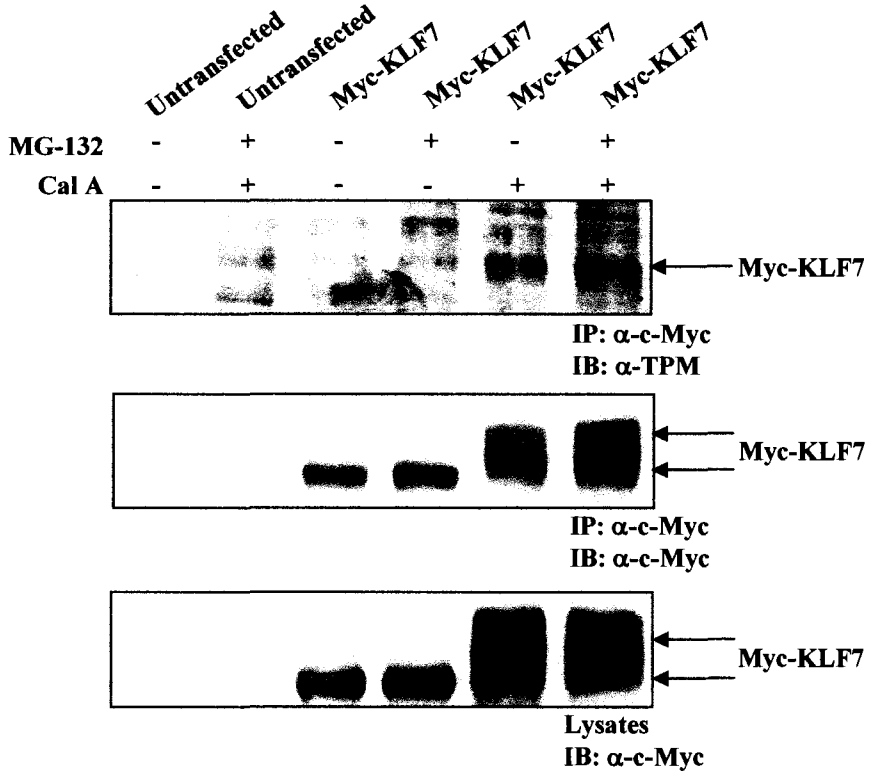

Figure 3.6- The TPM Phosphoantibody Reacts with Myc-KLF7. HEK 293 cells were either untransfected or were transiently transfected with Myc-KLF7. Approximately 24 h post-transfection, cells were untreated (-) or treated (+) with MG-132 (10 μM) and/or Calyculin A (100 nM) for 1 h. The cells were then lysed and the lysates were subjected to anti-c-Myc immunoprecipitation (IP). The resulting immune complexes were resolved by SDS/PAGE and immunoblotted (IB) with anti-TPM (*upper panel*) and anti-c-Myc (*middle panel*). Cleared cell lysates were also separated by SDS/PAGE and immunoblotted with anti-c-Myc (*lower panel*). The double arrows indicate the differentially modified forms of Myc-KLF7. These results were representative of three separate experiments.

observed at approximately 65 kDa in the treated cell lysate (Figure 3.7A). Alignment of the stained gel with an anti-FLAG immunoblot of the immunoprecipitant material confirmed the identity of this band as the highly modified form of FLAG-TAZ (Figure 3.7B). Unmodified FLAG-TAZ, isolated from the untreated cell lysate, co-migrated with the heavy chain of the mouse IgG.

The protein band corresponding to modified FLAG-TAZ was excised and subjected to in-gel trypsin digestion. The tryptic peptides were extracted from the gel piece, concentrated by speed vacuuming, and desalted with microtips containing C18 resin. The resultant tryptic peptides were then analysed by MALDI-TOF mass spectrometry. Analysis of the tryptic peptide mass fingerprint revealed a number of peptides with masses matching those predicted by the *in silico* digestion of TAZ conducted by the MS-Digest command of the Protein Prospector software (UCSF), confirming the identity of the excised protein as TAZ (Figure 3.8A). The TAZ tryptic peptides detected by MALDI-MS analysis are highlighted on the mass fingerprint by their experimentally determined m/z ratios. Importantly, we identified a tryptic peptide with a mass corresponding to that predicted for a tetra-phosphorylated peptide containing the TAZ TPM (2643.18 m/z), (K)^{55}EPDSGSHSRQSSTDSSGGHPGPR^{77}(L). This peptide contains one missed cleavage site, indicated by the underlined arginine (R) residue, which may be due to interference from the multiple phosphate groups on this peptide.

We further analysed the 2643.18 m/z peptide by tandem mass spectrometry (MS/MS) to obtain information regarding its amino acid sequence and phosphorylation status, as well as to attempt to locate the exact sites of phosphorylation. Post-source decay (PSD) MS/MS analysis of this peptide revealed phosphorylation on four serine or threonine residues, as demonstrated by four consecutive losses of approximately 98 m/z from the precursor ion, 2642.5 m/z (Figure 3.8B). A neutral loss of 98 m/z indicates the loss of phosphoric acid (H_3PO_4) from a phosphorylated serine or threonine residue. The

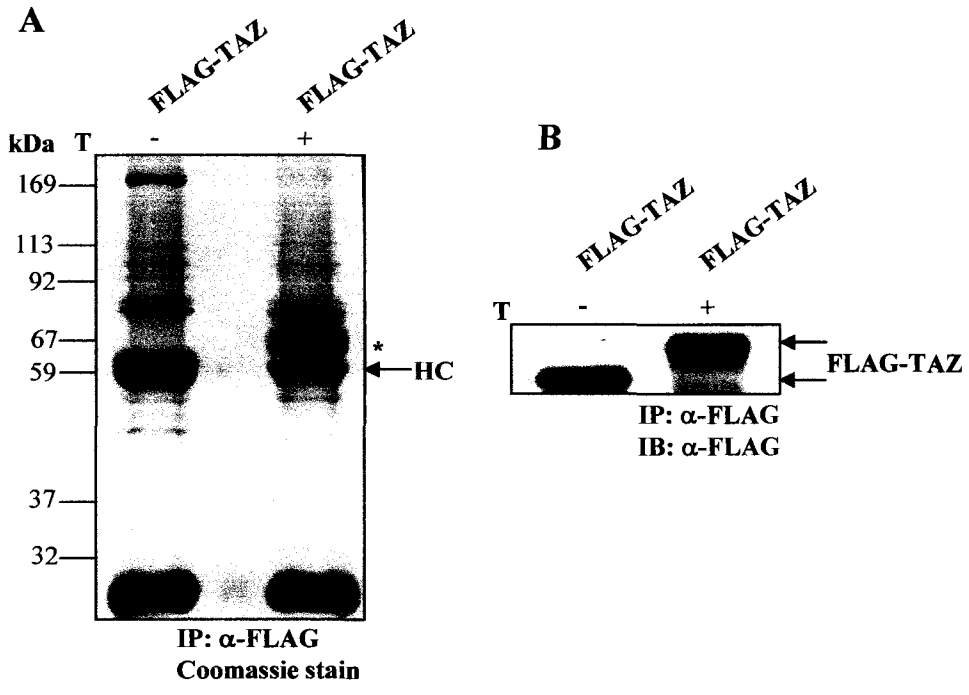

Figure 3.7- Large-Scale Anti-FLAG Immunoprecipitation. HEK 293 cells (~12x10^6) were transiently transfected with FLAG-TAZ. The cells were either untreated (-) or treated (+) with 10 μM MG-132 and 100 nM Calyculin A, collectively represented as T, for 1 h. Following cell lysis, the lysates underwent anti-FLAG immunoprecipitation (IP). The immune complexes were resolved by SDS/PAGE and proteins were visualized by **(A)** Coomassie staining or were **(B)** transferred and immunoblotted with anti-FLAG. The Coomassie stained gel was aligned with the anti-FLAG immunoblot to verify the identity of the treated FLAG-TAZ band, which is indicated with an asterisk (*). This band was excised from the polyacrylamide gel and subsequently prepared for in-gel trypsin digestion. Molecular weight markers (in kDa) are shown to the left of the Coomassie-stained gel. The IgG heavy chain is indicated (HC).

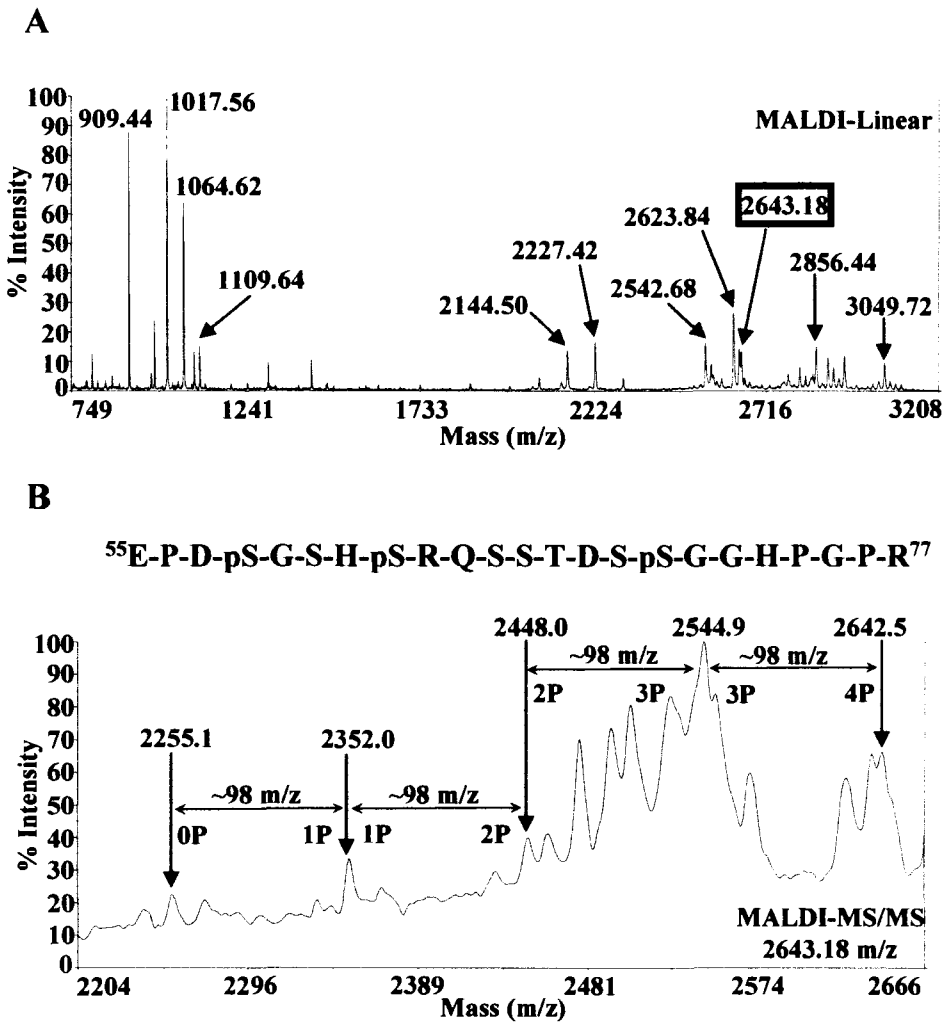

Figure 3.8- Mass Spectrometric Analysis of FLAG-TAZ Reveals a Tetra-Phosphorylated Tryptic Peptide Ion Presumed to Contain the TAZ TPM. The Coomassie stained band corresponding to modified FLAG-TAZ was excised and subjected to in-gel trypsin digestion. The resulting tryptic peptides were concentrated, desalted, and then analyzed by MALDI-TOF mass spectrometry. **(A)** MALDI-TOF peptide mass fingerprint of FLAG-TAZ. Ions matching those predicted for TAZ by MS-Digest are indicated by their experimental m/z ratios. The peptide ion (2643.18 m/z), predicted to contain the TAZ TPM, is highlighted. MALDI-MS/MS was performed on the 2643.18 m/z peptide ion. **(B)** Portion of the MALDI-MS/MS spectrum of 2643.18 m/z. The presence of 4 phosphate groups on this peptide was confirmed by four H_3PO_4 eliminations (loss of 98 m/z) from the precursor ion (2642.5 m/z).

MS/MS data also revealed a number of fragment ions matching the TPM tryptic peptide (Figure 3.9A,B). To verify the occurrence of phosphorylation at each of the predicted TAZ TPM sites, we closely examined the fragment ions detected through CID. The detection of a fragment ion at 508.78 m/z confirmed Ser58 as a phosphorylation site on this peptide, for this mass corresponds to a phosphorylated b_4 ion. Based upon the identification of the b_6 (653.38 m/z) and b_9 - 98 m/z (1015.07 m/z) fragment ions, we were able to rule out Ser60 as a phosphorylation site, while proving that Ser62 does indeed undergo phosphorylation. The presence of a fragment ion at 844.80 m/z, which matches a theoretically determined y_8 ion containing a single phosphate group, verified the phosphorylation of Ser70.

Analysis of the detected fragment ions enabled the unambiguous identification of three of the four phosphorylation sites as Ser58, Ser62, and Ser70. Since these three residues are those that were originally hypothesized to be phosphorylated as part of the TPM, their identification bolsters our claim that TAZ is a novel TPM-containing protein. Although, we were unable to unambiguously determine the location of the fourth phosphorylation site, the presence of fragment ions corresponding to b_9 - 98 m/z and y_{11} – 98 m/z directed our assignment of this phosphorylation site to either Ser65 or Ser66. Interestingly, Ser66 is located at the hypothesized third phosphorylation site of the putative TAZ TPM; thus, the possibility of a phosphorylation event at this site serves to strengthen our confidence in the existence of a veritable TAZ TPM. Our inability to delineate the exact location of this final phosphorylation site is likely due to signal suppression, resulting from the co-elution of at least two other peptides ions with the 2643.18 m/z peptide.

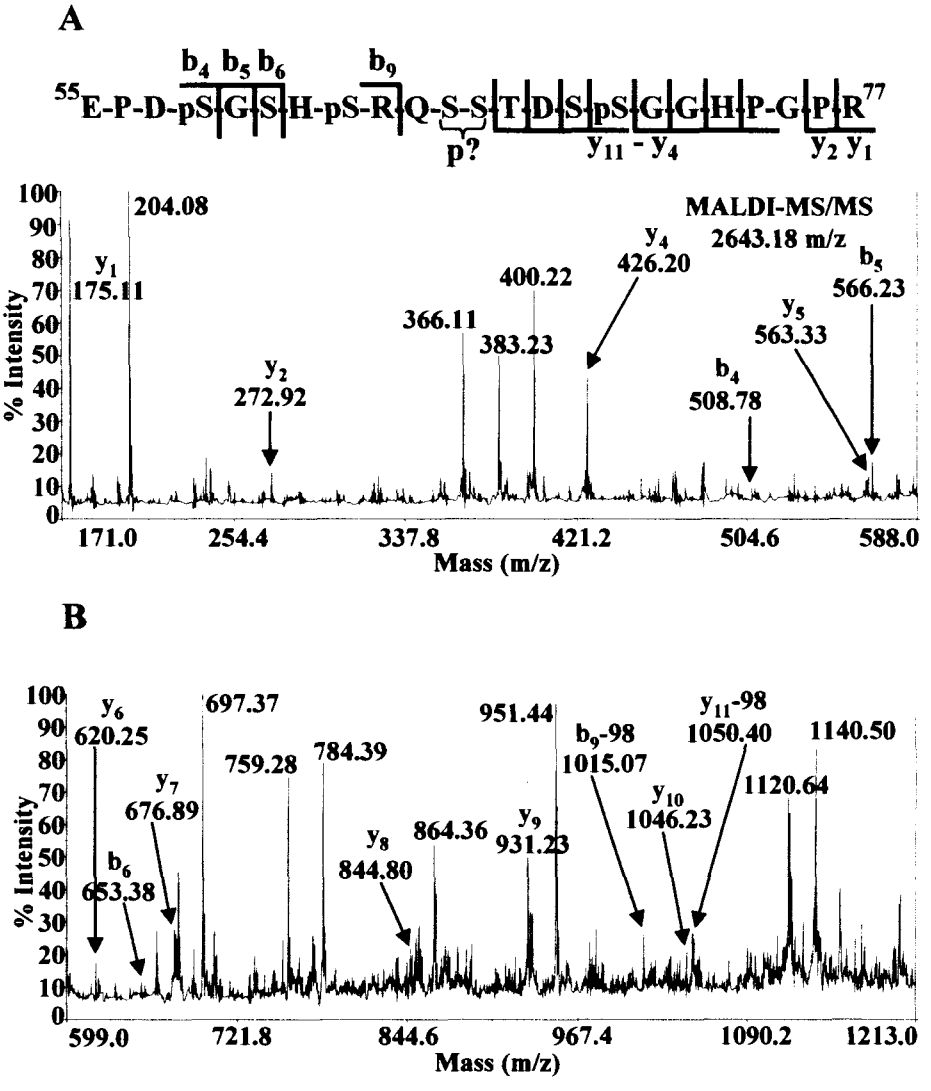

Figure 3.9- Localization of TAZ TPM Phosphorylation Sites by Tandem Mass Spectrometry. (A, B) Different portions of the MALDI-MS/MS spectrum of 2643.18 m/z. The fragment ions with m/z ratios matching those predicted by MS-Product for b and y ions, including b and y ions with a loss of H_3PO_4 (98 m/z), are labelled. The detected fragment ions verified the peptide to be that containing the TAZ TPM (shown in **(A)**). Three phosphorylation sites were identified at Ser58, Ser62, and Ser70 and are indicated by a small p before the Ser residue. The location of the fourth phosphorylation site remains uncertain, the possible sites are underlined (Ser66 or Ser67) and highlighted with a question mark (?).

3.3 Interaction of TPM-Containing Proteins with the F-box Protein, β-TrCP

3.3.1 Mutation of the KLF7 TPM Inhibits β-TrCP Binding

Phosphorylation of β-catenin at its TPM has been shown to facilitate its interaction with the F-box/WD40-repeat protein, β-TrCP [19]. Since, like β-catenin, KLF7 also contains a β-TrCP recognition sequence within its putative TPM (Figure 3.4), we wanted to investigate whether KLF7 could also associate with β-TrCP. To examine this potential interaction, HEK 293 cells were transiently co-transfected with Myc-KLF7 and FLAG-β-TrCP and either untreated or treated with proteasome and phosphatase inhibitors to increase the stoichiometry of phosphorylated KLF7. Following cell lysis, the cleared cell lysates were subjected to immunoprecipitation with anti-c-Myc-conjugated agarose to isolate exogenous Myc-KLF7, along with any interacting proteins. Anti-FLAG immunoblot analysis of these immune complexes, resolved by SDS/PAGE, revealed that FLAG-β-TrCP co-immunoprecipitated with Myc-KLF7 (Figure 3.10; *uppermost panel*). Importantly, FLAG-β-TrCP was only found to associate with Myc-KLF7 under treatment conditions, indicating the phosphorylation-dependent nature of the β-TrCP-KLF7 interaction, akin to that observed between β-TrCP and β-catenin [19].

In order to determine whether β-TrCP was interacting with KLF7 through recognition of the consensus β-TrCP binding site located within the KLF7 TPM, we generated a KLF7 TPM mutant, which harbours alanine substitutions at both Thr19 and Ser23 (KLF7 STDM; KLF7 Serine Threonine Double Mutant). As in the case of β-catenin, we believe that ordered phosphorylation of KLF7 at its TPM, culminating in the phosphorylation of Ser23 and Thr19, which exist within the β-TrCP consensus sequence, mediates β-TrCP binding. Co-immunoprecipitation analysis revealed that the TPM mutant of Myc-KLF7 could not associate with FLAG-β-TrCP, both in the presence or absence of phosphatase and proteasome inhibition (Figure 3.10; *uppermost panel*). Its

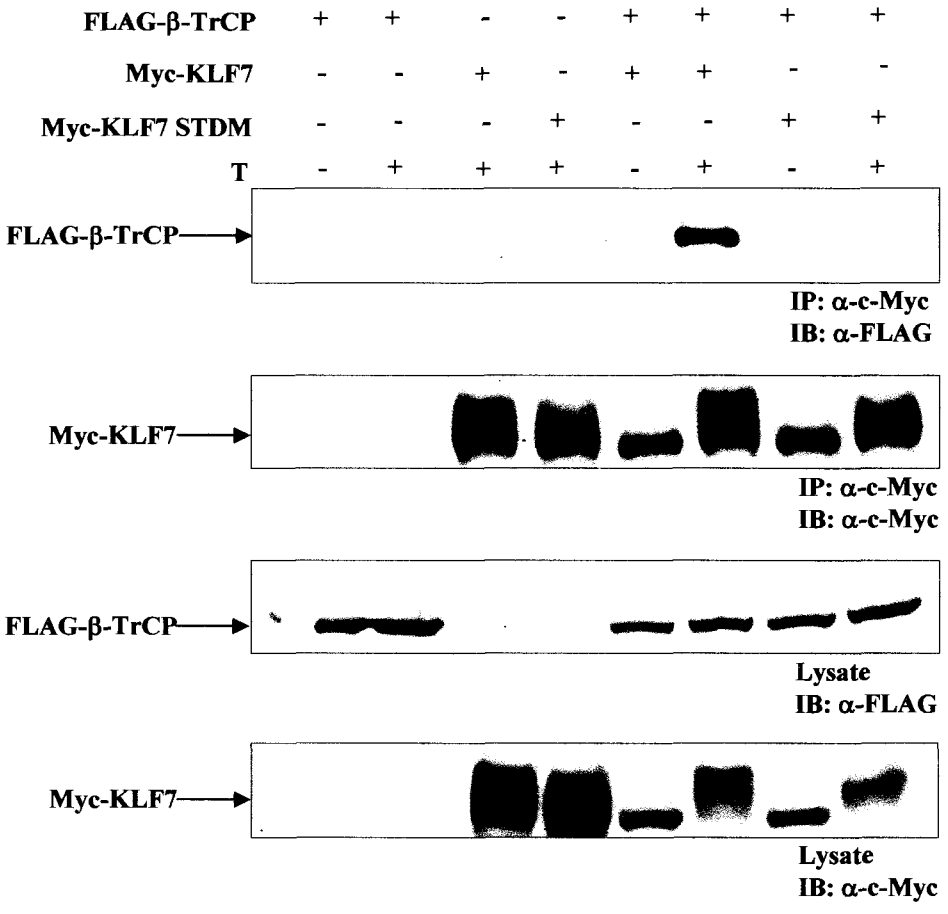

Figure 3.10- FLAG-β-TrCP Binds the KLF7 TPM. HEK 293 cells were transiently co-transfected with FLAG-β-TrCP alongside pFLAG-CMV-2 (empty vector), Myc-KLF7, or Myc-KLF7 STDM, as indicated by +/-. Twenty-four hours post-transfection, cells were either untreated (-) or treated (+) with MG-132 (10 μM) and Calyculin A (100 nM). Following 1 h treatment (T), the cells were lysed and subjected to anti-c-Myc immunoprecipitation. The immune complexes were washed, resolved by SDS/PAGE, and immunoblotted with anti-FLAG (*uppermost panel*) to determine whether FLAG-β-TrCP was co-immunoprecipitated and anti-c-Myc (*second upper panel*). The cell lysates were also resolved by SDS/PAGE and immunoblotted with anti-FLAG (*second lower panel*) and anti-c-Myc (*lowermost panel*). These results are representative of three separate experiments.

inability to bind the KLF7 TPM mutant indicates that β-TrCP interacts with KLF7 via phosphorylation-dependent recognition of the β-TrCP consensus sequence. It is worthwhile to note that anti-c-Myc immunoblot analysis of the cell lysates reveals two anti-c-Myc reactive bands in cells over-expressing Myc-KLF7 (Figure 3.10; *lowermost panel*). Interestingly, the slower migrating band is absent in the extracts from cells over-expressing the KLF7 TPM mutant, KLF7 STDM. This band likely represents a higher phosphorylated form of KLF7, which is abolished with the alanine mutations of Thr19 and Ser23, providing evidence that the aforementioned amino acid residues are indeed TPM phosphorylation sites.

3.3.2 The Function of the β-TrCP Consensus Site within the TAZ TPM Remains Unknown

Recent studies conducted by Tian *et al.*, unveiled TAZ as a binding partner of β-TrCP. The association of TAZ with β-TrCP, within the context of an $SCF^{\beta\text{-}TrCP}$ E3 ligase complex, was shown to facilitate the degradation of polycystin 2 (PC2), a calcium-permeable cation channel protein, responsible for regulating the entry and release of calcium from the endoplasmic reticulum (ER) [41]. Within this study, Tian *et al.* tested the function of two putative β-TrCP consensus sequences within mouse TAZ: $DS^{58}GSHS^{62}$ and $S^{302}REQS^{306}TDS^{309}GLG$. The first β-TrCP recognition sequence is contained within the TPM, whereas the second is in the remote C-terminal region. Mutational analyses, followed by co-immunoprecipitation, revealed the C-terminal β-TrCP recognition sequence as necessary for the TAZ/β-TrCP interaction, whereas, serine to alanine substitutions at the TPM consensus sequence appeared to have no effect on the binding of β-TrCP to TAZ [41].

The above study did not employ phosphatase or proteasome inhibitors in their analysis; therefore, we assessed the effect these treatments would have on the binding of

β-TrCP to TAZ. We generated the two TAZ mutants employed by Tian *et al.*, TAZ ΔC^{t}DSG and TAZ ΔTPM/ΔC^{t}DSG, which contain an alanine substitution at Ser314 of wild-type human TAZ (Ser309 of mouse TAZ) and of the human TAZ TPM mutant, respectively. The TAZ TPM mutant (TAZ ΔTPM) features alanine substitutions at Ser58, Ser62, Ser66, and Ser70. We then subcloned TAZ, TAZ ΔTPM, TAZ ΔC^{t}DSG, and TAZ ΔTPM/ΔC^{t}DSG into the pCS2+MT vector, producing N-terminally, Myc-tagged versions of these constructs.

Cells expressing these TAZ variants with FLAG-β-TrCP were treated with MG-132 and Calyculin A and anti-c-Myc immunoprecipitation was conducted to isolate the Myc-tagged TAZ constructs. Anti-FLAG immunoblot analysis demonstrated that the association between β-TrCP and TAZ is dependent upon an intact C-terminal β-TrCP binding site (Figure 3.11; *uppermost panel*), since both Myc-TAZ ΔC^{t}DSG and Myc-TAZ ΔTPM/ΔC^{t}DSG could not interact with FLAG-β-TrCP. Our results agree with those published by Tian *et al.*, as the potential enrichment of TPM-regulated TAZ did not appear to have any bearing on its interaction with β-TrCP, as indicated by the inability of FLAG-β-TrCP to co-immunoprecipitate with Myc-TAZ ΔC^{t}DSG, as well as by the binding of FLAG-β-TrCP to Myc-TAZ ΔTPM. It is interesting to note that the anti-FLAG immunoblot of the immunoprecipitant (Figure 3.11; *second upper panel*) shows the slower migration of TAZ in comparison to that of the TAZ TPM mutant, TAZ ΔTPM. This migratory difference is indicative of the higher phosphorylation status of TAZ, lending further credence to our previous assignments of Ser58, Ser62, Ser70, and potentially Ser66, as the phosphorylation sites of the TAZ TPM.

3.4 Ubiquitination of TAZ and KLF7 is Mediated by their Respective TPMs

Since the phosphorylation-dependent degradation of β-catenin has been shown to involve the ubiquitin-proteasome pathway [18,19], we next set out to determine whether

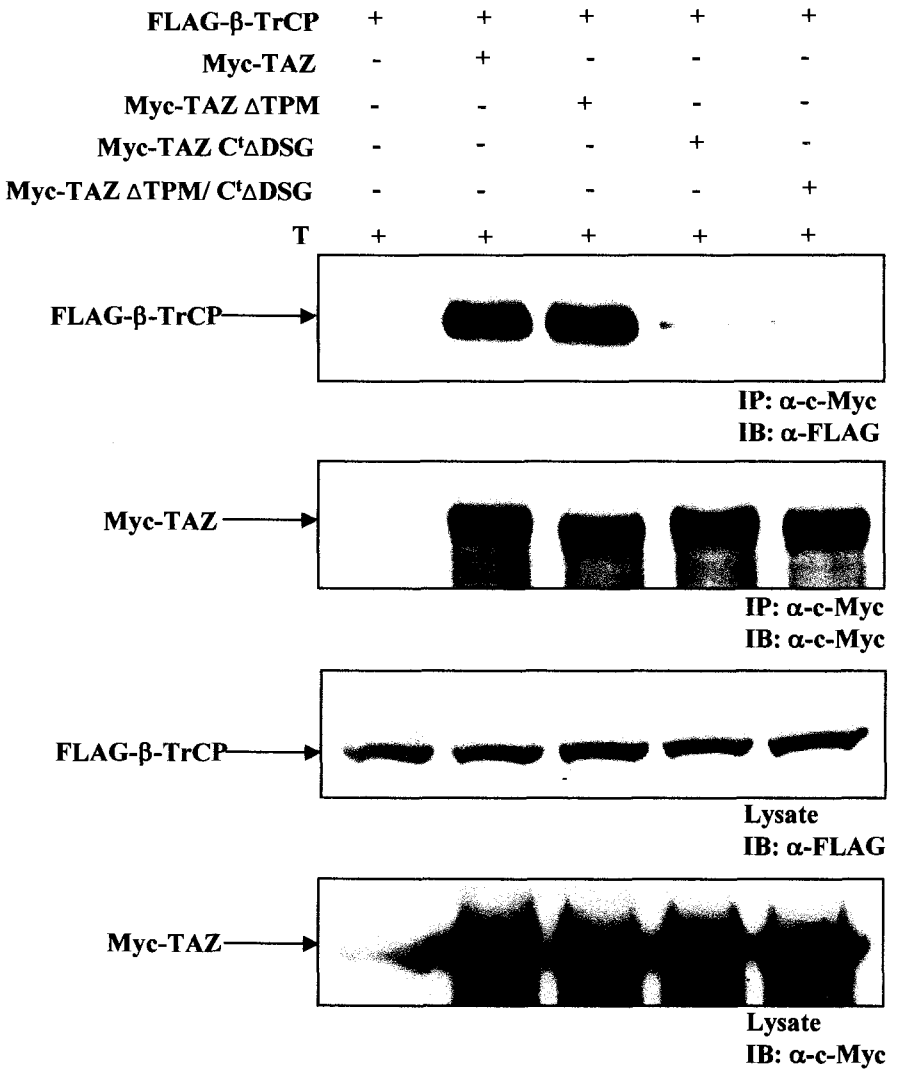

Figure 3.11- Interaction Between β-TrCP and TAZ Does Not Appear to Involve the TAZ TPM. HEK 293 cells were transiently co-transfected with FLAG-β-TrCP and Myc-TAZ, Myc-TAZ ΔTPM, Myc-TAZ C^{t}ΔDSG, or Myc-TAZ ΔTPM/ C^{t}ΔDSG, as shown by the +/-. Twenty-fours post-transfection, cells were treated (+) with 10 μM MG-132 and 100 nM Calyculin A. Following the 1 h treatment, cells were lysed and lysates were incubated with anti-c-Myc agarose. The immune complexes were resolved by SDS/PAGE and immunoblotted with anti-FLAG (*uppermost panel*) and anti-c-Myc (*second upper panel*). The lysates were also separated by SDS/PAGE and immunoblotted with anti-FLAG (*second lower panel*) and anti-c-Myc (*lowermost panel*). These results are representative of three separate experiments.

tetra-phosphorylation at the TPM induces the ubiquitination of both TAZ and KLF7. In order to assess the ubiquitination state of KLF7, HEK 293 cells, over-expressing Myc-KLF7, were either untreated or treated with phosphatase (Calyculin A) and proteasome (MG-132) inhibitors to increase the stoichiometry of proteins that are phosphorylated and/or ubiquitinated, in effect increasing the level of proteins ubiquitinated in response to phosphorylation. Following treatment and cell lysis, the lysates were incubated with anti-c-Myc-conjugated agarose, enabling the isolation of Myc-KLF7. Anti-ubiquitin immunoblot analysis displayed prominent banding solely for anti-KLF7 immune complexes treated with phosphatase and proteasome inhibitors, indicating that KLF7 may be regulated by ubiquitination (Figure 3.12; *upper panel*).

To further characterize the putative ubiquitination of KLF7, we investigated whether the TPM affects its ubiquitination status. HEK 293 cells, co-expressing HA-tagged ubiquitin alongside Myc-KLF7 or Myc-KLF7 STDM, were treated with phosphatase and proteasome inhibitors, since the potential ubiquitination of KLF7 was detected solely under treatment conditions (Figure 3.12; *upper panel*). Exogenously expressed KLF7 was isolated via anti-c-Myc immunoprecipitation. Anti-HA immunoblot analysis of the immune complexes revealed a detectable difference in the amount of HA-ubiquitin present within the extracts containing over-expressed wild-type KLF7 compared to those over-expressing KLF7 STDM, the TPM mutant (Figure 3.13; *upper panel*). These results verify the occurrence of ubiquitin-conjugated proteins within the immunoprecipitants over-expressing Myc-KLF7, while, depicting a lesser degree of HA-ubiquitin adducts in the samples generated from cells over-expressing Myc-KLF7 STDM. Immunoblot analysis of the immunoprecipitants with anti-c-Myc (Figure 3.13; *middle panel*) and of the cell lysates with the HA antibody (Figure 3.13; *lower panel*) demonstrate equal expression levels of the Myc-KLF7 constructs and of the HA-ubiquitin construct between samples. Thus, we suggest that phosphorylation of KLF7 at its TPM

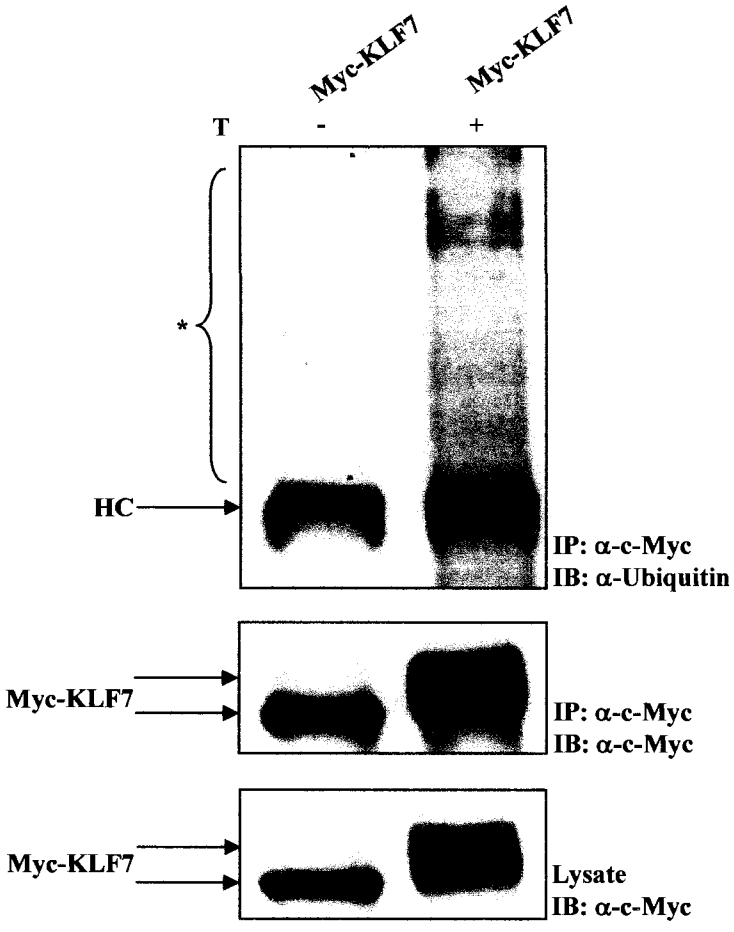

Figure 3.12- KLF7 Undergoes Ubiquitination. HEK 293 cells were transiently transfected with Myc-KLF7. The cells were either untreated (-) or treated (+) approximately 24 h post-transfection with 10 μM MG-132 and 100 nM Calyculin A for 1 h. Following treatment (T), the cells were lysed and the cleared cell lysates were incubated with anti-c-Myc-conjugated agarose. The immune complexes were extensively washed and resolved by SDS/PAGE, as were the cleared cell lysates. Immunoblot analysis was then conducted with anti-ubiqutin (*upper panel*) and anti-c-Myc (*middle, lower panels*). The double arrows indicate the differentially modified forms of Myc- KLF7. Potential higher molecular weight complexes of Myc-KLF7 and ubiquitin are highlighted with a bracket and an asterisk (*). The IgG heavy chain is indicated (HC). These results are representative of three separate experiments.

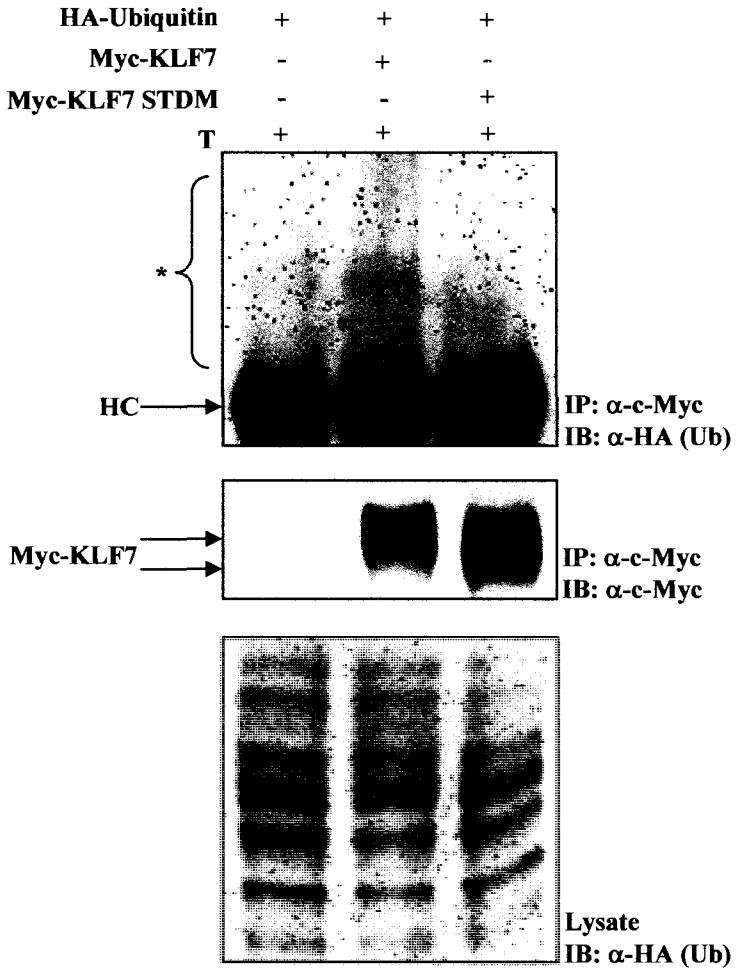

Figure 3.13- The KLF7 TPM is Necessary for Its Ubiquitination. HEK 293 cells were transiently co-transfected with HA-Ubiquitin (Ub) and Myc-KLF7 or Myc-KLF7 STDM, as indicated by the +/-. The cells were treated (T) with 10 μM MG-132 and 100 nM Calyculin A for 1 h approximately 24 h post-transfection. Following cell lysis, cleared lysates were subjected to anti-c-Myc immunoprecipitation. The resulting immune complexes were extensively washed, resolved by SDS/PAGE, and immunoblotted with anti-HA (*upper panel*) and anti-c-Myc (*middle panel*). The lysates were also separated by SDS/PAGE and immunoblotted with anti-HA (*lower panel*) to ensure comparable HA-ubiquitin over-expression between samples. Putative higher molecular weight complexes of Myc-KLF7 and HA-ubiquitin are indicated with an asterisk (*). The double arrows indicate the differentially modified forms of Myc-KLF7. The IgG heavy chain is indicated (HC). These results are representative of two separate experiments.

may be responsible for driving its putative ubiquitination, as the KLF7 TPM mutant appears unable to be ubiquitinated.

We next wanted to assay whether TAZ undergoes ubiquitination in response to phosphorylation at its TPM. HEK 293 cells co-expressing HA-ubiquitin and FLAG-TAZ or FLAG-TAZ SDM, which encodes FLAG-tagged TAZ harbouring serine to alanine mutations at Ser58 and Ser62, were subjected to co-immunoprecipitation analysis. Anti-HA immunoblot analysis of the immune complexes revealed a considerable degree of high-molecular weight, HA-ubiquitin-conjugated species within the extracts containing exogenous TAZ (Figure 3.14; *upper panel*). It is important to note that this extensive ubiquitination is only detected in the presence of proteasome and phosphatase inhibitors, hinting at the probable regulation of TAZ ubiquitination by phosphatases and the proteasome. The detection of HA-ubiquitin-adducts in these immune complexes indicates the presence of ubiquitinated TAZ and/or ubiquitinated binding partners of TAZ. As the extracts containing over-expressed TAZ SDM do not exhibit a significant amount of HA-ubiquitin-conjugated proteins, it is likely that the HA-ubiquitin adducts detected in the FLAG-TAZ immunoprecipitants are those of TAZ conjugated to HA-tagged ubiquitin chains of varying length. The absence of HA-ubiquitin-conjugated FLAG-TAZ SDM illustrates that phosphorylation at the TAZ TPM likely governs the putative ubiquitination of TAZ. An anti-FLAG immunoblot of the immune complexes (Figure 3.14; *middle panel*) and an anti-HA immunoblot of the original cell lysates (Figure 3.14; *lower panel*) demonstrate equal expression levels of FLAG-TAZ and FLAG-TAZ SDM, as well as that of HA-ubiquitin between samples, confirming that the differential ubiquitination can likely be attributed to the difference between the TAZ constructs investigated: an intact TAZ TPM.

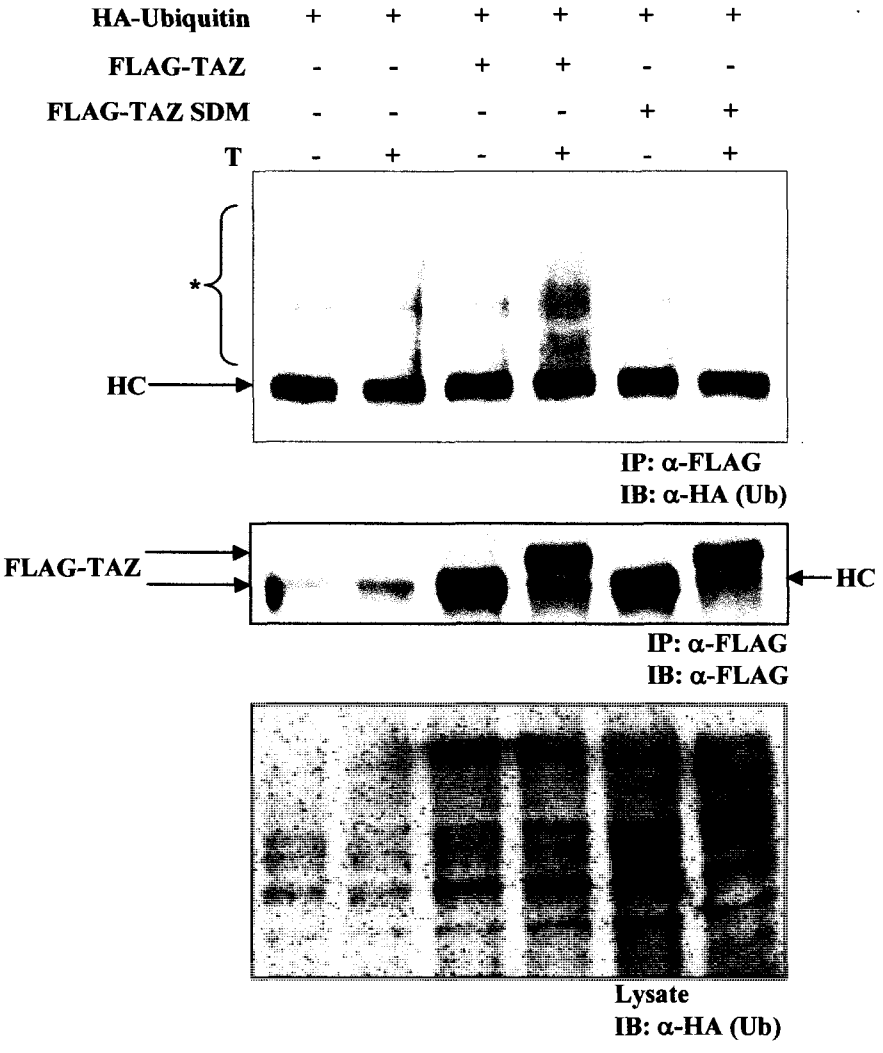

Figure 3.14- Ubiquitination of TAZ Requires an Intact TAZ TPM. HEK 293 cells were co-transfected with HA-ubiquitin (Ub) and FLAG-TAZ or FLAG-TAZ SDM, indicated by +/-. Approximately 24 h post-transfection, cells were untreated (-) or treated (+) with 10 μM MG-132 and 100 nM Calyculin A. Following 1 h treatment (T), cells were lysed and lysates were incubated with anti-FLAG-conjugated agarose. The immune complexes were extensively washed, resolved by SDS/PAGE, and immunoblotted with anti-HA (*upper panel*) and anti-FLAG (*middle panel*). Cell lysates were also separated by SDS/PAGE and immunoblotted with anti-HA (*lower panel*). Potential complexes of FLAG-TAZ and HA-ubiquitin are indicated by an asterisk (*). The double arrows highlight the differentially modified forms of FLAG-TAZ. The IgG heavy chain is indicated (HC). These results are representative of two separate experiments.

3.5 Investigation of the Effect of the TPM on TAZ and KLF7 Protein Stability

Proteins are commonly targeted to the proteasome for destruction by the conjugation of poly-ubiquitin chains to their lysine residue(s) [22]. Since we have shown that TAZ undergoes ubiquitination, we were interested in determining whether the TPM-mediated ubiquitination ultimately leads to its demise. In order to determine whether the ubiquitination plays a role in the regulation of TAZ turnover, we ectopically expressed FLAG-TAZ or FLAG-TAZ ΔTPM in HEK 293 cells. Approximately 48 hours post-transfection, cycloheximide (CHX; 200 μg/mL) was added to the cell culture medium to inhibit protein synthesis. At the indicated time intervals, the cells were lysed and equal amounts of extracted cellular protein were resolved by SDS/PAGE and immunoblotted with anti-FLAG and anti-actin (Figure 3.15). It was initially hypothesized that wild-type FLAG-TAZ would degrade at a considerably faster rate than would the TPM mutant based upon the inability of the mutant to be ubiquitinated; however, comparison of the turnover rate of FLAG-TAZ and FLAG-TAZ ΔTPM showed no significant difference in their half-lives (Figure 3.15A,B; *upper panels*). It is apparent from the anti-FLAG immunoblots that both FLAG-TAZ and FLAG-TAZ ΔTPM are quite stable over the time interval examined, which suggests that the ubiquitination of TAZ may have no bearing on the regulation of TAZ stability. Anti-actin immunoblot analyses revealed consistent actin levels between all of the samples, indicating equal protein loading (Figure 3.15A,B; *lower panels*).

We have shown that the proposed tetra-phosphorylation of KLF7 at its TPM enables its recognition by β-TrCP, an interaction that is likely responsible for the subsequent ubiquitination of KLF7. As this course of events has been shown to promote the proteasome-dependent degradation of β-catenin, we questioned whether KLF7 was destined for the same fate [16,18,19]. In order to determine if the aforementioned activities culminate in the degradation of KLF7, we assessed the stability of transiently

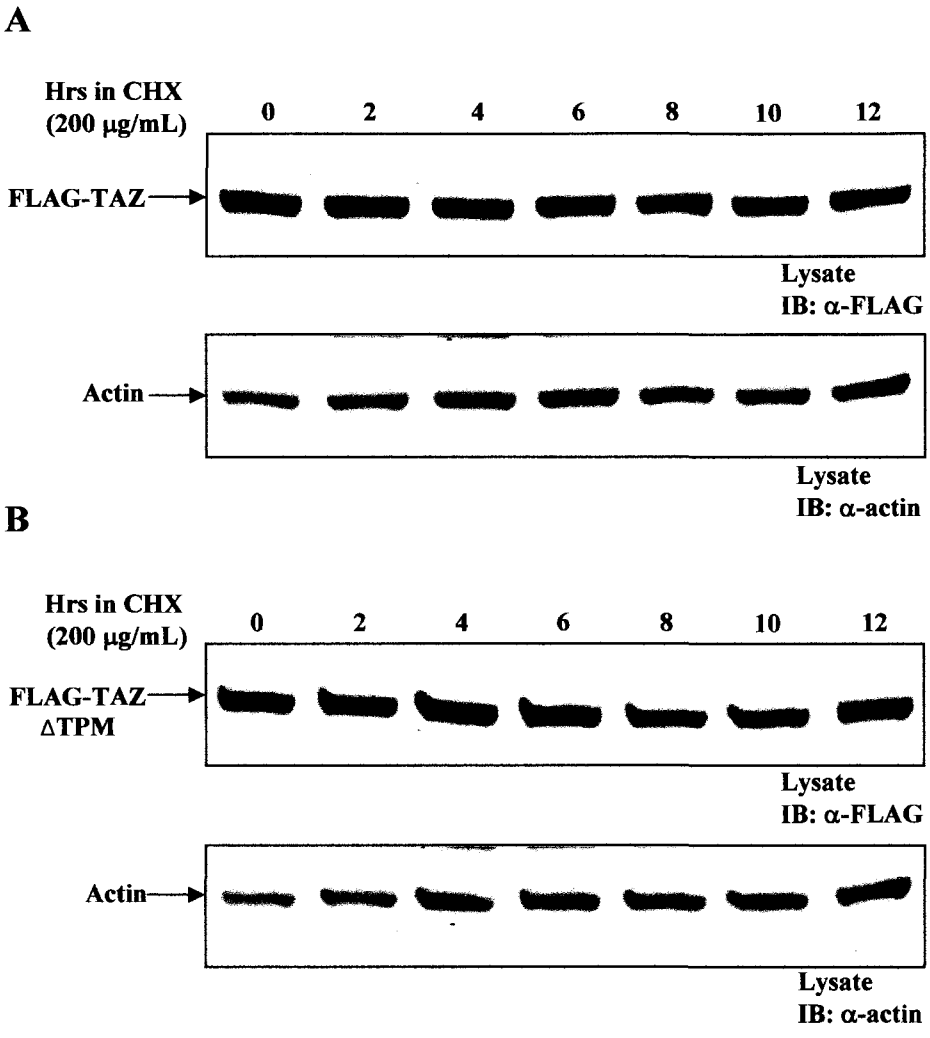

Figure 3.15- Effect of the TPM on TAZ Protein Stability. HEK 293 cells were transiently transfected with FLAG-TAZ or FLAG-TAZ ΔTPM. Cells were treated with 200 μg/mL cycloheximide (CHX) approximately 48 h post-transfection. At the indicated time points, the cells were lysed and prior to resolution by SDS/PAGE, the extracted cellular proteins were normalized via the Bradford method. **(A)** Anti-FLAG immunoblot analysis (*upper panel*) of the lysate samples over-expressing FLAG-TAZ. **(B)** Anti-FLAG immunoblot analysis (*upper panel*) of the cells over-expressing FLAG-TAZ ΔTPM. The anti-FLAG immunoblots were subsequently immunoblotted with anti-actin (*lower panels*) to ensure equal protein loading. These results are representative of four separate experiments.

transfected Myc-KLF7 and Myc-KLF7 STDM in HEK 293 cells treated with cycloheximide for increasing time intervals. The examination of KLF7 stability was conducted in the same manner as indicated previously for the assessment of TAZ stability. Equal amounts of protein, extracted from the cells over-expressing Myc-KLF7 or Myc-KLF7 STDM, were resolved by SDS/PAGE and subsequently immunoblotted with c-Myc and actin antibodies (Figure 3.16). Anti-c-Myc immunoblot analysis revealed a comparable turnover rate for both Myc-KLF7 and Myc-KLF7 STDM in the time interval spanning from 0 to 10 hours (Figure 3.16A,B; *upper panels*). Interestingly, within the last time interval investigated (10 - 12 hours), the level of wild-type Myc-KLF7 was considerably reduced, whereas, no significant decrease was detected for the TPM mutant of KLF7 during this time. Examination of the anti-actin immunoblots demonstrated similar levels of actin within all of the samples investigated, verifying equal protein loading (Figure 3.16A,B; *lower panels*).

We had expected that wild-type Myc-KLF7 would degrade at a much faster rate than its TPM mutant counterpart, as the mutant does not associate with β-TrCP, nor does it undergo ubiquitination; however, no conclusions can be drawn regarding the role of the KLF7 TPM in the governance of the half-life of KLF7 based upon our stability data. Since it appears that we may only have detected the onset of KLF7 degradation during the final time interval studied, further time intervals will have to be analysed to confirm that the wild-type protein continues to degrade, while the TPM mutant remains stable.

3.6 The Binding of TAZ by 14-3-3 is TPM-Dependent

In an attempt to understand the purpose of the TAZ TPM, we looked to the critical regulatory interaction between the 14-3-3 proteins and TAZ. Previous studies conducted by Kanai *et al.* revealed that 14-3-3 binding acts to sequester TAZ in the cytoplasm, thereby halting its transcriptional co-activation activities [42]. The

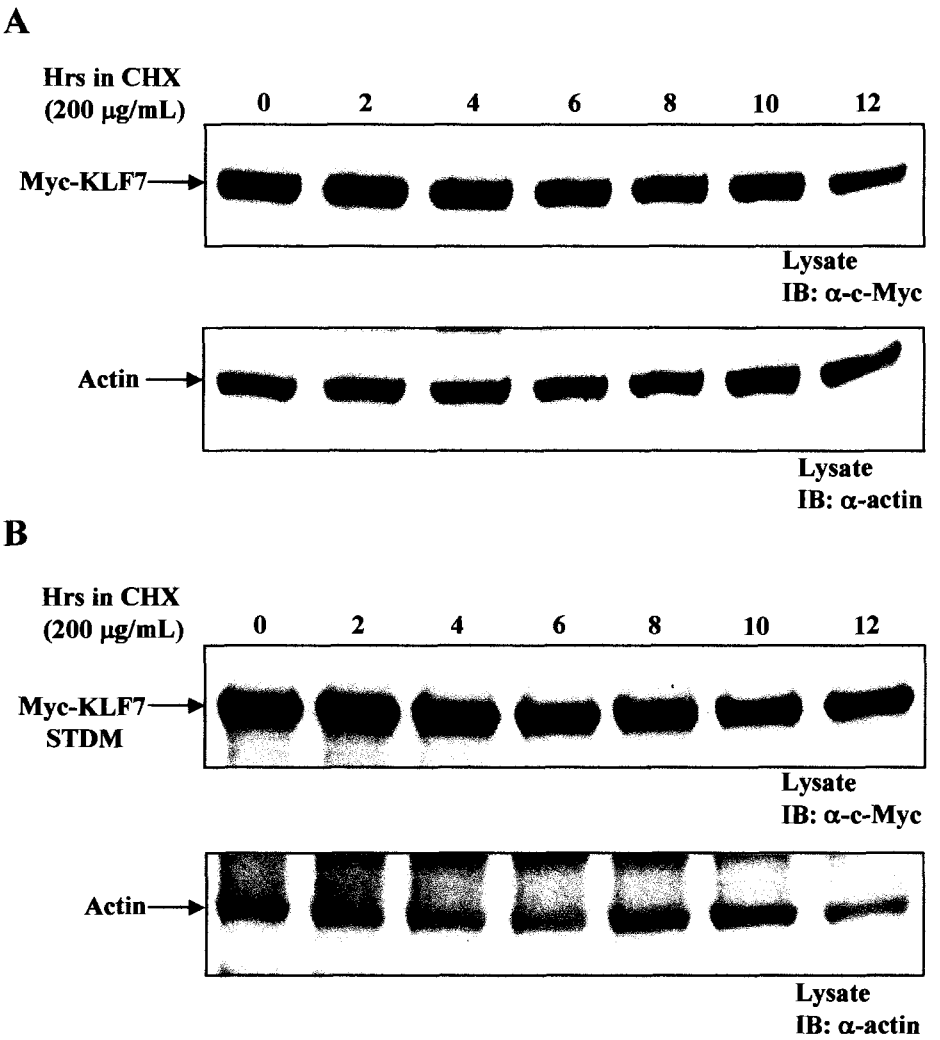

Figure 3.16- KLF7 Protein Stability is Regulated by Its TPM. HEK 293 cells were transiently transfected with Myc-KLF7 or Myc-KLF7 STDM. Forty-eight hours post-transfection, cells were treated with 200 μg/mL cycloheximide (CHX). The cells were lysed at the indicated time points and the amount of extracted cellular protein was normalized by the Bradford method. Cell lysates were resolved by SDS/PAGE and protein stability was assessed through anti-FLAG immunoblotting of the samples over-expressing **(A)** Myc-KLF7 (*upper panel*) or **(B)** Myc-KLF7 STDM (*upper panel*). The anti-FLAG immunoblots were also probed with anti-actin (*lower panels*) to ensure equal protein loading. These results are representative of two separate experiments.

phosphorylation-dependent nature of the association between 14-3-3 proteins and their target ligands holds true for the interaction between TAZ and 14-3-3, in that phosphorylation at Ser89 of TAZ, catalyzed by the Lats kinase, is necessary for 14-3-3 binding [42,43]. In order to determine whether activities dictated at or by the TAZ TPM influence its interaction with 14-3-3, co-immunoprecipitation experiments were conducted. We generated a TAZ mutant containing an alanine substitution at Ser89 (TAZ S89A), which was previously shown to diminish the interaction between TAZ and 14-3-3 [42]. We over-expressed FLAG-TAZ, FLAG-TAZ ΔTPM, and FLAG TAZ S89A in 3T3-L1 mouse pre-adipocytes. Cleared cell lysates were then subjected to anti-FLAG-conjugated agarose to enable isolation of FLAG-tagged TAZ. Anti-14-3-3 immunoblot analysis demonstrated that 14-3-3 could indeed co-immunoprecipitate with FLAG-TAZ, while, as expected, TAZ S89A could not associate with 14-3-3 (Figure 3.17; *upper panel*). Interestingly, no 14-3-3 was detected in the TAZ ΔTPM immunoprecipitants, indicating that the TPM is necessary for the interaction of TAZ with 14-3-3 proteins.

The analogous experiment in HEK 293 cells depicted the existence of an interaction between 14-3-3 and FLAG-TAZ ΔTPM, albeit at a lower affinity than that observed for wild-type TAZ (Figure 3.18; *upper panel*). The fact that the TPM mutant of TAZ can still interact with 14-3-3 in HEK 293 cells, while there appears to be no detectable interaction in 3T3-L1 cells, indicates that the influence of the TAZ TPM on 14-3-3 binding may be cell-type specific.

3.7 TPM Mutants of TAZ and KLF7 Strongly Inhibit Adipocyte Differentiation in 3T3-L1 Preadipocyte Cells

Perhaps the most intriguing facet of the identification of TAZ and KLF7 as TPM-containing proteins is their functional similarity to β-catenin, which remains the only bona fide TPM protein reported to date [16]. A commonality between these three TPM-

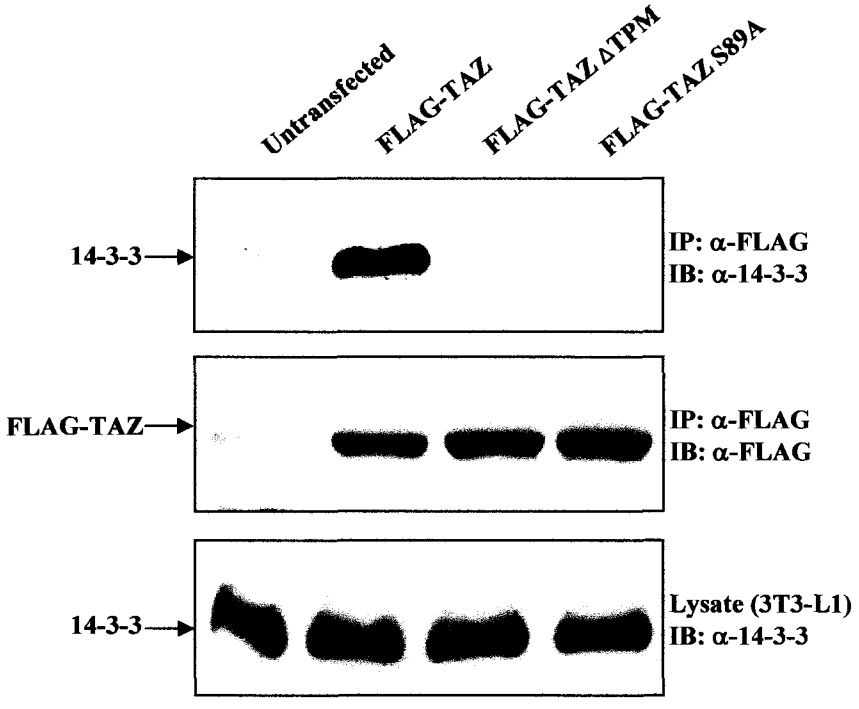

Figure 3.17- TAZ ΔTPM Does Not Associate with 14-3-3 in 3T3-L1 Preadipocytes. Mouse 3T3-L1 preadipocyte cells were untransfected or transiently transfected with FLAG-TAZ, FLAG-TAZ ΔTPM, or FLAG-TAZ S89A. Twenty-four hours post-transfection, the cells were lysed and the cleared cell lysates were subjected to anti-FLAG immunoprecipitation (IP). The resulting immune complexes were resolved by SDS/PAGE and subsequently immunoblotted (B) with a pan-14-3-3 antibody (*upper panel*) and a FLAG antibody (*middle panel*). Cell lysates were also separated by SDS/PAGE and immunoblotted with a pan-14-3-3 antibody (*lower panel*) to detect the amount of endogenous 14-3-3. These results are representative of two experiments.

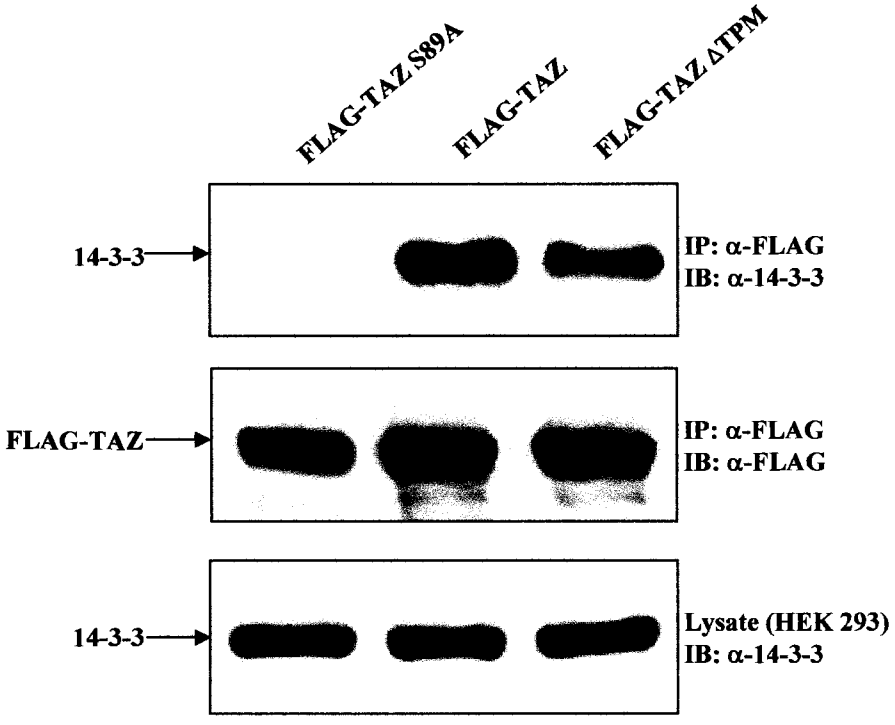

Figure 3.18- Mutation of the TAZ TPM Diminishes the Interaction Between TAZ and 14-3-3 in HEK 293 Cells. HEK 293 cells were transiently transfected with FLAG-TAZ S89A, FLAG-TAZ, or FLAG-TAZ ΔTPM. Cells were lysed approximately 24 h post-transfection and the cleared cell lysates were incubated with anti-FLAG-conjugated agarose. The resulting immune complexes were resolved by SDS/PAGE and immunoblotted (IB) with a pan-14-3-3 antibody (*upper panel*) and a FLAG antibody (*middle panel*). The cleared cell lysates were also resolved by SDS/PAGE and subsequently immunoblotted with a pan-14-3-3 antibody (*lower panel*). These results are representative of two separate experiments.

containing, transcriptional mediators is their regulation of adipocyte differentiation. β-catenin signalling has been implicated in the inhibition of adipogenesis by halting the transcription of a subset of genes necessary for proper adipocyte formation [44]. The fate of mesenchymal stem cells (MSCs) to differentiate into osteoblasts or adipocytes has been shown to be governed by TAZ protein levels, with TAZ acting to stimulate osteogenesis, while simultaneously inhibiting adipocyte differentiation [45]. KLF7 has also been linked to the inhibition of adipogenic differentiation potential in model preadipocyte and adipocyte cell lines through the transcriptional repression of a number of adipocyte-specific genes [46,47].

In light of the similar impact that TAZ and KLF7 have on adipocyte differentiation, we questioned whether these outcomes were a functional consequence of activities centred at their TPMs. In order to assess the effect of the TPM on adipogenesis, we analysed the adipogenic progression in mouse 3T3-L1 preadipocyte cells over-expressing the wild-type and TPM mutant forms of both TAZ and KLF7. We also transiently transfected cells with the empty pFLAG-CMV-2 vector DNA to control for any effect the transfection reagents may have on adipogenesis. Approximately 30 - 36 hours post-transfection, when the cells were perceived to be 100% confluent, differentiation was induced via the addition of cell culture medium supplemented with 10% FBS, 1X isobutylmethylxanthine (IBMX), 1X dexamethasone, and a 1X insulin solution. At this time, control samples were lysed and the lysates were resolved by SDS/PAGE and subjected to anti-FLAG (Figure 3.19A) or anti-c-Myc (Figure 3.20A) immunoblot analyses to confirm successful expression and comparable expression levels between the constructs under investigation. Following a 72 hour period of differentiation, the cell culture media was replaced with insulin media, consisting of 10% FBS and a 1X insulin solution. Fresh insulin media was provided 48 hours after the initial weaning of the cells from induction media, at which time significant lipid accumulation was visible. Forty-eight hours following the second insulin change, the

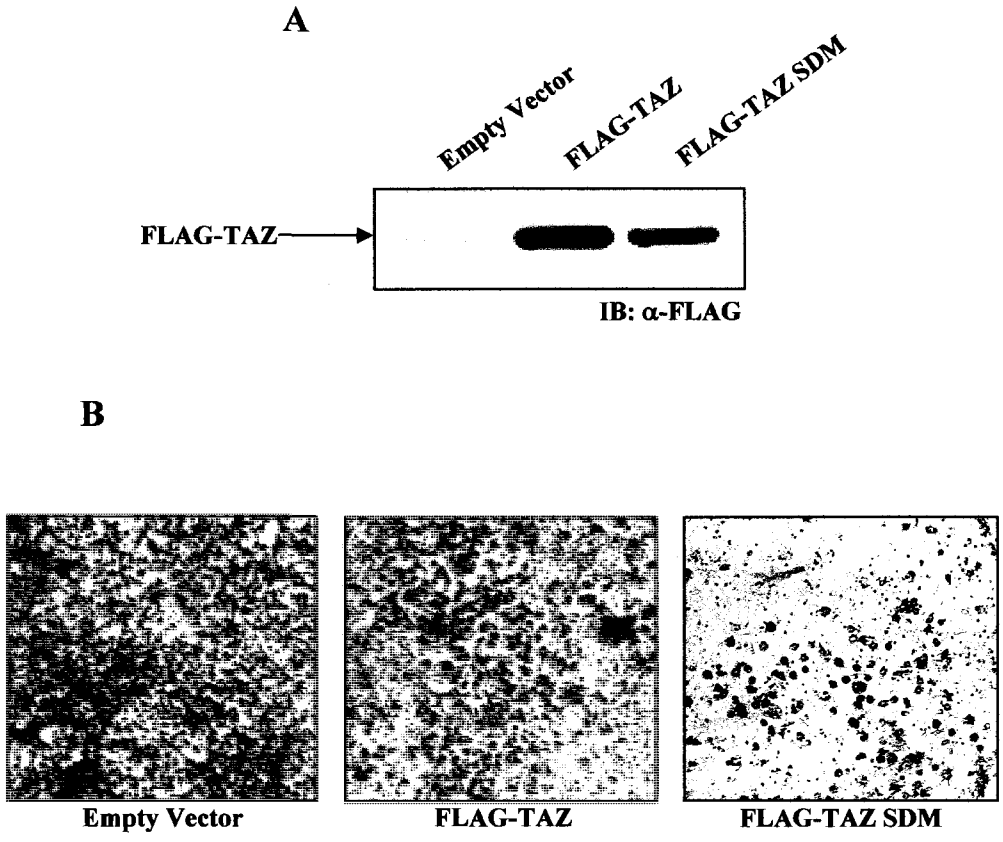

Figure 3.19- TPM-Mediated Activities Regulate the TAZ-Induced Inhibition of Adipogenesis. Mouse 3T3-L1 preadipocyte cells were transiently transfected with pFLAG-CMV-2 (empty vector), FLAG-TAZ, or FLAG-TAZ SDM. Transfection control cells were lysed 24 h post-transfection. Cell lysates were resolved by SDS/PAGE and **(A)** anti-FLAG immunoblot analysis was performed. 3T3-L1 cells were exposed to IBMX, dexamethasone, insulin, and FBS ~24-30 h post-transfection to induce adipocyte differentiation. After 72 h, the culture medium was replaced with insulin media and 48 h later fresh insulin media was supplied. The cells were monitored until the desired degree of differentiation was reached (~48 h after the second insulin media change). The cells were then fixed and stained for neutral lipids with Oil Red O. **(B)** Phase contrast images of the cells were taken at 50x magnification. These results are representative of seven separate experiments.

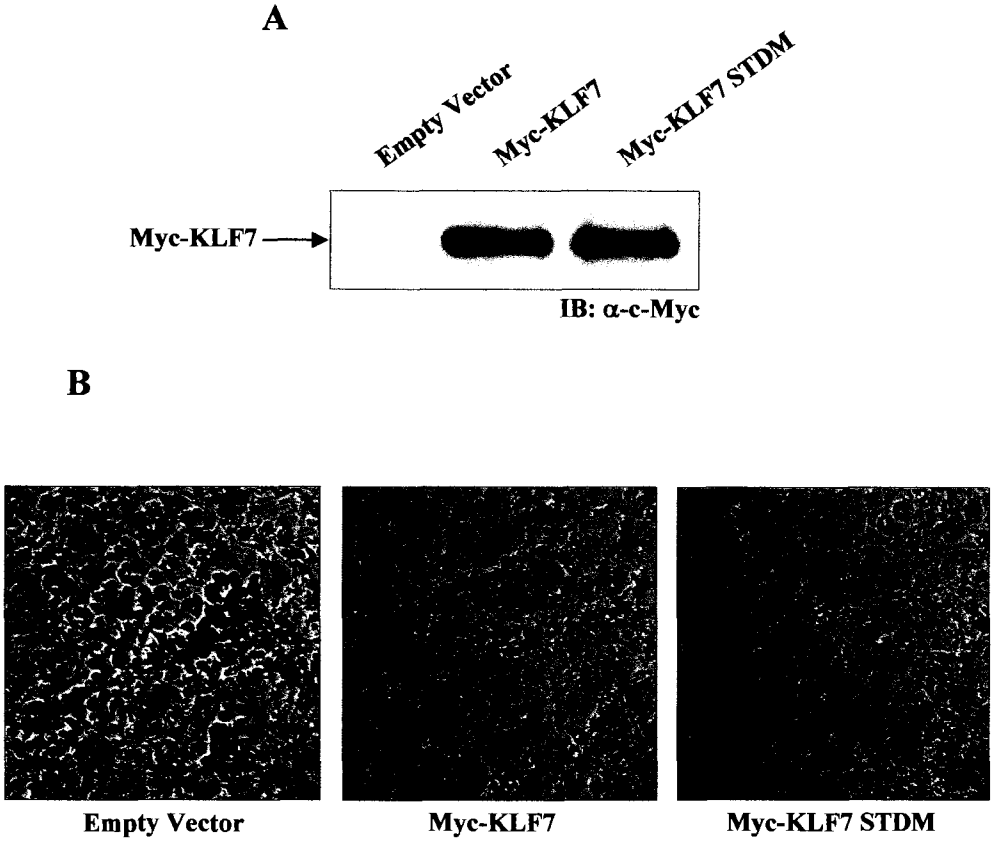

Figure 3.20- KLF7 STDM Strongly Inhibits Adipocyte Differentiation. Mouse 3T3-L1 preadipocyte cells were transiently transfected with pFLAG-CMV-2 (empty vector), Myc-KLF7, and Myc-KLF7 STDM. Approximately 24 h post-transfection, transfection control cells were lysed. The lysates were separated by SDS/PAGE and **(A)** immunoblotted with anti-c-Myc. To induce adipogenesis, confluent cells were exposed to IBMX, dexamethasone, insulin, and FBS ~24-30 h post-transfection. After 72 h, the cells were incubated in insulin media for 48 h, following which fresh insulin media was supplied. Once the desired degree of differentiation was reached, ~48 h after the second change of insulin media, the cells were fixed and subsequently stained for neutral lipids with Oil Red O. **(B)** Phase contrast images of the Oil Red O stained cells were taken at a magnification of 100x. These results are representative of two separate experiments.

3T3-L1 cells were fixed and stained with Oil Red O (ORO), a fat-soluble dye capable of binding neutral lipids, whose presence is suggestive of adipocyte maturation.

Phase contrast images of the differentiated 3T3-L1 cells were taken following ORO staining. Cells housing ORO-stained lipids appear darker in contrast than do cells lacking significant lipid accumulation. It can be seen from Figure 3.19B that the over-expression of FLAG-TAZ indeed limits the adipogenic differentiation progression of preadipocyte cells when compared to those which were mock transfected, a finding that was previously published by Hong *et al.* [45]. Intriguingly, we reproducibly observed levels of adipocyte differentiation drastically lower for the TPM mutant of TAZ than those documented for the wild-type protein. We were also able to reproduce the results reported by Kanazawa *et al.*, which revealed that the over-expression of KLF7 in preadipocyte cells inhibited adipogenesis [46]. This is evident within Figure 3.20B, as 3T3-L1 cells over-expressing Myc-KLF7 exhibited a lesser degree of ORO staining than did the mock-transfected cells. Most importantly, however, we again observed that the TPM mutant of KLF7 further inhibited adipocyte differentiation compared to wild-type KLF7. The ability of the TPM mutants of both TAZ and KLF7 to inhibit adipogenesis to a greater extent than their respective wild-type proteins suggests that events orchestrated by their TPMs likely influence their regulation of adipocyte differentiation.

PART II) A Comprehensive Analysis of TAZ Phosphorylation Sites

3.8 TAZ is a Heavily Phosphorylated Protein

3.8.1 Phosphorylation Accounts for the Mobility Shift of Treated FLAG-TAZ

Throughout our characterization of TAZ as a novel TPM-containing protein, anti-FLAG immunoblot analyses reproducibly revealed a pronounced, upward mobility shift

of FLAG-TAZ upon phosphatase and proteasome inhibition (Figures 3.5, 3.7, 3.14). We hypothesized that this slower migration of FLAG-TAZ was likely attributable to phosphorylation, as treatment solely with Calyculin A, a potent Ser/Thr phosphatase inhibitor, could induce the upward shift (Figure 3.5). To substantiate our claim that the mobility shift of treated FLAG-TAZ is due to the addition of numerous phosphate groups, we performed a dephosphorylation assay. HEK 293 cells, over-expressing FLAG-TAZ, were either untreated or treated with proteasome and phosphatase inhibitors to increase the stoichiometry of phosphorylated FLAG-TAZ. Following anti-FLAG immunoprecipitation, which was performed in order to isolate FLAG-TAZ, the resultant immune complexes were washed and divided evenly between two samples. The first sample was incubated with 3 units of calf intestinal alkaline phosphatase (1 unit/μL) for 30 minutes at 37 °C. The second sample was incubated as outlined above; however, no alkaline phosphatase was added. Lysate samples, with and without the addition of alkaline phosphatase, were also put through the dephosphorylation assay and all of the dephosphorylation reactions were terminated by boiling the samples in SDS protein loading dye. Immunoprecipitant and lysate samples were then resolved by SDS/PAGE, immobilized on PVDF membrane, and analysed by immunoblotting with anti-FLAG.

Immunoblot analysis of the samples not subjected to alkaline phosphatase once again displayed the difference in mobility between untreated and treated FLAG-TAZ, with treated FLAG-TAZ migrating much slower than its untreated counterpart (Figure 3.21). Examination of the anti-FLAG immunoprecipitants incubated with alkaline phosphatase revealed that treated FLAG-TAZ underwent a considerable shift downward to a molecular weight comparable to that of untreated FLAG-TAZ. Since the mobility shift could be counteracted by alkaline phosphatase-induced dephosphorylation, it is believed that phosphorylation is indeed the source of the mobility shift and that TAZ is likely a heavily phosphorylated protein.

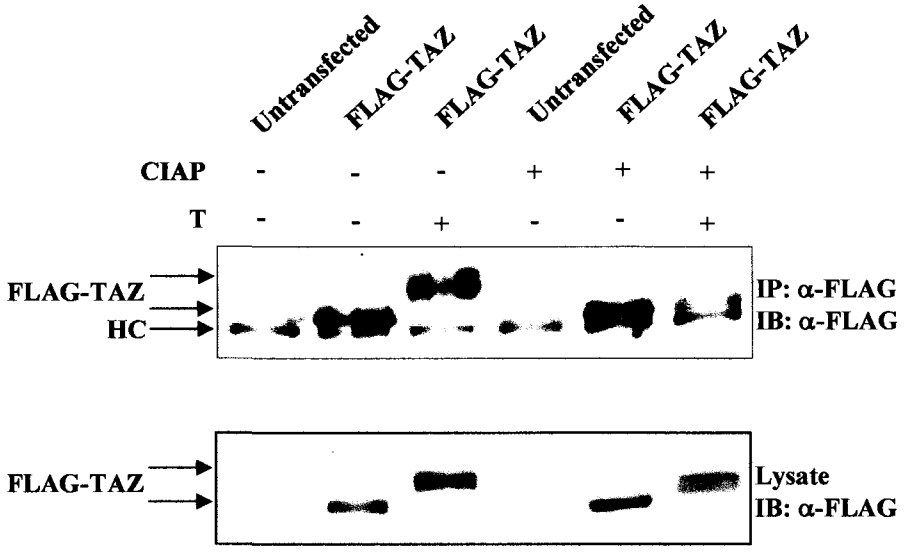

Figure 3.21- TAZ Mobility Shift is Abolished by Its Dephosphorylation with Alkaline Phosphatase. HEK 293 cells were either untransfected or transiently transfected with FLAG-TAZ. Approximately 24 h post-transfection, cells were left untreated (-) or were treated (+) with 10 μM MG-132 and 100 nM Calyculin A for 1 h. Following treatment (T), the cells were lysed and cleared cell lysates were subjected to anti-FLAG immunoprecipitation (IP). The resulting immune complexes, as well as lysate samples, were incubated with (+) or without (-) 3 units of calf-intestinal alkaline phosphatase (CIAP) for 30 min. at 37°C. Dephosphorylation reactions were quenched by boiling the immune complexes and lysate samples at 95°C in 2X or 6X SDS/PAGE protein loading dye, respectively. Both the immune complexes (*upper panel*) and lysates (*lower panel*) were resolved by SDS/PAGE and subsequently analyzed by immunoblotting (IB) with anti-FLAG. The double arrows indicate the differentially phosphorylated forms of TAZ. The IgG heavy chain is indicated (HC). These results are representative of three separate trials.

3.8.2 Identification of TAZ Phosphorylation Sites by Mass Spectrometry

Since reversible protein phosphorylation is a common form of post-translational modification implicated in the regulation of numerous aspects of protein function, it is probable that a major advancement in the understanding of the cellular role of TAZ may be achieved with the delineation and characterization of its multiple phosphorylation sites. Therefore, we performed a global analysis of TAZ phosphorylation sites using mass spectrometry. TAZ tryptic peptides were derived from a Coomassie-stained protein band corresponding to FLAG-TAZ that was isolated from cells treated with proteasome and phosphatase inhibitors, ensuring a high stoichiometry of phosphorylated FLAG-TAZ (Figure 3.7A,B). The tryptic peptides were co-crystallized with α-cyano-4-hydroxycinnamic acid matrix on a MALDI target plate and subsequently analysed via MALDI-TOF mass spectrometry in linear mode.

The resultant peptide mass fingerprint, depicted in Figure 3.22, reveals a number of tryptic peptides matching those of FLAG-TAZ. These peptides are indicated on the mass spectrum by their experimentally determined m/z ratios. Among the tryptic peptides attributed to FLAG-TAZ were a number of putative phosphopeptides. We detected five unique phosphorylated peptides, each containing at least one putative phosphorylation site. Two of the five potential FLAG-TAZ phosphopeptides appear to be multiply phosphorylated, with the lesser phosphorylated peptides separated from their higher phosphorylated counterparts by ~80 m/z, a mass difference attributed to the addition of a phosphate group. Within Figure 3.22, the number of symbols used to label the potential phosphopeptides is representative of the number of phosphorylation sites presumed to be present.

In order to unambiguously establish the identity and phosphorylation status of each of the putative FLAG-TAZ phosphopeptides, we performed tandem mass

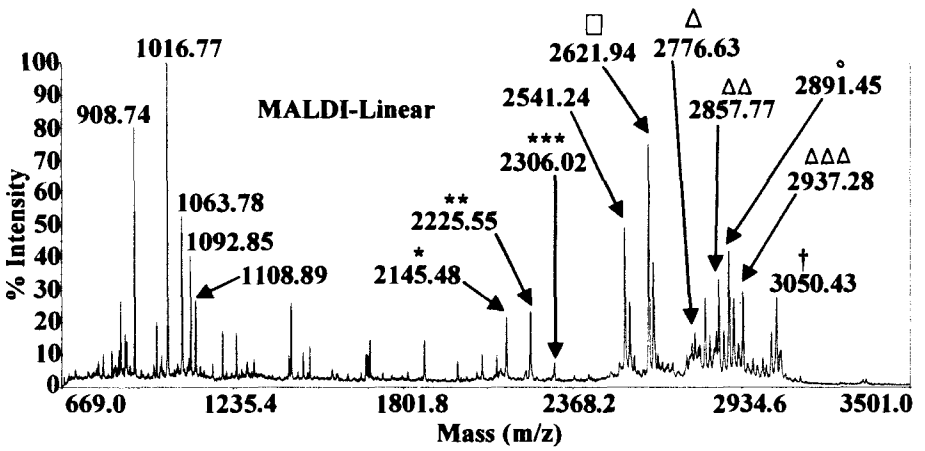

Figure 3.22- Mass Spectrometric Analysis of FLAG-TAZ Reveals a Number of Putative Phosphopeptides. The tryptic peptides derived from the Coomassie stained band indicated in Figure 3.7 were analyzed by MALDI-TOF mass spectrometry in linear mode in an attempt to identify putative TAZ phosphopeptides. The MALDI-TOF peptide mass fingerprint of FLAG-TAZ is shown above. Tryptic peptide ions matching those predicted for TAZ by MS-Digest are indicated by their experimentally determined m/z ratios. Putative phosphopeptides, also predicted by MS-Digest, are denoted by the following symbols: *, □, Δ, °, †. The number of symbols in the label indicates the phosphorylation status of the putative phosphopeptide. This spectra is representative of four separate experiments.

spectrometry (MS/MS). Location of the exact site(s) of phosphorylation within the peptides was attempted through analysis of the resultant fragment ion spectra.

2145.48 m/z, 2225.55 m/z, 2306.02 m/z- Within Figure 3.22, we detected a series of tryptic peptides with masses corresponding to the TAZ peptide, $(R)^{290}$SITNNSSDPFLNGGPYHSR^{308}(E), containing one (2145.48 m/z), two (2225.55 m/z), and three (2306.02 m/z) phosphate groups. The MS/MS spectrum of the peptide ion at 2306.02 m/z exhibited four peaks separated by approximately 98 m/z, a difference attributable to the neutral loss of phosphoric acid (H_3PO_4) from a phosphoserine or phosphothreonine, proving that this peptide, which contains five serine/threonine residues, is indeed triply phosphorylated (Figure 3.23A). Examination of the fragment ions of the singly phosphorylated tryptic peptide (2145.48 m/z) revealed a number of carboxy-terminal (y) ions matching those predicted for the TAZ peptide spanning amino acid residues 290 to 308, $(R)^{290}$SITNNSSDPFLNGGPYHSR^{308}(E). A number of the most abundant peaks (y_7, y_7 - 98 m/z, y_{10}, y_{11}) detected in the MS/MS spectrum, as well as numerous less prominent ones, represent phosphopeptide fragments containing only one phosphorylatable residue, Ser307 (Figure 3.23B). Taken together, this MS/MS data enabled the unambiguous identification of Ser307 as a novel TAZ phosphorylation site.

Interestingly, two major peptide peaks detected in the MS/MS analysis of 2145.48 m/z do not support our identification of Ser307 as a phosphorylation site. The 773.22 m/z and 1245.29 m/z peptide peaks can be matched to masses predicted for y_7 and y_{11} fragment ions, however, only in the absence of a phosphate group on Ser307 (Figure 3.23B). The 773.22 m/z peptide was also detected in the MS/MS spectra of both the doubly and triply phosphorylated peptides. Since we are highly confident in our assignment of Ser307 as a phosphorylation site, we believe that phosphorylation at Ser307 may oppose phosphorylation at one or more of the amino-terminally located Ser/Thr residues (Ser290, Thr292, Ser295, Ser296). However, identification of the other

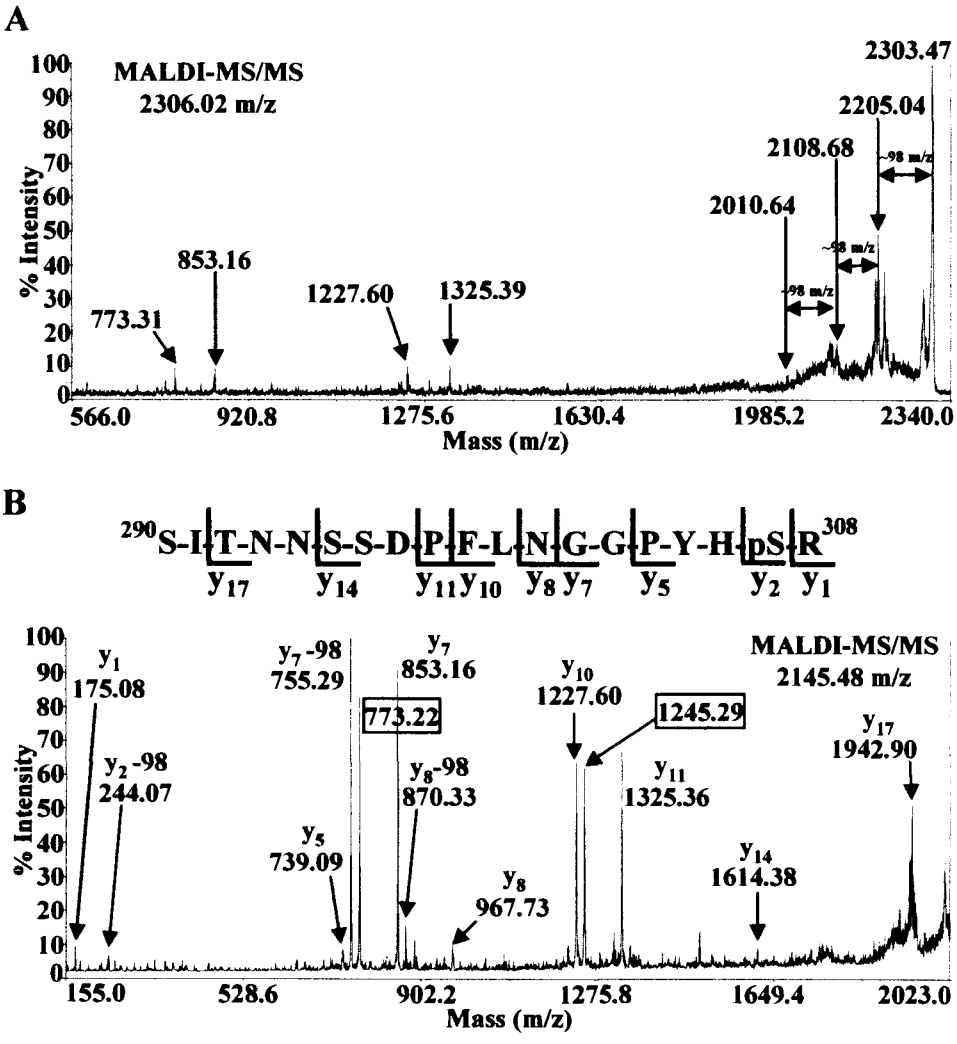

Figure 3.23- Identification of Ser307 as a TAZ Phosphorylation Site. (A) A portion of the MS/MS spectrum of the peptide at 2306.02 m/z. Three consecutive losses of 98 m/z from the precursor ion (2303.47 m/z) confirmed the presence of 3 phosphate groups on this peptide. **(B)** A segment of the MS/MS spectrum of the singly phosphorylated peptide at 2145.48 m/z. The fragment ions (b and y) with m/z ratios matching those predicted by MS-Product, including y ions with a loss of H_3PO_4 (98 m/z), are labelled. The detected fragment ions verified the TAZ peptide to be ^{290}SITNNSSDPFLNGGPYHSR^{308}, as well as enabled the unambiguous identification of Ser307 as a TAZ phosphorylation site (pS). The boxed m/z ratios are those which oppose the identification of Ser307 as a phosphorylation site.

phosphorylation sites within this peptide was not feasible with the MS/MS data obtained, which is likely explained, at least in part, by the close proximity of the other potential phosphorylation sites.

2621.94 m/z- Our MS analysis of FLAG-TAZ revealed a tryptic peptide with an experimental m/z ratio of 2621.94, which corresponds to a TAZ peptide predicted to be singly phosphorylated (Figure 3.22). The presence of one phosphate group on this peptide ion was confirmed via tandem mass spectrometry, as we detected a major peak at 2520.64 m/z, which is approximately 98 m/z less than the precursor ion, 2618.34 m/z (Figure 3.24). The MS/MS spectrum presented numerous fragment ions characteristic of the following TAZ peptide, (K)^{158}AMNQPLNHMNLHPAVSSTPVPQR^{180}(S) (Figure 3.25A,C). Interestingly, analysis of the MS/MS spectrum provided compelling evidence suggesting that Ser173, Ser174, and Thr175 all undergo phosphorylation (Figure 3.25B). The ions detected at 777.21 m/z (y_6) and 679.15 m/z (y_6 - 98 m/z) suggest the phosphorylation of Thr175, a proline-directed site, as they represent the mass of the peptide fragment ^{175}TPVPQR^{180} containing one phosphate group. On the other hand, we were also able to detect fragment ions at 697.22 m/z, a mass predicted for an unphosphorylated y_6 ion (^{175}TPVPQR^{180}), and at 864.47 m/z and 766.20 m/z, indicating a phosphorylated y_7 ion (^{174}STPVPQR^{180}), which includes Ser174. The detection of these y ions implies that Ser174 also undergoes phosphorylation. Finally, we were also able to localize a phosphate group to Ser173, due to the identification of a y_7 ion at 784.26 m/z, which represents the peptide ^{174}STPVPQR^{180} in an unphosphorylated form.

It is important to note that we were unable to detect a doubly or triply phosphorylated form of this peptide; therefore, it is possible that phosphorylation at any one of these residues is dependent upon the phosphorylation status of the other two sites. The extremely close proximity of these three TAZ phosphorylation sites likely favours our notion of phosphorylation dependency, as the occurrence of multiple negatively

A

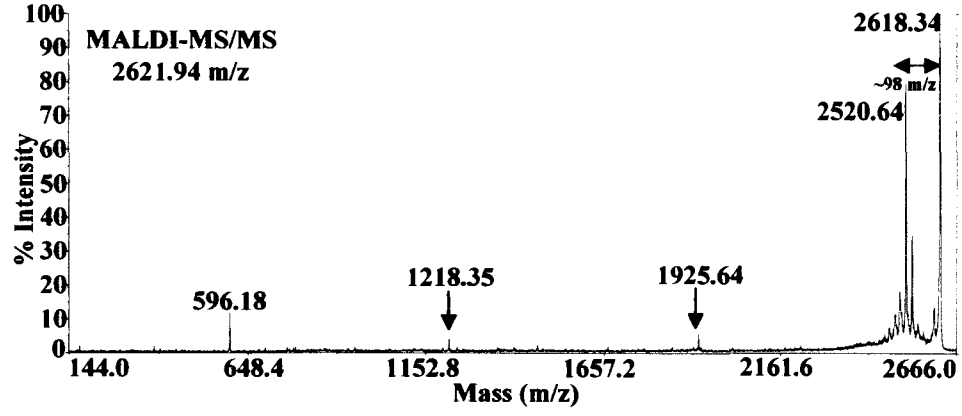

B

^{158}A-M-N-Q-P-L-N-H-M-N-L-H-P-A-V-S-S-T-P-V-P-Q-R^{180}

Figure 3.24- MALDI-MS/MS Analysis of 2621.94 m/z. (A) The MS/MS spectrum of the TAZ tryptic peptide at 2621.94 m/z is shown. The loss of 98 m/z from the precursor ion (2618.34 m/z), represented by the double-ended arrow, confirmed the presence of a single phosphoserine or phosphothreonine residue in this TAZ peptide. **(B)** The singly phosphorylated tryptic TAZ peptide matching 2621.94 m/z.

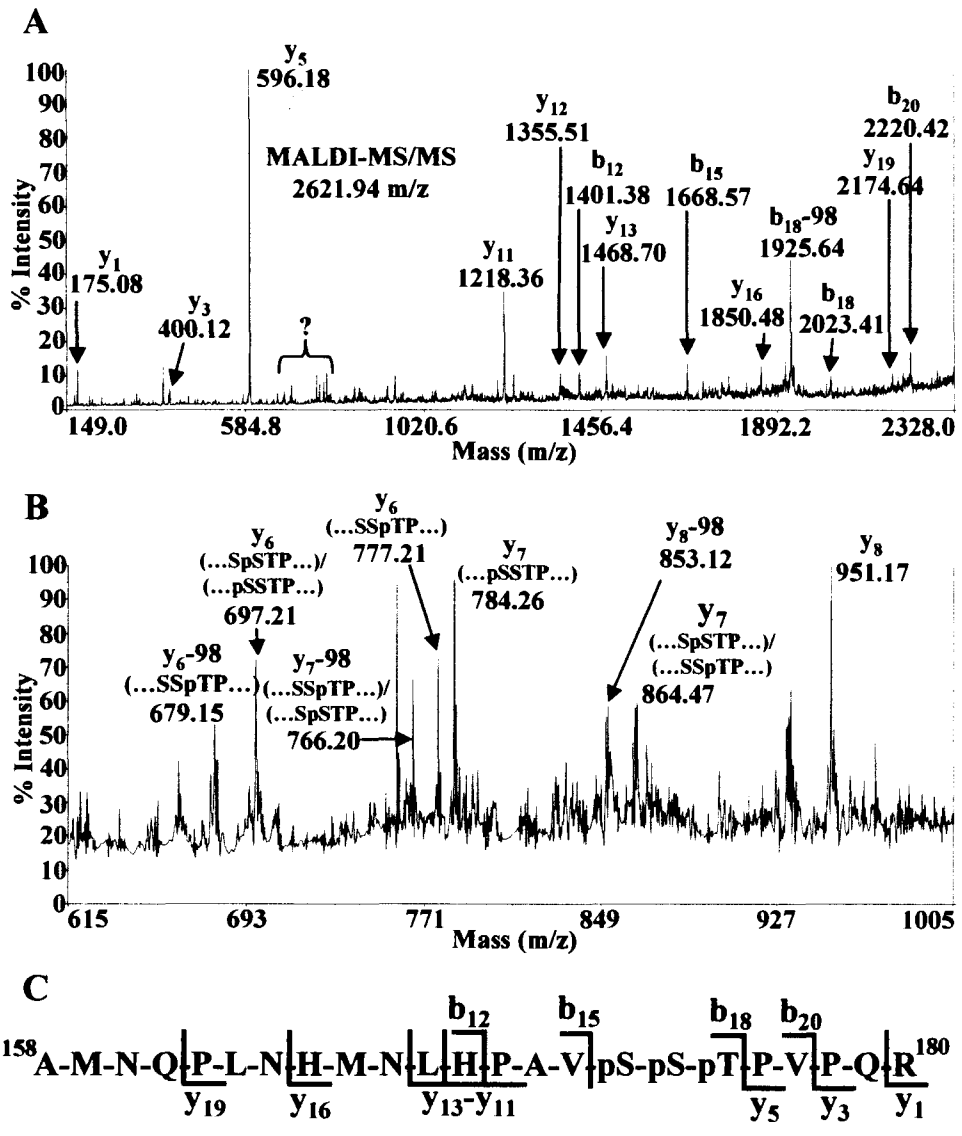

Figure 3.25- Identification of Ser173, Ser174, and Thr175 as TAZ Phosphorylation Sites. (A) A portion of the MS/MS spectrum of 2621.94 m/z. The b and y fragment ions with m/z ratios matching those predicted by MS-Product, including ions with a loss of H_3PO_4 (98 m/z), are labelled. The question mark (?) indicates the region of the MS/MS spectrum that was enlarged in **(B)**. The fragment ions denoted in **(B)** revealed Ser173, Ser174, and Thr175 as TAZ phosphorylation sites (pS, pT). The fragment ions that enabled the identification of each of the sites are indicated. **(C)** The fragment ions confirmed the TAZ peptide under investigation to be ^{158}AMNQPLNHMNLHPAVSSTPVPQR^{180}.

charged phosphate groups on consecutive residues would likely introduce considerable electrostatic repulsion in the region of the peptide. Thus, we hypothesize that, at any given time, only one of the three indicated phosphorylation sites is phosphorylated with that site undergoing dephosphorylation before the phosphorylation of another site can be achieved.

2776.63 m/z, 2857.77 m/z, 2937.28 m/z- Through MALDI-MS analysis of the FLAG-TAZ tryptic peptides, we detected a series of putative phosphopeptides with masses corresponding to a TAZ peptide containing one (2776.63 m/z), two (2857.77 m/z), or three (2937.28 m/z) phosphate groups (Figure 3.22). To ascertain the phosphorylation status of this peptide, we consulted the MS/MS spectrum of the peptide ion assumed to be triply phosphorylated (2937.28 m/z), which presents two consecutive neutral losses of approximately 98 m/z from the precursor ion (2933.08 m/z), indicating that this peptide is at least doubly phosphorylated (Figure 3.26A). A third loss of 98 m/z is not evident on the MS/MS spectrum; however, this does not disprove the presence of a third phosphorylation site on this peptide, as the detection of fragment ions was likely suppressed by the co-elution of a second putative TAZ peptide (2938.28 m/z_{av}).

MS/MS analysis of the singly phosphorylated TAZ peptide (2776.63 m/z) revealed a number of fragment ions corresponding to amino acid residues 87 to 114 of TAZ, $(R)^{87}$SHSSPASLQLGTGAGAAGSPAQQHAHLR^{114}(Q) (Figure 3.26B). In our attempt to identify the phosphorylation site on this peptide, detection of the fragment ion series, y_{11} to y_{16}, ruled out Ser105 as a phosphorylation site. Our detection of fragment ions y_{18}, y_{20}, and y_{21} also disqualified Thr98 as the phosphorylated residue in this peptide. The presence of b ions with masses matching those predicted for unphosphorylated b_4 and b_5 fragment ions enabled the identification of the phosphorylated residue as Ser93 by eliminating Ser87, Ser89, and Ser90 as candidate phosphorylation sites. Furthermore, the detection of y_{23} and y_{24} – 98 m/z ions, which correspond to masses of phosphorylated

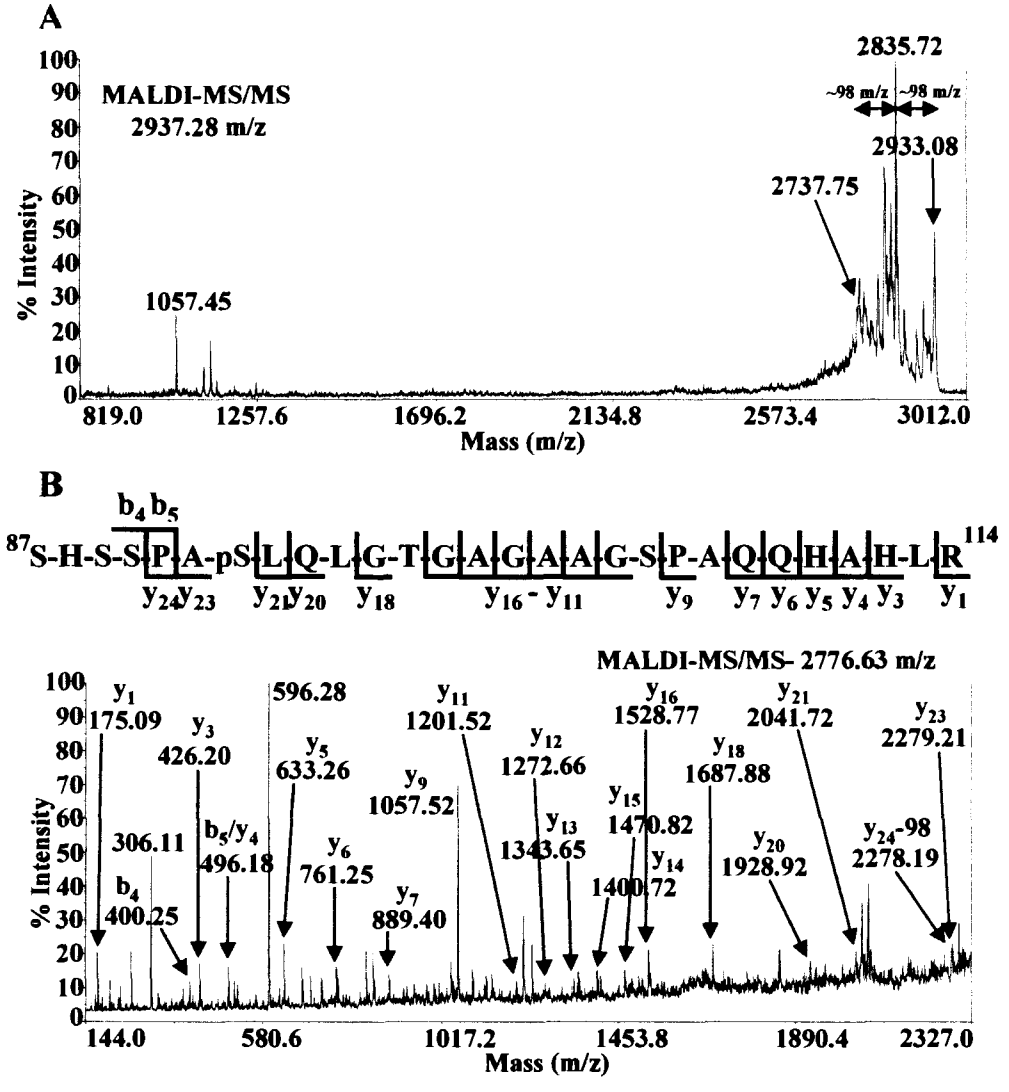

Figure 3.26- Identification of Ser93 as a TAZ Phosphorylation Site. **(A)** Part of the MS/MS spectrum of 2937.28 m/z. The double elimination of H_3PO_4, as shown by 2 consecutive losses of 98 m/z from the precursor ion (2933.08 m/z), confirmed the presence of 2 phosphate groups. The fragment ions did not confirm the existence of a third phosphate group. **(B)** A portion of the MS/MS spectrum of the singly phosphorylated peptide at 2776.63 m/z. The b and y fragment ions with m/z ratios matching those predicted by MS-Product are labelled. The fragment ions confirmed the TAZ peptide to be ^{87}SHSSPASLQLGTGAGAAGSPAQQHAHLR^{114}. Unambiguous identification of Ser93 as a TAZ phosphorylation site (pS) was also possible.

TAZ ions, confirmed our assignment of Ser93 as a TAZ phosphorylation site on this singly phosphorylated peptide.

Insufficient MS/MS data obtained for the phosphopeptides presumed to contain two (2857.77 m/z) and three (2937.28 m/z) phosphate groups, respectively, hindered our attempt to locate the other phosphorylation sites within this peptide. The occurrence of three of the six phosphorylatable residues within the first four amino acid residues of this peptide exacerbated our feat of identifying the other two sites. Although, the detected fragment ions for this peptide did not clearly depict Ser89 as a phosphorylation site, studies have revealed that TAZ does indeed undergo phosphorylation at Ser89, an event proven necessary for 14-3-3 recognition [42,43]. Taken together with our identification of Ser93 as a novel TAZ phosphorylation site, there likely remains at least one more phosphorylation site to be determined amidst the amino acid residues of this TAZ peptide.

2891.45 m/z- Examination of the MS spectra portraying the FLAG-TAZ tryptic peptides revealed a peptide ion with an m/z ratio of 2891.45, which matches that of a theoretical TAZ tryptic peptide containing one phosphate group (Figure 3.22). MS/MS analysis of this putative phosphopeptide confirmed the presence of a single phosphate group, as we detected the neutral loss of phosphoric acid from the precursor ion, 2888.45 m/z (Figure 3.27). Analysis of the fragment ions confirmed that the peptide included residues 264 to 289 of TAZ, (R)^{264}QLPMEAETLAPVQAAVNPPTMTPDMR^{289}(S) (Figure 3.28). Within this TAZ peptide, there exists three Thr residues positioned at amino acid residues 271, 283, and 285. The detection of fragments ions at 601.21 m/z and 699.20 m/z, which match the theoretical masses of the phosphorylated y_5 and $y_5 - 98$ m/z ions, allowed us to unambiguously discern Thr285 as the site of phosphorylation in this singly phosphorylated TAZ peptide, as the y_5 ion contains only one putative phosphorylatable residue (Figure 3.28A,B). Interestingly, Thr285 is immediately

A

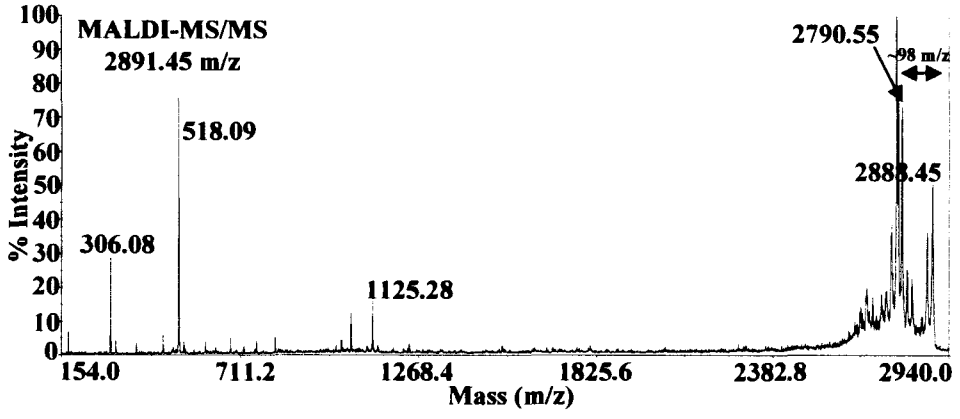

B

^{264}Q-L-P-M-E-A-E-T-L-A-P-V-Q-A-A-V-N-P-P-T-M-T-P-D-M-R^{289}

Figure 3.27- MALDI-MS/MS Analysis of 2891.45 m/z. **(A)** The MS/MS spectrum of the tryptic peptide at 2891.45 m/z is shown. The elimination of H_3PO_4, evidenced by the loss of 98 m/z from the precursor ion (2888.45 m/z), confirmed the presence of a single phosphoserine or phosphothreonine on this peptide. **(B)** The singly phosphorylated tryptic peptide ion matching 2891.45 m/z.

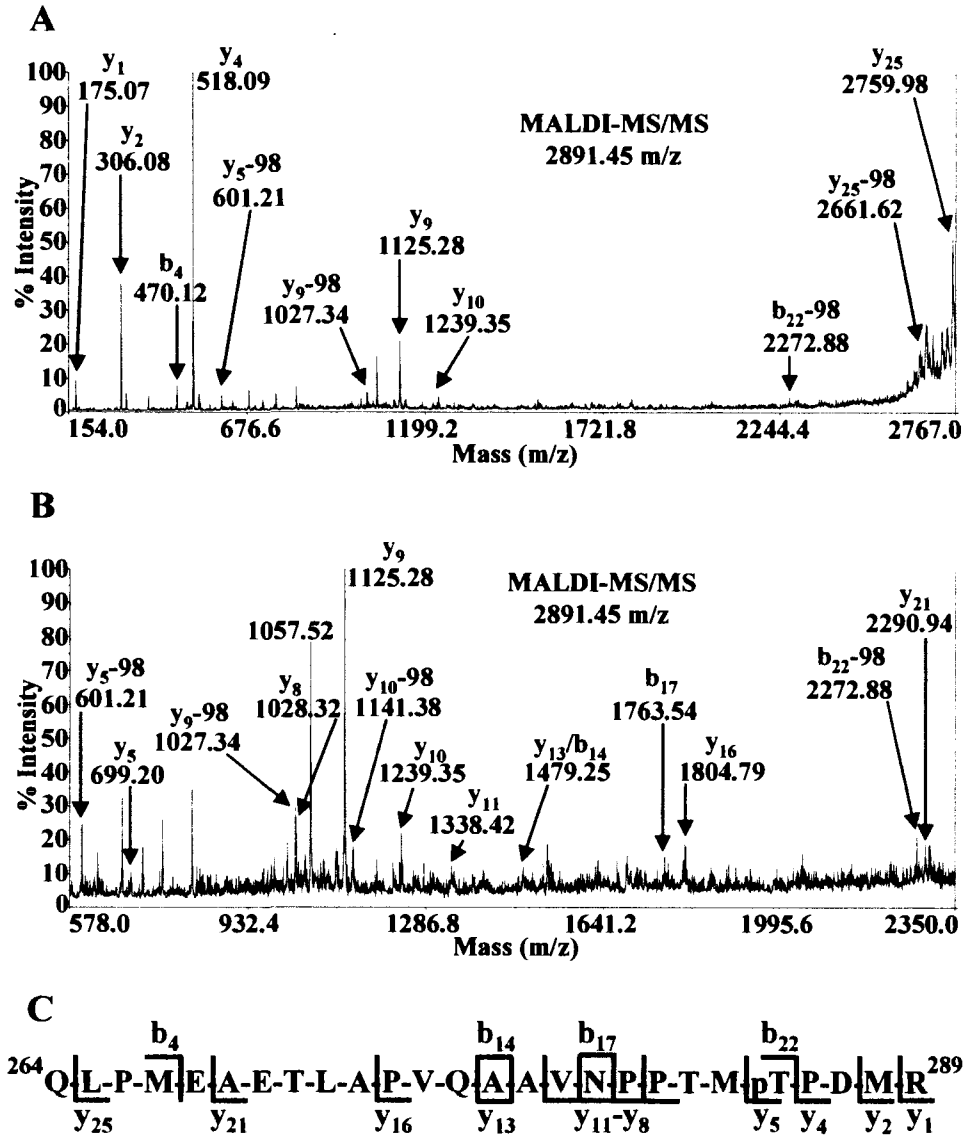

Figure 3.28- Identification of Thr285 as a TAZ Phosphorylation Site. (A,B) Different portions of the MS/MS spectrum of 2891.45 m/z. The b and y fragment ions with m/z ratios matching those predicted by MS-Product, including ions showing a loss of H_3PO_4 (98 m/z), are labelled. **(C)** The detected fragment ions enabled the identification of the tryptic peptide as QLPMEAETLAPVQAAVNPPTMTPDMR, which encompasses TAZ amino acids 264 to 289. It was also possible to unambiguously identify Thr285 as the phosphorylation site (pT) on this TAZ peptide.

followed by a proline residue (Pro286), suggesting that this newly identified TAZ phosphorylation site may be a proline-directed phosphorylation site.

3050.43 m/z- The peptide mass fingerprint resulting from the MALDI-MS analysis of the FLAG-TAZ tryptic peptides displayed a peak at 3050.43 m/z, which corresponds to a TAZ peptide containing one phosphate group (Figure 3.22). MS/MS analysis of the tryptic peptide ion at 3050.43 m/z confirmed that this peptide is indeed singly phosphorylated, as a neutral loss of approximately 98 m/z was evident from the parent ion (3046.69 m/z) (Figure 3.29A). Numerous fragment ions, mainly y ions, were detected, which matched those expected for the TAZ peptide (R)^{115}QQSYDVTDELPLPPGWEMTFTATGQR^{140}(Y) (Figure 3.29B). Based upon the detection of fragment ions at 461.06 m/z and 532.22 m/z, which represent unphosphorylated y_4 and y_5 ions, respectively, we were able to eliminate Thr137 as the site of phosphorylation in this peptide. It was also possible to rule out Thr135 as the phosphorylated residue, as we observed fragment ions matching unphosphorylated y_6 (632.96 m/z) and y_7 (780.27 m/z) ions. The detection of numerous y ions ranging from y_8 (881.27 m/z) to y_{18} (2030.94 m/z) further narrowed down the identity of the phosphorylated amino acid residue by disqualifying Thr133, as the masses of these fragment ions match those calculated for the unphosphorylated ions. Examination of the MS/MS spectrum of this TAZ peptide also revealed masses corresponding to unphosphorylated y_{21} (2346.90 m/z) and y_{22} (2461.01 m/z) ions, enabling the exclusion of Thr121 as the phosphorylation site on this peptide. Thus, through the process of elimination, it appears that Ser117 undergoes phosphorylation. Furthermore, we detected peaks at 425.15 m/z and 587.13 m/z, which match the masses predicted for phosphorylated b_3 and b_4 fragment ions, respectively. As there is only one Ser/Thr residue within these fragment ions, we were able to unambiguously identify Ser117 as a novel TAZ phosphorylation site within this peptide.

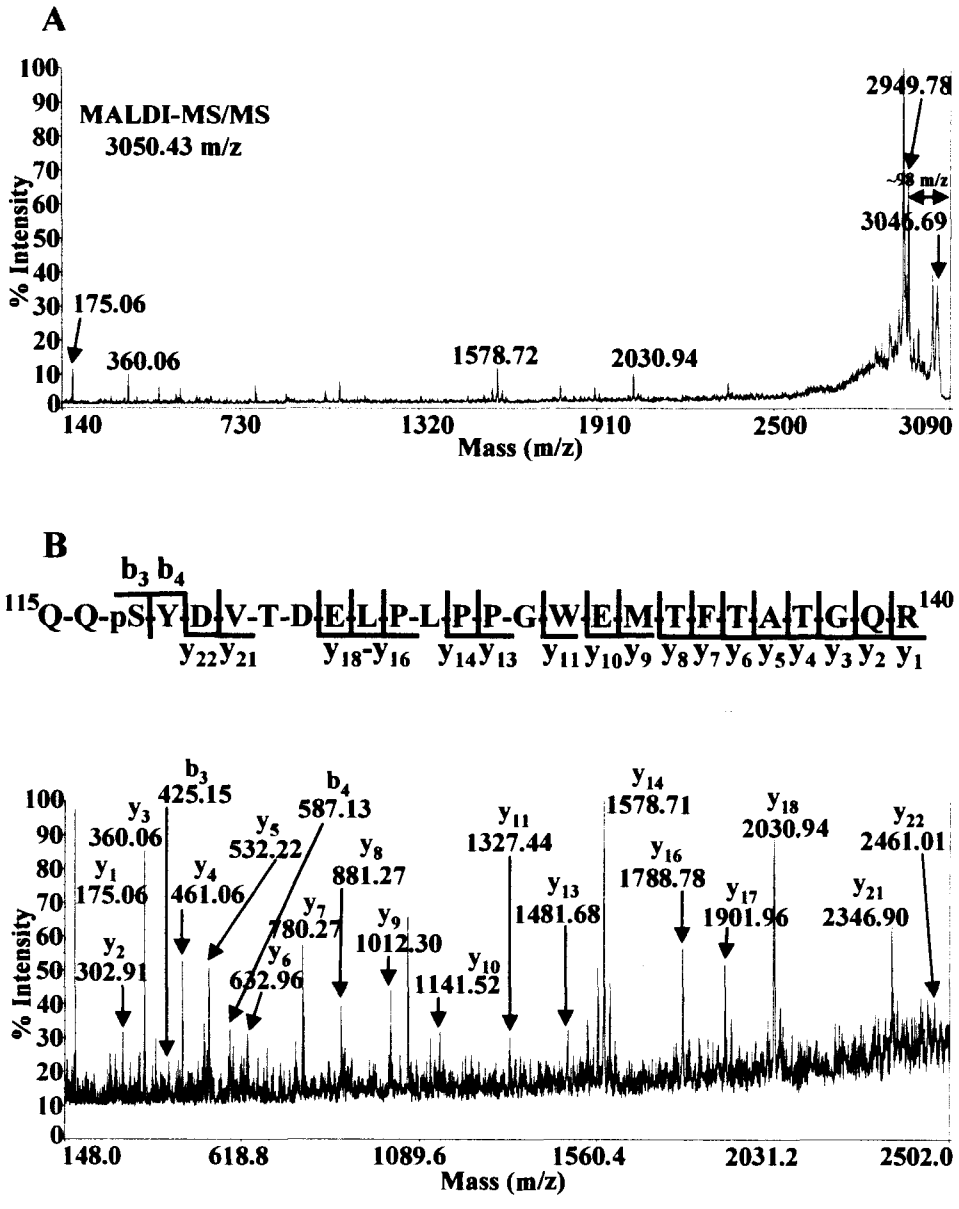

Figure 3.29- Identification of Ser117 as a TAZ Phosphorylation Site. (A) MS/MS spectrum of the TAZ tryptic peptide at 3050.43 m/z. The loss of 98 m/z from the precursor ion (3046.69 m/z) confirmed the peptide to be singly phosphorylated. **(B)** Part of the MS/MS spectrum of 3050.43 m/z. The b and y fragment ions matching those predicted by MS-Product are labelled. The pattern of detected fragment ions verified the TAZ peptide to be ^{115}QQSYDVTDELPLPPGWEMTFTATGQR^{140}, as well as enabled the unambiguous identification of Ser117 as a phosphorylation site (pS) on TAZ.

In our comprehensive investigation of TAZ phosphorylation, we were able to detect five unique TAZ phosphopeptides using mass spectrometry. We observed that two of the five TAZ phosphopeptides were triply phosphorylated, while the remaining three phosphopeptides were proven to be singly phosphorylated. Most importantly, we were successful in unambiguously identifying seven TAZ phosphorylation sites. A summary of the TAZ phosphorylation data and a schematic diagram of TAZ illustrating the location of the identified phosphorylation sites can be found in Table 3.1 and Figure 3.30, respectively.

3.9 Phosphorylation of Ser93 Diminishes the Interaction Between TAZ and 14-3-3

Since the cytoplasmic sequestration of TAZ by 14-3-3 has proven to be a very critical mechanism regulating TAZ transcriptional co-activation activities, our identification of Ser93 as a novel TAZ phosphorylation site was intriguing, as it is located in close proximity to Ser89, the phosphorylation site responsible for the phosphorylation-dependent recognition of TAZ by 14-3-3 [42]. Hence, we wondered whether the occurrence of phosphorylation at Ser93 would in some manner impact the interaction between TAZ and 14-3-3. In order to investigate the consequence of Ser93 phosphorylation on 14-3-3 binding, we generated two FLAG-TAZ mutant constructs through substitution of Ser93 with an alanine (FLAG-TAZ S93A) or an aspartate residue (FLAG-TAZ S93D). Substituting Ser93 with an alanine residue produces a form of FLAG-TAZ that cannot be phosphorylated at position 93; whereas, substitution with an aspartate residue serves to mimic constitutive phosphorylation at Ser93. We transiently transfected these FLAG-TAZ mutant constructs, as well as wild-type TAZ (FLAG-TAZ) and the 14-3-3 binding mutant of TAZ (FLAG-TAZ S89A) in HEK 293 cells. Approximately 24 hours post-transfection, the cells were lysed and the cleared cell lysates were subjected to anti-FLAG immunoprecipitation. The resulting anti-FLAG

m/z	Peptide Sequence	# of Sites
2145.48	^{290}SITNNSSDPFLNGGPYH$\overset{307}{\underline{S}}$R^{308}	1
2225.55	^{290}SITNNSSDPFLNGGPYH$\overset{307}{\underline{S}}$R^{308}	2
2306.02	^{290}SITNNSSDPFLNGGPYH$\overset{307}{\underline{S}}$R^{308}	3
2621.94	^{158}AMNQPLNHMNLHPAV$\overset{173\text{-}175}{\underline{SST}}$PVPQR^{180}	1
2776.63	^{87}SHSSPA$\overset{93}{\underline{S}}$LQLGTGAGAAGSPAQQHAHLR^{114}	1
2857.77	^{87}SHSSPA$\overset{93}{\underline{S}}$LQLGTGAGAAGSPAQQHAHLR^{114}	2
2937.28	^{87}SHSSPA$\overset{93}{\underline{S}}$LQLGTGAGAAGSPAQQHAHLR^{114}	3
2891.45	^{264}QLPMEAETLAPVQAAVNPPTM$\overset{285}{\underline{T}}$PDMR^{289}	1
3050.43	^{115}QQ$\overset{117}{\underline{S}}$YDVTDELPLPPGWEMTFTATGQR^{140}	1

Table 3.1- Summary of TAZ Phosphopeptides Detected by Mass Spectrometry. The table lists the m/z ratios and the sequences of the TAZ phosphopeptides identified by mass spectrometric analysis of FLAG-TAZ. The number of phosphate groups either proven or presumed to be on the phosphopeptides is also shown. Phosphorylation sites that were unambiguously identified through our analysis are underlined and their numerical position within peptide is indicated.

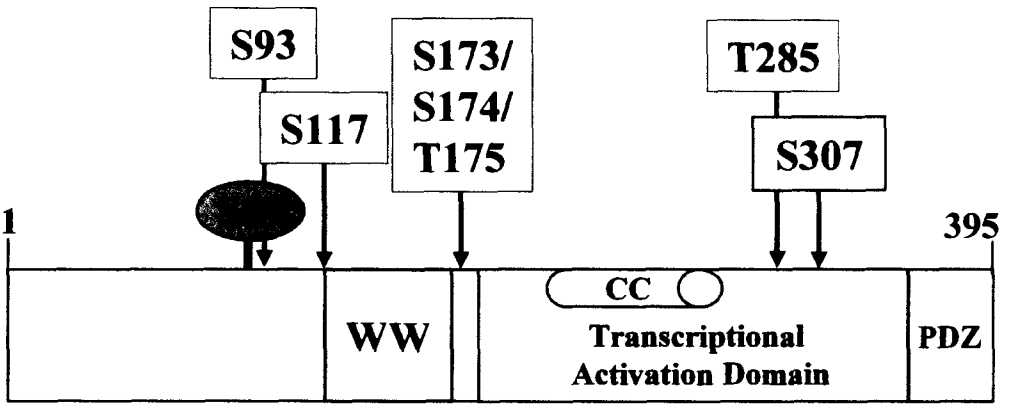

Figure 3.30- Schematic Model of TAZ. The identified TAZ phosphorylation sites are shown here (boxed) with reference to key TAZ regions (WW, WW domain; CC, Coiled-coil domain; PDZ, PDZ-binding motif; S89, 14-3-3 binding site).

immune complexes were resolved by SDS/PAGE and subsequently immunoblotted with a pan-14-3-3 antibody, so as to detect any co-immunoprecipitated 14-3-3 (Figure 3.31; *upper panel*).

As it has been previously reported, we observed that endogenous 14-3-3 could indeed co-immunoprecipitate with FLAG-TAZ, but not with FLAG-TAZ S89A, since the interaction between TAZ and 14-3-3 is reliant upon Ser89 phosphorylation [42]. Interestingly, anti-14-3-3 immunoblot analysis revealed little 14-3-3 in the FLAG-TAZ S93D immunoprecipitants, indicating that phosphorylation at Ser93 may, to some extent, disrupt the association between TAZ and 14-3-3. In agreement with this result, FLAG-TAZ S93A was shown to have no bearing on 14-3-3 binding, as it was able to bring down as much 14-3-3 as did wild-type FLAG-TAZ. Thus, these findings suggest that the phosphorylation of Ser93 influences the interaction between TAZ and 14-3-3, ultimately governing the ability of TAZ to function as a transcriptional co-activator through regulation of its cytoplasmic sequestration.

3.10 The Phosphorylation-Defective Mutant, TAZ S117A, Strongly Inhibits Adipocyte Differentiation

In their assessment of the modular structure of TAZ, Kanai *et al.* noted that TAZ contains a centrally located WW domain [42]. It has been well documented that WW-domain-containing transcriptional co-activators utilize their WW domains in the binding of transcription factors, most favourably binding to those transcription factors possessing Pro-rich motifs, such as the Leu/Pro-Pro-Xxx-Tyr (L/PPXY) motif optimally bound by TAZ. Thus, numerous researchers have assessed whether the binding of TAZ to its target transcription factors is afforded by its WW domain [42,45,48-51]. Within our comprehensive study of TAZ phosphorylation sites, we unambiguously identified Ser117 as a novel TAZ phosphorylation site, an intriguing finding since Ser117 maps to a region

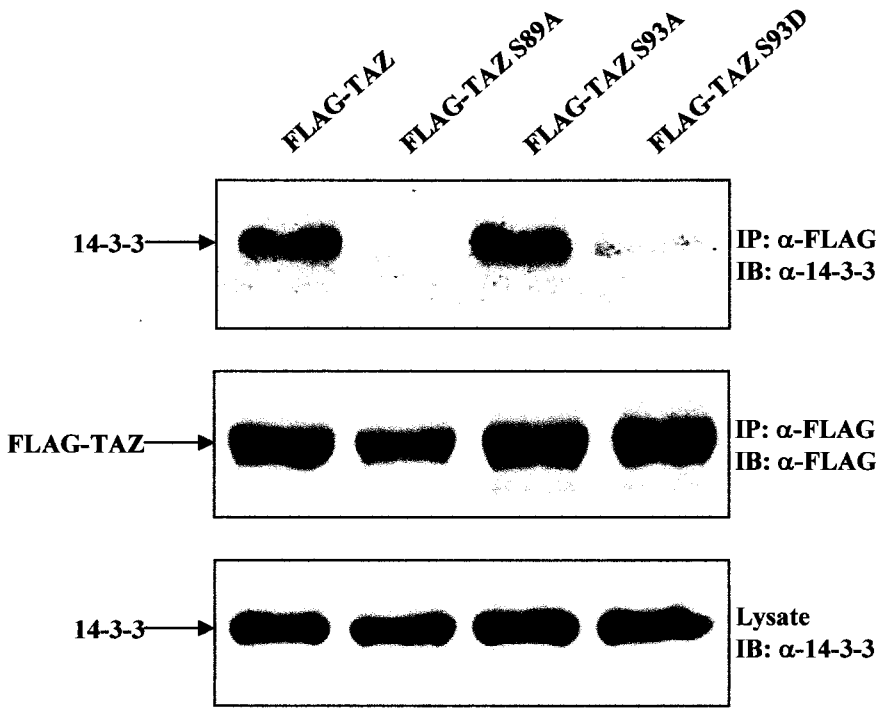

Figure 3.31- TAZ S93D Resists 14-3-3 Binding. HEK 293 cells were transiently transfected with FLAG-TAZ, FLAG-TAZ S89A, FLAG-TAZ S93A, and FLAG-TAZ S93D. Twenty-four hours post-transfection cells were lysed and subjected to anti-FLAG immunoprecipitation (IP). The resulting immune complexes were resolved by SDS/PAGE and immunoblotted (IB) with a pan-14-3-3 antibody (*upper panel*) and a FLAG antibody (*middle panel*). Endogenous 14-3-3 levels were assayed by immunoblot analysis of SDS/PAGE-resolved lysates with a pan-14-3-3 antibody (*lower panel*). These results are representative of 3 separate experiments.

of TAZ located immediately N-terminal to its WW domain (Figure 3.30). Given the close proximity of Ser117 to the WW domain, we questioned whether the presence of a phosphate group at Ser117 would influence the manner in which TAZ interacts with the subset of transcription factors believed to associate with TAZ through its WW domain.

In order to indirectly examine whether phosphorylation on Ser117 influences the WW-domain-mediated binding of TAZ to (L/P)PXY motif-containing transcription factors, we tested the interaction of TAZ with peroxisome proliferator-activated receptor γ (PPARγ), a transcription factor critical for the proper differentiation of adipocytes [45]. It was shown by Hong *et al.* that the binding of TAZ to PPARγ, which involves the recognition of the (L/P)PXY motif of PPARγ by the WW domain of TAZ, results in the repression of the transcriptional activities of PPARγ, ultimately, leading to a decrease in adipocyte differentiation [45]. Since the integrity of the TAZ-PPARγ interaction is inversely related to the capacity of the cells to differentiate into adipocytes, we indirectly examined the functional consequence of Ser117 phosphorylation by assessing the degree of adipogenesis achieved in mouse 3T3-L1 preadipocyte cells. We generated a phosphorylation defective mutant (FLAG-TAZ S117A) by substituting Ser117 with an alanine residue, creating a TAZ variant that cannot undergo phosphorylation at this position. A second TAZ phosphorylation mutant was generated by replacing Ser117 with an aspartic acid residue (FLAG-TAZ S117D) to mimic a form of TAZ that is constitutively phosphorylated on Ser117.

Approximately 30 hours post-transfection, undifferentiated 3T3-L1 cells that had been transiently transfected with FLAG-TAZ, FLAG-TAZ S117A, or FLAG-TAZ S117D were induced to differentiate by replacing the culture medium with medium supplemented with 10% FBS, 1X dexamethasone, 1X IBMX, and 1X insulin. At this point, a subset of transfected cells were lysed with the resulting cell lysates being resolved by SDS-PAGE, transferred to PVDF membrane, and immunoblotted. Anti-FLAG immunoblot analysis revealed the success of transfection, as well as comparable

expression levels between the various TAZ constructs (Figure 3.32A). The remaining preadipocyte cells were then subjected to an eight-day differentiation regimen, as described previously, following which the differentiated cells were stained with Oil Red O (ORO) to examine the degree of adipocyte differentiation.

Phase contrast images of the differentiated 3T3-L1 cells were taken immediately following ORO staining, with cells heavily laden with ORO-stained lipids appearing darker in contrast than those lacking significant lipid accumulation. It can be seen in Figure 3.32B, that we were successful in reproducing the result put forth by Hong *et al.*, in that FLAG-TAZ over-expression hinders adipogenic differentiation, which can be seen through a comparison of the degree of adipogenesis observed in the mock (empty vector) transfected cells [45]. Interestingly, we reproducibly observed that FLAG-TAZ S117A over-expression reduced adipocyte differentiation to a level markedly lower than that documented for wild-type TAZ. In accordance with these results, we also found that cells over-expressing FLAG-TAZ S117D appeared to differentiate to a degree comparable to, or slightly higher than, wild-type FLAG-TAZ over-expressing cells.

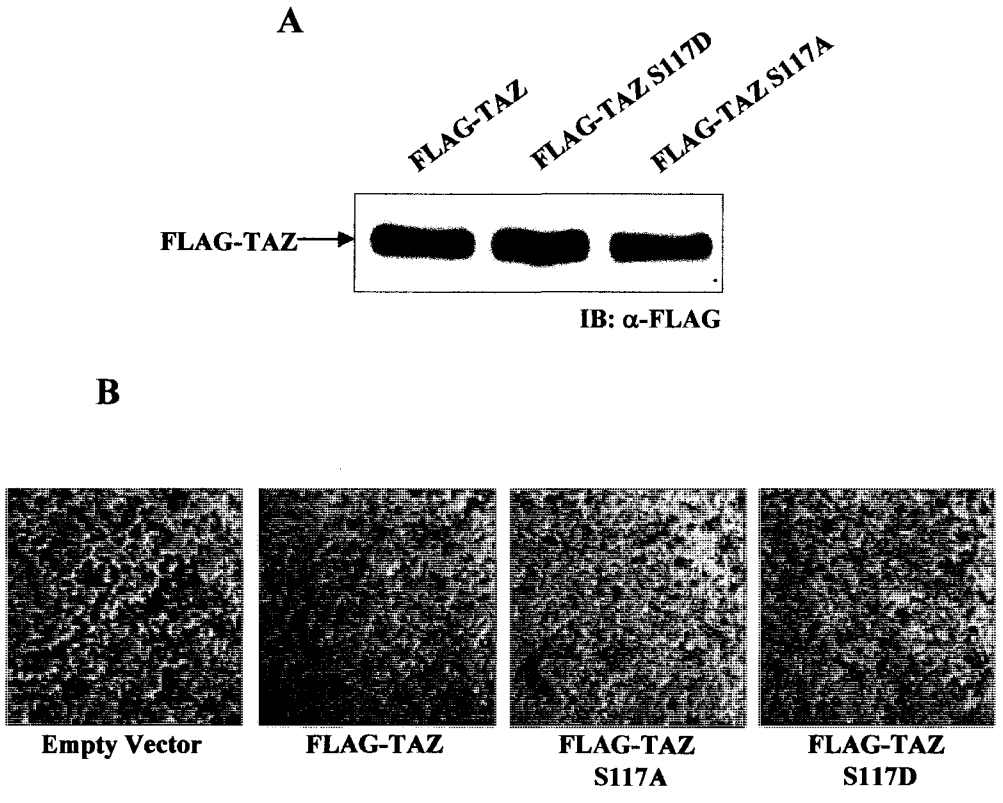

Figure 3.32- TAZ S117A Greatly Hinders Adipogenesis. Mouse 3T3-L1 preadipocyte cells were transiently transfected with pFLAG-CMV-2 (empty vector), FLAG-TAZ, FLAG-TAZ S117A, FLAG-TAZ S117D. Approximately 24 h post-transfection, transfection control cells were lysed. The lysates were separated by SDS/PAGE and **(A)** immunoblotted with anti-FLAG. To induce adipogenesis, confluent cells were exposed to IBMX, dexamethasone, insulin, and FBS ~24-30 h post-transfection. After 72 h, the cells were incubated in insulin media for 48 h, following which fresh insulin media was supplied. Once the desired degree of differentiation was reached, ~48 h after the second change of insulin media, the cells were fixed and subsequently stained for neutral lipids with Oil Red O. **(B)** Phase contrast images of the Oil Red O stained cells were taken at a magnification of 100x. These results are representative of two separate experiments.

Chapter 4

Discussion and Future Work

Within this study, we identified two transcriptional regulators, TAZ and KLF7, which contain tetra-phosphorylation motifs (TPMs) akin to that first discovered in the proto-typical TPM protein, β-catenin. Our characterization of the TAZ and KLF7 TPMs revealed significant similarities, as well as differences, with respect to the regulatory roles afforded by the β-catenin TPM. We also provide the first direct evidence that TAZ is a highly phosphorylated protein. Through mass spectrometric analysis, we successfully located ten TAZ phosphorylation sites, of which three were mapped to the TPM.

PART I) Identification and Characterization of TPM-Containing Proteins

4.1 Anti-TPM is a Bona Fide Phosphoantibody

In order to facilitate the identification of putative TPM-containing proteins, we utilized a novel phosphoantibody raised against a degenerate TPM phosphopeptide library of the form, pSXXXpSXXXpSXXXpS, in immunoblotting procedures. The specificity of this TPM phosphoantibody was evaluated through its reactivity with differentially phosphorylated synthetic peptides, a β-catenin tetra-phosphorylation mutant (β-catenin ΔTPM), and phosphoprotein-enriched cellular lysates (Figures 3.1, 3.2, 3.3). Dot blot analysis of the differentially phosphorylated peptide libraries revealed that the TPM antibody reacted most strongly with the tetra-phosphorylated peptides, while

exhibiting no reactivity with the unphosphorylated peptide library (Figure 3.1). These findings illustrate the phosphospecific nature of the TPM antibody. It was also observed that the TPM antibody showed relatively low binding specificity with the singly, doubly, and triply phosphorylated peptide libraries. Although, this reactivity further validates the phosphospecificity of the antibody, it shows it not to be specifically reactive with proteins phosphorylated in a TPM. The fact that the intensity of the TPM phosphoantibody interactions with the various phosphopeptide libraries increases with the number of phosphate groups on the peptides suggests the antibody to be highly recognizant of multiply phosphorylated proteins. This lack of specificity for TPM-containing proteins can be explained by the polyclonal nature of the TPM phosphoantibody, as there likely exists phosphospecific antibodies with varying epitopes within the antibody preparation. Thus, the TPM phosphoantibody may be made up of antibodies that react with singly, doubly, triply, and tetra phosphorylated proteins.

Acidic proteins have long interfered with phosphoprotein enrichment methods that rely on electrostatic interactions between negatively charged phosphate groups and immobilized metal cations, as acidic amino acids, such as aspartate and glutamate, mimic the chemistry of phosphate groups [10]. For the same reason, phosphoantibodies tend to non-specifically bind to highly acidic proteins. Within our global analysis of TPM-containing proteins in HEK 293 cells, we observed a number of diffuse, TPM phosphoantibody-reactive bands that did not show an increase in intensity with phosphatase and proteasome inhibition, as would be expected for true TPM proteins (Figure 3.3). We attributed these bands to acidic proteins, as their phosphoantibody recognition was not diminished upon alkaline phosphatase incubation (data not shown). Preliminary large-scale purification efforts resulted in the anti-TPM immunoprecipitation and subsequent mass spectrometric identification of the highly acidic protein, tropomyosin (data not shown). Interestingly, amino acid sequence analysis of human tropomyosin revealed four glutamate residues separated from one another by three

arbitrary residues in a TPM-like fashion. Thus, it is possible that the acidic proteins reactive with the TPM phosphoantibody, like tropomyosin, feature acidic amino acid residues in the proper spacing.

In an effort to elucidate the TPM phosphoproteome, we do intend to pursue a large-scale identification of TPM-containing proteins in a variety of cell types. The isolation of putative TPM proteins from crude cell lysates will be afforded through the generation of a chromatographic column containing covalently conjugated TPM phosphoantibody. The ability of the TPM phosphoantibody to react non-specifically with phosphoproteins containing less than four phosphate groups, as well as acidic proteins, is not anticipated to be a major obstacle in the identification of TPM proteins, as mass spectrometry will be utilized to identify the isolated proteins, filter out any non TPM-containing proteins, and to unambiguously map the phosphorylation sites that constitute their respective TPMs.

4.2 TAZ and KLF7 are Novel TPM-Containing Proteins

Small-scale immunoblot analyses focused on detecting the complement of TPM-containing proteins within HEK 293 cells revealed a number of putative TPM proteins through their reactivity with the TPM phosphoantibody, as well as by their increased intensity upon phosphatase and proteasome inhibition (Figure 3.3A). Correlation of bioinformatic data compiled through a pattern search of the human SwissProt database with the TPM sequence, DS/TGXXS/TXXXS/TXXXS/T (Appendix 1), with our immunological data (Figure 3.3A,B) revealed two proteins, TAZ and KLF7, with intriguing similarities to β-catenin, as putative TPM-containing proteins.

TAZ, also referred to as WWTR1 (WW domain-containing transcriptional regulator 1), was initially identified in a screen for 14-3-3 binding proteins [42]. It was discovered that 14-3-3 binding retained TAZ within the cytoplasm, hindering its nuclear

localization. The localization of TAZ to the nucleus, as well as to the plasma membrane, was shown to be mediated by interaction of its C-terminal, PDZ-binding motif with unknown PDZ domain-containing proteins [42]. The inability of TAZ to enter the nucleus diminishes its transcriptional co-activation abilities, which have been shown to mediate the expression of genes linked to the development of bone, fat, muscle, lung, heart, and limb [41,45,48-50,52-55].

KLF7, or ubiquitous KLF (UKLF), named for its broad expression profile, belongs to a zinc-finger transcription factor family, primarily characterized by the presence of a C-terminal, DNA-binding domain, consisting of three zinc fingers of the Cys_2-His_2 type, and by the conserved amino acid sequence connecting the zinc fingers, which was initially observed in the Drosophila segmentation protein, Krüppel [56]. Intensive studies centred on delineating the role of KLF7 in neurogenesis revealed that its transcriptional regulation is critical for proper differentiation, maturation, and phenotype maintenance of neurons [57-64]. Transcriptional mediation afforded by KLF7 has also been implicated in adipogenesis and insulin biosynthesis and secretion [46,47].

Within this study, we have provided evidence confirming the presence of a TPM within both TAZ and KLF7. Firstly, highly modified forms of over-expressed FLAG-TAZ and Myc-KLF7, whose levels were enhanced by phosphatase and proteasome inhibition, were found to react with the TPM phosphoantibody in immunoblot experiments (Figures 3.5, 3.6). The recognition of modified TAZ and KLF7 by anti-TPM was entirely dependent upon phosphatase inhibition, suggesting that phosphorylation of their respective TPMs is highly regulated by the interplay of yet to be identified kinases and phosphatases.

Secondly, mutational analyses of the putative TAZ and KLF7 TPM phosphorylation sites resulted in the generation of potentially lesser phosphorylated versions of these proteins. Separation by SDS-PAGE revealed that Myc-KLF7 STDM, which contains alanine substitutions at both Thr19 and Ser23, migrated at a relatively

faster rate than did wild-type Myc-KLF7 (Figure 3.13), as well as lacked an upper anti-c-Myc reactive band observed within the wild-type protein that can likely be attributed to a higher modified form of Myc-KLF7 (Figure 3.10). FLAG-TAZ ΔTPM, which features an alanine substitution at each of the four putative TAZ TPM phosphorylation sites, also migrated at a faster rate than did FLAG-TAZ (Figure 3.11). The increased mobility observed for the TPM mutant forms of KLF7 and TAZ suggested that the mutations made affected the phosphorylation state of the protein, corroborating our identification of TAZ and KLF7 as TPM proteins.

Finally, mass spectrometric (MS) analysis of phosphorylated FLAG-TAZ revealed a tryptic peptide ion with an m/z ratio matching that predicted for a peptide containing the TAZ TPM with four phosphate groups (2643.18 m/z; Figure 3.8). The mapping of these TAZ phosphorylation sites by tandem mass spectrometry (MS/MS) was an important undertaking, as there exists 8 phosphorylatable S/T residues within the vicinity of the TAZ TPM (^{57}DSGSHSRQSSTDSS^{70}). MS/MS analysis of this phosphopeptide verified its tetra-phosphorylation and mapped three of the phosphate groups to the predicted TAZ TPM sites: Ser58, Ser62, and Ser70 (Figures 3.8, 3.9). Although we were unable to explicitly locate the site of the fourth phosphate group, the series of fragment ions detected via MS/MS did enable us to trace it to either Ser65 or Ser66. Our inability to distinguish between Ser65 and Ser66 as a phosphorylation site on the TAZ TPM peptide can partly be attributed to the presence of fragment ions from a number of prominent TAZ peptide ions (2539.71 m/z, 2555.71 m/z, 2572.57 m/z, 2621.05 m/z) within the MS/MS spectrum. As Ser66 is a predicted TPM phosphorylation site, with additional attention paid to the separation of the TAZ phosphopeptides prior to MS/MS by means such as high performance liquid chromatography (HPLC), we will likely be able to unambiguously identify TAZ as a TPM protein.

4.3 Biochemical Characterization of the TAZ and KLF7 TPMs

Amino acid sequence alignments of KLF7 and TAZ orthologues revealed their TPMs to be entirely conserved in closely related mammals (Figures 4.1, 4.2). This conservation suggests that the KLF7 and TAZ TPMs may be involved in the regulation of their activities, comparable to the roles afforded by the β-catenin TPM. Although sequence information for TAZ and KLF7 from more distinctly related vertebrate species is limited, sequence analysis of the available orthologues illustrated that a greater part of the TPM of both TAZ and KLF7 is conserved, with the exception of the C-terminal-most phosphorylation sites (Ser70 of human TAZ; Thr31 of human KLF7). The emergence of the aforementioned C-terminal phosphorylation sites of TAZ and KLF7 in higher mammals likely evolved as an additional layer of regulation for the processes governed by the phosphorylation events at the sites conserved across all species. Interestingly, the consensus β-TrCP binding sequence, DSGXXS, is highly conserved within all of the TAZ and KLF7 orthologues.

4.3.1 TPM-Dependent Binding of β-TrCP Likely Facilitates KLF7 Ubiquitination

Within our investigation of the KLF7 TPM, we uncovered a novel interaction between KLF7 and β-TrCP (Figure 3.10). The interaction between β-TrCP and a majority of its known substrates, including IκBα, Snail, Vpu, and β-catenin, has been shown to be phosphorylation-dependent, requiring the phosphorylation of two serine residues (DpSGXXpS) [19,65,66]. Our results show that the recognition of KLF7 by β-TrCP is likely also reliant on phosphorylation, as the interaction was detected solely upon phosphatase inhibition, which allows for the accumulation of potentially phosphorylated KLF7. Furthermore, alanine substitutions at the putative phosphorylation sites (Thr19 and Ser23) in the proposed β-TrCP consensus sequence, ^{18}D<u>T</u>GYF<u>S</u>^{23}, abolished the

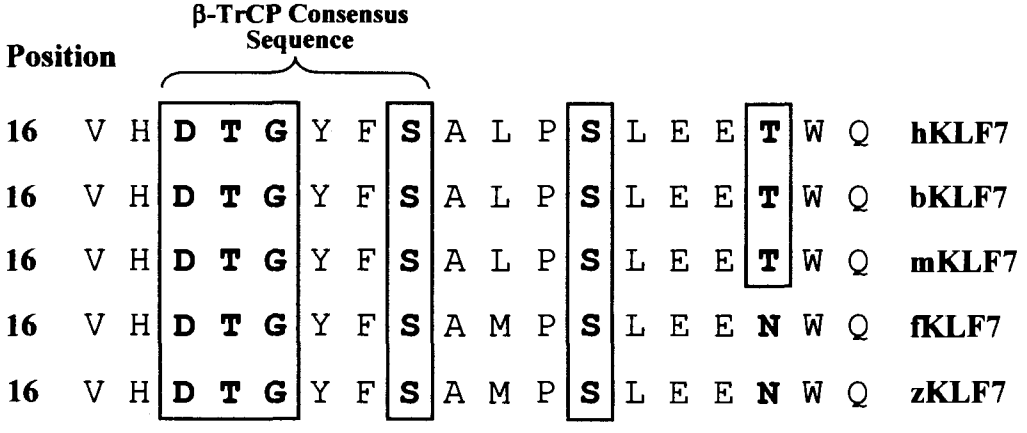

Figure 4.1- Amino Acid Sequence Alignment of the N-terminal Region of KLF7 Orthologues. The serine/threonine residues constituting the KLF7 TPM are boxed. The highly conserved β-TrCP consensus sequence (DTGYFS) is also highlighted. The amino acid positions at which the alignments were initiated are indicated at left. (hKLF7, human KLF7; bKLF7, boar KLF7; mKLF7, mouse KLF7; fKLF7, frog KLF7; zKLF7, zebrafish KLF7)

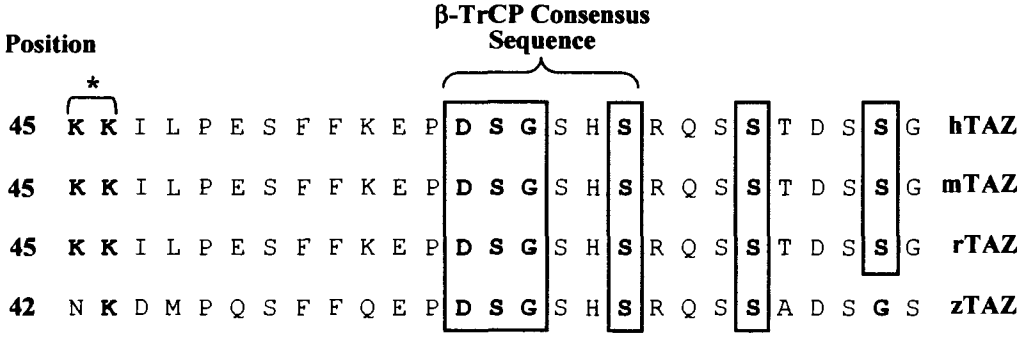

Figure 4.2- N-terminal Sequence Alignment of TAZ Orthologues. The serine residues comprising the TAZ TPM are boxed. The highly conserved β-TrCP consensus sequence (DSGSHS) is also highlighted. Putative ubiquitination sites are marked by an asterisk (*). The amino acid positions at which the alignments were initiated are indicated at left. (hTAZ, human TAZ; mTAZ, mouse TAZ; rTAZ, rat TAZ; zTAZ, zebrafish TAZ)

binding of KLF7 by β-TrCP, suggesting that their interaction is mediated by the phosphorylation of this consensus sequence. It will be interesting to determine whether sequential phosphorylation of Thr31 and Ser27, the two C-terminal TPM sites, is necessary for the putative phosphorylation events at Ser23 and Thr19, as has been shown for the phosphorylation of the β-catenin TPM [16]. In order to address the possibility of hierarchical phosphorylation at the KLF7 TPM, the integrity of the KLF7-β-TrCP interaction will be assessed using KLF7 phosphorylation mutants of Thr31 and Ser27.

The binding of β-TrCP to phosphorylated β-catenin has been shown to facilitate the degradation of β-catenin via the ubiquitin-proteasome pathway [18-21]. We provide evidence here that, like β-catenin, KLF7 also undergoes ubiquitination in a manner dependent upon its TPM. Firstly, KLF7 ubiquitination was apparent only in cells subjected to phosphatase inhibition, which suggested a link between KLF7 phosphorylation and its subsequent ubiquitination (Figure 3.12). Secondly, little to no ubiquitination was detected on KLF7 STDM, the KLF7 TPM mutant incapable of binding β-TrCP (Figure 3.13). Thus, it appears that TPM phosphorylation, specifically the phosphorylation of the sites comprising the inherent β-TrCP consensus sequence (Ser23 and Thr19), is essential for KLF7 ubiquitination. The dependence of KLF7 ubiquitination on an intact β-TrCP binding site suggests that the binding of KLF7 by β-TrCP enables the ubiquitination of KLF7 through its recruitment of the ubiquitination apparatus. Further studies are required to fully ascertain a causative relationship between β-TrCP recognition and KLF7 ubiquitination. Such studies may include an analysis of the ubiquitination state of KLF7 in response to the over-expression of an F-box deletion mutant of β-TrCP, a dominant negative mutant that cannot bind to the Skp1/Cul1 complex, but retains its capacity to bind to its substrates [67]. It will also be important to verify that the ubiquitin conjugates detected are indeed derived from KLF7 and not from other proteins capable of co-precipitating with KLF7. In order to circumvent such ambiguity in the analysis of ubiquitinated proteins, we will make use of a denaturing step

proposed by Rotin *et al.*, wherein, cell lysates are boiled in 1 – 2% SDS, prior to immunoprecipitation, to eliminate all protein-protein interactions that may lead to erroneous results [68].

Given our findings that KLF7 contains an N-terminally located TPM that is responsible for both its interaction with β-TrCP and its ubiquitination, it is tempting to suggest that KLF7 is also degraded in a manner dependent upon its TPM, analogous to the phosphorylation-dependent degradation of β-catenin [18-21]. Our initial attempts at determining whether KLF7 stability is mediated by actions at its TPM have been largely inconclusive. Timed-course analysis of cycloheximide-treated HEK 293 cells revealed the KLF7 TPM mutant, KLF7 STDM, to be fairly stable over the 12 hour time period; whereas, it appears that wild-type KLF7 may be destabilized after the 10 hour mark (Figure 3.16). The levels of wild-type KLF7 and KLF7 STDM present at time intervals extending beyond 12 hours of cycloheximide incubation must be assessed to confirm the degradation of KLF7, as well as its reliance upon the KLF7 TPM. The evaluation of KLF7 turnover will likely benefit from the utilization of a more sensitive method, such as pulse-chase analysis, which involves the tracing of radioactively labeled proteins over a defined time period following a short period of *in vivo* radioactive protein labeling. Since the analysis of protein stability requires the examination of different cell populations over time, the generation of cell lines stably expressing KLF7 and KLF7 STDM will likely limit any differences in their expression due to variations in transfection efficiency between the cell populations.

4.3.2 TAZ Binds to an $SCF^{\beta\text{-}TrCP}$ E3 Ligase Complex to Facilitate the Ubiquitin-Mediated Proteolysis of PC2

Earlier, we alluded to the presence of a consensus β-TrCP phosphodegron motif within the TAZ TPM, ^{57}DSGSHS^{62}, whose existence and conservation in TAZ

orthologues (Figure 4.2) hinted at the potential for an interaction between β-TrCP and TAZ. During the course of our analysis of the TAZ TPM, the results of a study conducted by Tian *et al.* were released, which indeed demonstrated an interaction between TAZ and β-TrCP; however, this interaction did not involve the TPM-encompassed β-TrCP consensus sequence, as we had expected, rather it occurred through the binding of β-TrCP to an atypical β-TrCP phosphodegron within the C-terminal of mouse TAZ, ^{306}STDSGLG^{312}, which corresponds to ^{311}STDSGLG^{317} of human TAZ [41]. Analysis of the novel association between TAZ and β-TrCP introduced a new functional role for TAZ, that being as an E3 ligase adapter protein. TAZ was found to serve as a scaffold protein, bringing β-TrCP within the vicinity of a second TAZ binding protein, polycystin 2 (PC2), a transmembrane protein responsible for the regulation of calcium entry into and release from the endoplasmic reticulum. The binding of PC2 and β-TrCP by TAZ enabled the β-TrCP-mediated ubiquitination of PC2, setting the stage for the subsequent proteolytic degradation of PC2 [41]. Interestingly, the kidneys of surviving TAZ knockout ($TAZ^{-/-}$) mice exhibited severe cyst formation, accompanied by an abnormal accumulation of PC2, which were both attributed to a reduction in PC2 degradation. These findings highlighted the importance of TAZ, not only in the regulation of ubiquitin-mediated PC2 proteolysis, but also in the development of proper renal structures [41].

Since β-TrCP substrate recognition has been shown to be highly dependent upon phosphorylation, the fact that Tian *et al.* did not uncover a physical association between β-TrCP and the consensus β-TrCP binding site within the TAZ TPM suggested to us that the phosphorylation of the TAZ TPM might be sensitive to dephosphorylation by unknown phosphatases. This notion was supported by our inability to detect the TAZ TPM in untreated cells through both immunoblotting (Figure 3.5) and mass spectrometry (data not shown). Thus, under conditions we had proven favorable to the phosphorylation of the TAZ TPM, we assessed whether an interaction between β-TrCP

and the TPM-contained β-TrCP consensus sequence could be unveiled. Our study within HEK 293 cells, treated with both phosphatase and proteasome inhibitors, once again demonstrated the binding of β-TrCP to the uncharacteristic binding site located in the TAZ C-terminal, while failing to reveal an association between β-TrCP and the TAZ TPM (Figure 3.11).

4.3.3 TPM Phosphorylation Facilitates TAZ Ubiquitination

Notwithstanding our findings and those published by Tian *et al.* that illustrate the functional importance of the C-terminal β-TrCP binding site, we believe that the TAZ TPM plays a critical functional role in the regulation of TAZ activities. Consistent with this hypothesis is the conservation of the TAZ TPM from lower invertebrates to more complex mammals (Figure 4.2). Of particular interest is the highly conserved nature of the putative β-TrCP binding motif found within the TAZ TPM and its resemblance to the equivalent consensus sequences in known β-TrCP substrates, such as β-catenin, IκBα, Snail, Vpu, and the newly identified KLF7 [19,65,66]. Such observations strongly imply that a common mechanism may exist for the regulation of the activities of TAZ and the aforementioned proteins. Studies have shown that the binding of β-TrCP to its substrates, including β-catenin, IκBα, and Vpu, initiates their ubiquitination, ultimately marking them for degradation by the proteasome [18-21,65,66]. Therefore, despite the lack of a detectable association between β-TrCP and the TAZ TPM, we questioned whether TAZ was also subject to ubiquitin-mediated degradation.

Within this study, we demonstrate that TAZ does indeed undergo ubiquitination in a manner dependent upon phosphorylation of its TPM, which was indicated by the detection of TAZ ubiquitination chiefly under phosphatase and proteasome inhibition, treatment conditions shown to favor TPM phosphorylation (Figure 3.14). Further evidence for the reliance of TAZ ubiquitination on its TPM was gained from the fact that

no ubiquitin adducts were found to co-precipitate with the partial TAZ TPM mutant (TAZ SDM), which contains alanine substitutions at the two serine residues comprising the putative β-TrCP binding site, Ser58 and Ser62. Although under the conditions tested the interaction between β-TrCP and TAZ does not require the TAZ TPM, this phosphomotif is essential for TAZ ubiquitination. Of course, it will be important to confirm the ubiquitination state of TAZ using the denaturing lysis protocol developed by Rotin *et al.*, as was proposed earlier for the verification of KLF7 ubiquitination [68]. However, the differential ubiquitination state of wild-type and TPM-compromised TAZ is highly suggestive of TPM-dependent TAZ ubiquitination. It will also be of interest to determine whether sequential phosphorylation of Ser70 and Ser66, the more C-terminal phosphorylation sites of the TAZ TPM, is a prerequisite for the phosphorylation of Ser62 and Ser58, which has been documented for the phosphorylation of the β-catenin TPM [16]. Future studies will examine the occurrence of hierarchical phosphorylation at the TAZ TPM through an assessment of the ubiquitination state of TAZ phosphorylation mutants containing single substitutions at the four TPM phosphorylation sites.

It is of interest to note that sequence analysis permitted the discovery of four lysine residues in the N-terminus of human TAZ that represent potential sites of ubiquitination (data not shown). Structural studies focused on delineating the mechanism underlying the lysine specificity of the E3 ligase, $SCF^{\beta\text{-}TrCP1}$, revealed the distance between the β-TrCP binding site and the targeted lysine residue as a principal determinant of ubiquitination efficiency [20]. Preferential ubiquitination has been demonstrated for lysine residues spaced 9 – 14 amino acids from the aspartate residue of the β-TrCP consensus sequence in both β-catenin and IκBα [20,21]. Intriguingly, analysis of the positions of the N-terminal lysine residues of human TAZ revealed that two of the four residues, Lys45 and Lys46, are located 11 and 12 amino acid residues, respectively, from the TPM (Figure 4.2). In future studies, it will be interesting to assess whether mutation of these Lys residues diminishes TAZ ubiquitination.

Based upon our finding that TAZ undergoes ubiquitination in response to TPM phosphorylation, we predicted that ubiquitin-conjugated TAZ is destined for degradation via the proteasome, an outcome that has been well documented for ubiquitinated β-catenin [18-21]. Through a timed-course analysis of cycloheximide-treated HEK 293 cells, we revealed both TAZ and its TPM mutant, TAZ ΔTPM, to be largely stable over the 12 hour time period (Figure 3.15). The stability of TAZ ΔTPM was anticipated, as we have shown that mutation of the TPM inhibits its ubiquitination, possibly eliminating the means by which TAZ is marked for degradation. However, the constant protein level of wild-type TAZ over the time period studied did not support our premise of ubiquitin-mediated TAZ degradation, suggesting that TPM-directed ubiquitination has no bearing on TAZ protein stability. We hesitantly report the results of this timed-course study, as an assay of the same lysates for endogenous β-catenin failed to illustrate the rapid degradation of β-catenin. The employment of more sensitive techniques, namely pulse-chase analysis, will likely prove beneficial to our examination of TAZ protein stability. As was previously discussed for our future investigations into KLF7 protein stability, it is likely that the analysis of TAZ degradation would also benefit from the development of stable TAZ and TAZ ΔTPM cell lines.

In support of the hypothesis that the ubiquitin-proteasome pathway is involved in the regulation of TAZ, we show that endogenous TAZ is only detected through anti-TAZ immunoblotting in the presence of phosphatase and proteasome inhibitors, which suggests that TAZ may be constitutively degraded *in vivo* (Figure 3.3). Furthermore, in their study of PC2 degradation, Tian *et al.* provide evidence that TAZ, like PC2, may be degraded as a result of its incorporation into the $SCF^{\beta\text{-}TrCP}$ E3 ligase complex. Mutation of Ser306 or Ser309 of mouse TAZ, the critical serine residues that comprise the C-terminal β-TrCP binding site, was found not only to abolish the binding of TAZ by β-TrCP, but also to stabilize the protein levels of TAZ [41]. Although, commented on only briefly, this preliminary result is intriguing to us, as it hints at the potential for the

regulation of TAZ by degradation, as well as links this putative regulatory mechanism to β-TrCP binding.

Since the most common method of protein degradation involves the proteasome and Tian *et al.* demonstrate that TAZ stability appears to be dependent upon β-TrCP binding, it is likely that the potential turnover of TAZ will involve the ubiquitin-proteasome system. In an attempt to mesh our findings with those published by Tian *et al.*, we have formulated a theory of TAZ degradation, which integrates TPM-dependent ubiquitination with β-TrCP binding at the C-terminal binding site on TAZ. We speculate that the putative degradation of TAZ may take place in the context of a feedback loop, where the degradation of TAZ is initiated, in order to halt the degradation of PC2 or other target proteins (Figure 4.3). It may be that during periods where PC2 degradation or the degradation of other target protein is no longer required, a signal is emitted which results in the liberation of bound β-TrCP from the TAZ C-terminal binding site and its subsequent binding to the β-TrCP consensus sequence located within the TAZ TPM. It is also possible that, instead of the same β-TrCP molecule jumping from one site to the other, a second molecule of β-TrCP may be recruited to the putative N-terminal β-TrCP binding site. Lastly, we propose that the binding of β-TrCP to the TPM-located consensus sequence will facilitate TAZ ubiquitination through its recruitment of the ubiquitination apparatus, ultimately leading to the degradation of TAZ via the proteasome. In both scenarios, the presence of β-TrCP at the C-terminal binding site is believed to be necessary for the putative binding of β-TrCP to the TPM, providing a potential explanation for the dependency of TAZ degradation on this site presented by Tian *et al.* [41].

It is obvious that future investigations will be needed to determine the mechanism of TAZ degradation. Initially, it will be important to confirm the regulation of TAZ by degradation and its dependence upon the binding of TAZ by β-TrCP at the C-terminal binding site, as the study published by Tian *et al.* provides fairly limited data on these

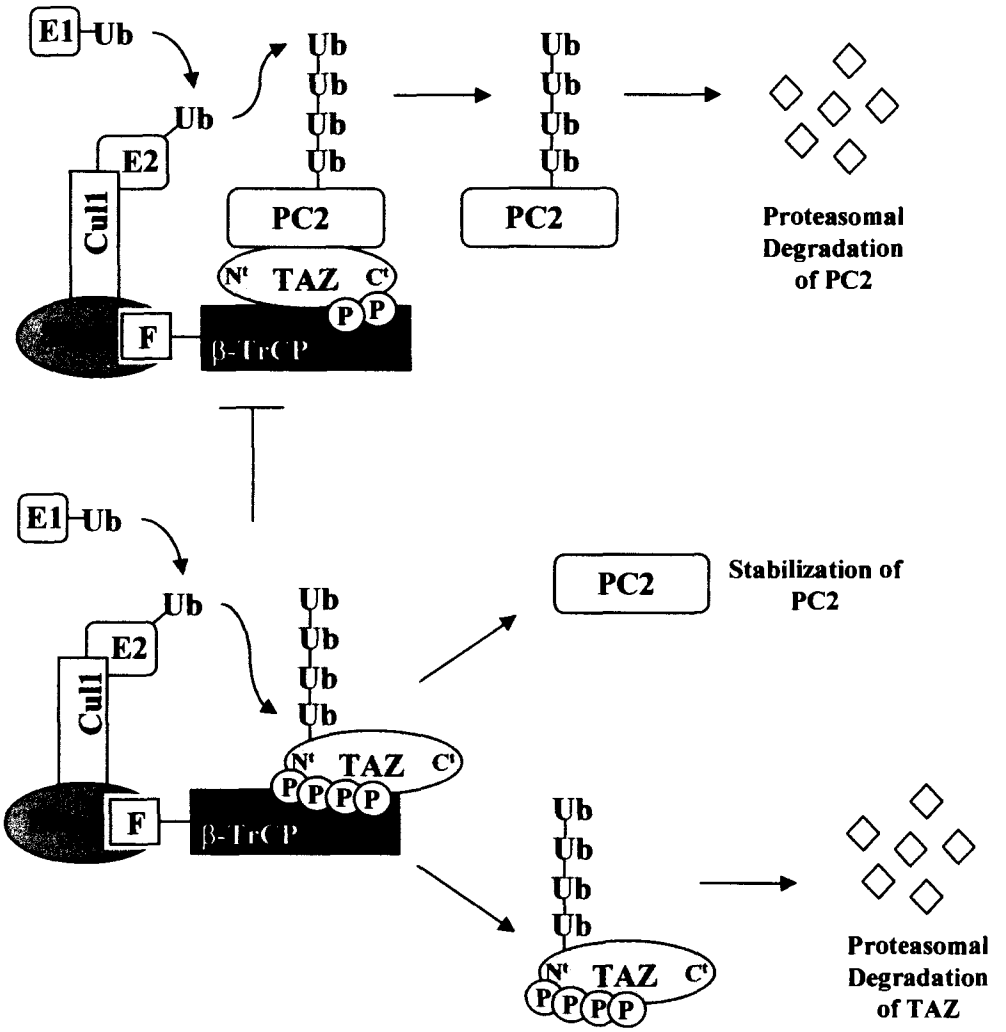

Figure 4.3- Model Depicting the Regulation of PC2 Turnover by TPM-Mediated TAZ Degradation [41]. Phosphorylation of TAZ at Ser311 and Ser314 of human TAZ facilitates the binding of β-TrCP, present within an SCF (Skp1/Cul1/F-box) complex, to an atypical β-TrCP binding site within the C-terminus (C^t) of TAZ. TAZ functions as an E3 adapter protein to bring β-TrCP within the vicinity of TAZ-bound PC2, facilitating the poly-ubiquitination and proteasomal degradation of PC2 [41]. Our theory suggests that during periods where PC2 stabilization is favored, the phosphorylation of the TAZ TPM is induced, generating a docking site for β-TrCP within the N-terminus (N^t) of TAZ. This event initiates the release of PC2 from the destruction complex and results in the ubiquitination and proteasomal degradation of TAZ. (E1, ubiquitin (Ub)-activating enzyme; E2, ubiquitin (Ub)-conjugating enzyme)

subjects [41]. Given that we are able to verify these results, likely through pulse-chase analysis with wild type TAZ and TAZ $C^t\Delta DSG$, we next want to reassess the effect of the TPM on the stability of TAZ using an identical approach with wild type TAZ and TAZ ΔTPM, as we proposed earlier. Finally, we intend to characterize the relationship between the C-terminal β-TrCP binding site and the TAZ TPM to determine whether the ubiquitination of TAZ is dependent upon β-TrCP binding at the TAZ C-terminal. This study will involve a comparison of the ubiquitination states of wild type TAZ and TAZ $C^t\Delta DSG$, the TAZ mutant harboring serine to alanine substitutions at the critical residues of the C-terminal β-TrCP binding site.

Interestingly, a fairly recent study has revealed that another E3 ligase adapter protein is itself degraded in the context of the degradation complex that it is responsible for assembling. Virus protein U (Vpu) is an integral membrane protein of the human immunodeficiency virus type 1 (HIV-1) that has been implicated in the degradation of CD4, the cell-surface co-receptor targeted by HIV particles for entrance into the host cell [1,66]. Vpu mediates the degradation of newly synthesized CD4, present within the endoplasmic reticulum (ER), by binding both CD4 and human β-TrCP, ultimately facilitating the association of CD4 with the E3 ligase, $SCF^{\beta\text{-}TrCP}$. As a result of its interaction with β-TrCP, CD4 is ubiquitinated and degraded by the host cell proteasome [66]. The ability of Vpu to function as an E3 ligase adapter has long been recognized; however, only recently was Vpu discovered as a bona fide β-TrCP substrate. It was found that the binding of β-TrCP to the Vpu phosphorylation motif, ^{51}DpSGNEpS^{56}, also resulted in the ubiquitination of Vpu and in its subsequent degradation by the proteasome [66]. Since CD4 degradation is linked to enhanced virion release and is thus, necessary to ensure viral propagation, it is thought that by halting the down-regulation of CD4 through the degradation of Vpu, the host cell can attempt to combat the progression of the virus [66]. All in all, the discovery of such a degradation mechanism tied to the

regulation of an E3 ligase adapter protein supports our proposition that TAZ may also be regulated in such a manner.

4.3.4 The TAZ TPM Influences the Critical Regulatory Interaction Between TAZ and 14-3-3

The human 14-3-3 protein family is comprised of seven highly conserved isoforms, denoted β, ε, γ, η, σ, τ, and ζ, that have been implicated in numerous cellular signaling pathways, including those that govern cell cycle progression, apoptosis, and transcription [69]. 14-3-3s are ubiquitously expressed, 30 kDa acidic proteins that engage in both homo- and heterodimer formation to enable ligand binding. In most cases, phosphorylation of the target protein is a pre-requisite for 14-3-3 binding, as each of the 14-3-3 monomers contains a phosphoserine/phosphothreonine-binding pocket [69]. The function of 14-3-3 binding is to regulate the target protein through an alteration of its behavior, which includes its conformation, protein-protein interactions, and intracellular localization [69].

As we alluded to earlier, TAZ was identified in an *in vitro* screening for proteins capable of interacting with 14-3-3 [42]. This study, conducted by Kanai *et al.*, revealed that 14-3-3 binding resulted in the retention of TAZ within the cytoplasm and was dependent upon the phosphorylation of TAZ on Ser89 [42]. Moreover, the 14-3-3-mediated cytoplasmic sequestration of TAZ was shown to inhibit the transcriptional co-activity of TAZ, as it effectively reduces the amount of TAZ present in the nucleus [42]. Interestingly, TAZ also contains a consensus PDZ-binding motif within its C-terminal, whose influence on TAZ localization was found to oppose that of 14-3-3. Mutational analysis illustrated the PDZ-binding motif to be responsible for localizing TAZ both to the nucleus, in the form of discrete foci, and to the plasma membrane. This motif was shown to be necessary for the transcriptional co-activation abilities of TAZ, a finding that

can likely be explained by the fact that it directs TAZ to the nucleus [42]. Based upon their results, Kanai *et al.* depict the regulation of TAZ localization as a competition between PDZ-mediated membrane and nuclear targeting and the cytoplasmic sequestration of TAZ by 14-3-3 proteins [42]. Although, the intricacies of TAZ regulation remain to be elucidated, it does appear that a major means of directing TAZ function is through control of its spatial orientation.

In light of the critical role of 14-3-3 in the regulation of TAZ and in an attempt to establish the function of the TAZ TPM, we questioned whether there existed a connection between the TPM and the binding of TAZ by 14-3-3. Through co-immunoprecipitation analysis, we were able to show that serine to alanine substitutions of the critical TPM residues abolished the interaction between 14-3-3 and TAZ in 3T3-L1 preadipocyte cells (Figure 3.17). The inability of the TPM mutant of TAZ (TAZ ΔTPM) to associate with 14-3-3 indicates that events occurring at the TPM, likely phosphorylation, make possible the binding of TAZ by 14-3-3. One possible scenario explaining the influence of the TAZ TPM on 14-3-3 binding depicts the phosphorylation of the TAZ TPM as a priming event for the phosphorylation of Ser89. This theory suggests that TPM phosphorylation enhances Ser89 phosphorylation in some manner, possibly through a favorable change in TAZ conformation (Figure 4.4A). Considering our identification of Ser93 as a TAZ phosphorylation site, a second putative scenario can be contrived. We show that, despite the presence of Ser89 and an intact TPM, 14-3-3 cannot interact with TAZ S93D, a TAZ mutant that mimics constitutive phosphorylation on Ser93 (Figure 3.31). This finding provides evidence that the phosphorylation of TAZ at Ser93 inhibits the binding of 14-3-3. Thus, it may be that TPM phosphorylation promotes TAZ recognition by 14-3-3 through inhibition of Ser93 phosphorylation or promotion of Ser93 dephosphorylation (Figure 4.4B).

In order to confirm the dependence of 14-3-3 binding on the TAZ TPM, we intend to determine whether the subcellular localization of the TAZ TPM mutant (TAZ

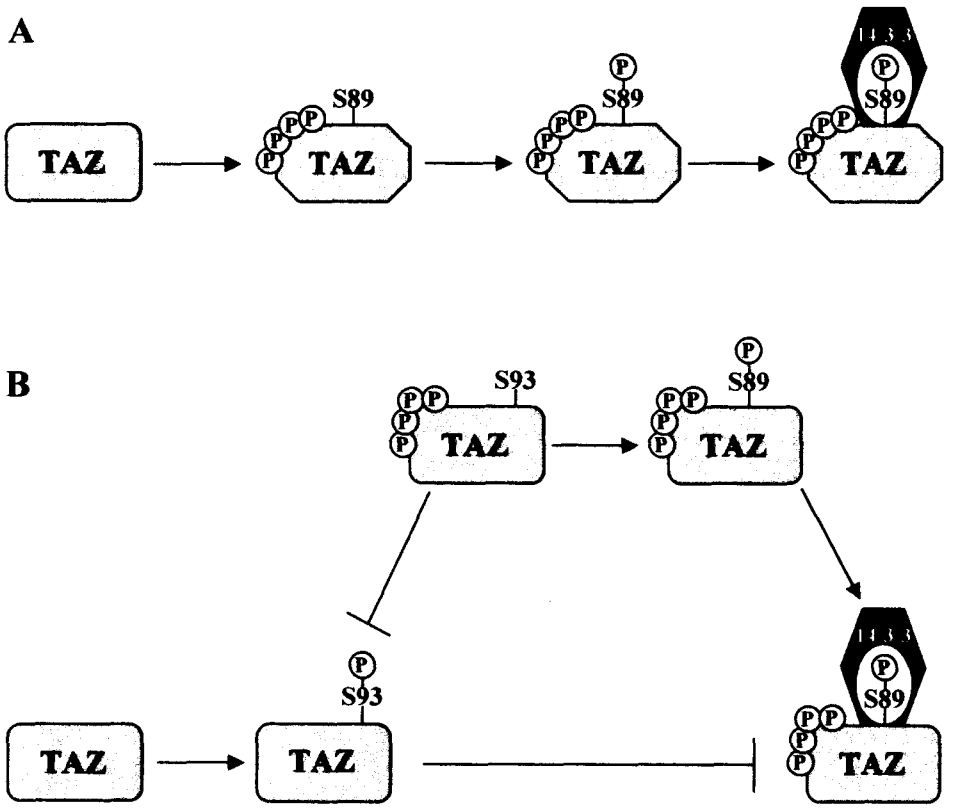

Figure 4.4- Models Illustrating the TPM-Dependence of 14-3-3 Binding of TAZ. 14-3-3 binding of TAZ is dependent upon the phosphorylation of TAZ on Ser89 (S89). **(A)** One scenario suggests that the phosphorylation of TAZ at the TPM induces a conformational change in TAZ that enhances the phosphorylation of Ser89. **(B)** Another possibility involves the negative regulatory phosphorylation site, Ser93 (S93). TAZ phosphorylated on Ser93 resists 14-3-3 binding. Thus, phosphorylation of the TAZ TPM might oppose Ser93 phosphorylation or promote the dephosphorylation of Ser93. The absence of phosphorylated Ser93 may make possible the phosphorylation of Ser89 or may unmask a previously phosphorylated Ser89.

ΔTPM) matches that of TAZ S89A, the TAZ mutant that is known to escape 14-3-3 binding. In future studies, we also want to further prove that the influence of the TPM on the association of 14-3-3 with TAZ is indeed a result of TPM phosphorylation. Serine to glutamate/aspartate substitutions of the TPM residues, which will mimic a constitutively phosphorylated TAZ TPM, will likely make this study possible. As our studies were conducted with TAZ ΔTPM, which contains serine to alanine substitutions at each of the four TPM residues, it will also be important to ascertain whether the binding of 14-3-3 is dependent upon all four TPM residues or is merely influenced by the residues located in closest proximity to Ser 89 and/or Ser93. Furthermore, it may be possible to elucidate the effect of the TAZ TPM on 14-3-3 binding by analyzing the phosphorylation states of both Ser89 and Ser93 in response to over-expression of a mutant form of TAZ containing a constitutively phosphorylated TPM. In the instance that our first theory holds true, Ser89 phosphorylation would be expected to increase as a result of the over-expression of the aforementioned TAZ mutant. If our second scenario were valid, the level of Ser89 phosphorylation would still be expected to increase; however, it would be accompanied by a decrease in Ser93 phosphorylation. The monitoring of TAZ phosphorylation at Ser89 and Ser93 could be conducted using phosphoantibodies or mass spectrometry.

Since we have also shown that the TPM governs the ubiquitination of TAZ, it is tempting to speculate that the binding of TAZ by 14-3-3 may be linked in some manner to this ubiquitination. One possibility involves the 14-3-3-mediated export of TAZ from the nucleus, followed by its ubiquitination and proteasomal degradation in the cytoplasm. Such a scheme has been implicated in the regulation of the protein levels of the FOXO proteins, a group of transcription factors implicated in the cellular response to growth signals and nutrients, oxidative stress, and genomic damage [70]. The activities and fates of the FOXO proteins are dictated by specific post-translational modifications, which are induced by various extracellular signals [70]. Most interesting to our study is the phosphorylation of nuclear FOXO by various kinases in response to growth signaling,

which favors the inactivation of FOXO-mediated gene expression. Multisite phosphorylation has been shown to facilitate the nuclear export of FOXO through the actions of a series of inhibitory phosphorylations that culminate in the binding of FOXO by 14-3-3 and the exportin, CRM1 [70]. 14-3-3- and CRM1-bound FOXO is escorted to the cytoplasm, where it engages with an E3 ligase and is consequently ubiquitinated, targeting it for proteasomal degradation [70]. Relating our findings that the TAZ TPM is required for both its ubiquitination and 14-3-3 binding with the regulation of FOXO degradation described above suggests that TPM phosphorylation of nuclear TAZ sets the stage for its association with 14-3-3. The binding of 14-3-3 to nuclear TAZ has previously been shown to promote the export of TAZ from the nucleus [42]. Once in the cytoplasm, TAZ may engage with β-TrCP and as a result be subjected to ubiquitination in a manner dependent upon the TPM. Finally, ubiquitinated TAZ may then be targeted to the proteasome for degradation.

The signal-dependent inactivation of the cell cycle phosphatase, Cdc25C, provides the basis for our second hypothesis concerning the potential interplay of TAZ ubiquitination and 14-3-3 binding. While our first proposition introduced the possibility that the binding of TAZ by 14-3-3 and TAZ ubiquitination occur consecutively, this theory suggests that these two events take place in an isolated fashion. Through dephosphorylation and thus, activation, of the cyclin-dependent kinase Cdc2/cyclin B1 complex, Cdc25C progresses the cell cycle into mitosis [71]. Cdc25C activity is heavily influenced by phosphorylation, especially phosphorylation of Ser216, which has been implicated in two distinct mechanisms of Cdc25C inactivation. Cdc25C inactivation is imperative to the induction of G2 arrest in situations where entry into mitosis would be unfavorable [71]. Firstly, in response to DNA damage, Ser216 phosphorylation facilitates the binding of Cdc25C by 14-3-3, which results in the inactivation of Cdc25C through cytoplasmic sequestration. The second means of Cdc25C inactivation is dependent upon the induction of G2 arrest by the tumor suppressor protein, $p14^{ARF}$. In

this case, the phosphorylation of Cdc25C on Ser216 promotes the ubiquitination and proteasomal degradation of Cdc25C [71]. In each of these cases, Ser216 phosphorylation is catalyzed by a different kinase, indicating that the method of Cdc25C inactivation is mediated by the activation of specific signaling pathways. Most interesting to us, is the fact that phosphorylation of a single site can elicit two responses depending upon the upstream kinases. It is thought that the existence of two modes of Cdc25C inactivation enables the cell to both initiate (cytoplasmic sequestration) and maintain (proteasomal degradation) G2 arrest [71]. In line with this notion for the dual functionality of Ser216 phosphorylation, it can be hypothesized that the TPM-dependent binding of TAZ by 14-3-3 may provide a temporary inhibition of TAZ transcriptional co-activation through its exclusion from the nucleus, while the TPM-mediated ubiquitination of TAZ may serve to sustain the inhibition of TAZ-related gene expression through TAZ degradation.

Our understanding of the role of the TPM in the regulation of TAZ will likely benefit from future investigations focused on elucidating whether either of the theories outlined above are applicable. In order to determine if the ubiquitination of TAZ is dependent upon its binding by 14-3-3, we intend to analyze the ubiquitination state of the TAZ mutant that is incapable of interacting with 14-3-3 (TAZ S89A). Given that the turnover of TAZ is the result of its ubiquitination, it would also be interesting to assess whether the stability of TAZ is ultimately dictated by its ability to interact with 14-3-3. Long-term studies dedicated to identifying the kinase, or kinases, responsible for phosphorylating the TAZ TPM will be important, as such information will allow us to ascertain whether the implicated signaling pathway(s) favor the binding of TAZ by 14-3-3 and/or the ubiquitination of TAZ. This knowledge will ultimately enable us to determine if these TPM-mediated events are directly related, in a manner resembling the turnover of the FOXO proteins, or are distinct from one another, as observed in the regulation of Cdc25C.

Interestingly, the dependence of 14-3-3 binding on the TAZ TPM appears to be somewhat cell-type specific. Where the TAZ TPM mutant, TAZ ΔTPM, completely escapes 14-3-3 binding within 3T3-L1 preadipocyte cells, we show that, within HEK 293 cells, TAZ ΔTPM retains its capacity to bind to 14-3-3, albeit to a lesser degree than wild-type TAZ (Figures 3.17, 3.18). This variation in the dependence of 14-3-3 binding of TAZ on the TPM suggests that certain signaling pathways targeting TAZ may not be as prevalent within HEK 293 cells as they are in 3T3-L1 cells. For example, given our hypothesis that Ser93 phosphorylation interferes with 14-3-3 binding, it is possible that the kinase responsible for this phosphorylation event may be down-regulated in HEK 293 cells. In this instance, the TPM would have limited bearing upon the 14-3-3 binding of TAZ, as it would not be required to inhibit the phosphorylation of Ser93, as would be the case in 3T3-L1 cells. As TAZ has been implicated in the inhibition of adipocyte differentiation [45], 3T3-L1 cells are more physiologically relevant, suggesting that the TPM-mediated 14-3-3 binding of TAZ may be a physiological event. With this in mind, it will be intriguing to determine whether the interaction between TAZ and 14-3-3 occurs in a TPM-dependent manner in other TAZ-relevant cell lines, including osteoblasts, myoblasts, mesenchymal stem cells (MSCs), and lung epithelial cells [45,48,49,52].

4.4 Functional Characterization of the TAZ and KLF7 TPMs

TAZ, KLF7, and β-catenin have all been shown to function as transcriptional mediators in the regulation of adipogenesis, the process by which pluripotent mesenchymal stem cells (MSCs) differentiate into lipid-storing adipocytes [72]. This functional parallel between the archetype TPM protein, β-catenin, and the newly identified TPM proteins, TAZ and KLF7, is intriguing, as it offers the possibility that common regulatory mechanisms afforded through their respective TPMs govern the progression of adipogenesis.

Interestingly, studies have revealed that adipogenesis is sensitive to the protein levels of β-catenin, highlighting the importance of its TPM in adipocyte differentiation, as TPM phosphorylation directs the ubiquitin-mediated degradation of β-catenin [18-21]. Firstly, the over-expression of a β-catenin TPM mutant (β-catenin S37A), which is capable of escaping ubiquitination and degradation because of a compromised β-TrCP binding site, was found to reduce the degree of adipocyte differentiation in mouse fibroblast cells [44]. Secondly, treatment with lithium chloride (LiCl), an inhibitor of GSK3β, inhibited the ability of adipose-derived MSCs (AMSCs) to differentiate into adipocytes, while stimulating osteogenesis [73]. This inhibition of adipogenic differentiation potential was attributed to the stabilization of cytoplasmic β-catenin through the inhibition of GSK3β, one of the kinases responsible for phosphorylating the β-catenin TPM.

4.4.1 KLF7 Inhibits Adipogenesis in Preadipocyte Cell Lines

Much of the research conducted on KLF7 to date has been focused on its transcriptional activities during neurogenesis; however, recent years have seen the introduction of KLF7 as a transcriptional mediator of adipogenesis [46,47,74]. In two separate studies, KLF7 over-expression was shown to reduce the adipogenic potential of both human and mouse preadipocyte cells [46,47]. In the present study, we reproduced the results first published by Maeda *et al.*, which revealed the inhibition of adipogenesis by the over-expression of KLF7 within mouse 3T3-L1 preadipocyte cells [46]. In an extension of the previous investigation, we analyzed the effect of the KLF7 TPM mutant (KLF7 STDM) on preadipocyte differentiation (Figure 3.20). Our results revealed that by compromising the integrity of its TPM, the inhibitory capacity of KLF7, in the context of adipogenesis, could be heightened, suggesting a role for the TPM in the regulation of adipogenesis by KLF7. The possibility that KLF7, like β-catenin, may be regulated by

TPM-dependent degradation provides a putative explanation for its inhibition of adipogenic differentiation, whereby the steady state levels of KLF7 control the degree of adipocyte differentiation. The existence of such a regulatory strategy suggests that the stabilization of KLF7, possibly through inhibition of the associated kinase(s) or another member of the degradation machinery, leads to a reduction in adipocyte differentiation; whereas, under conditions favoring adipocyte formation, KLF7 would be constitutively degraded in response to phosphorylation of its TPM. A recent study interested in elucidating the pro-adipogenic mechanisms of catechins, a form of polyphenol flavenoids present in green tea, provides support for our hypothesis concerning the relation between KLF7 protein levels and adipogenic progression. Within their investigation, Cho *et al.* demonstrated that a reduction in KLF7 protein levels due to (-)-catechin treatment of 3T3-L1 preadipocyte cells was accompanied by a dramatic increase in adipogenesis [74]. Taken together, these findings largely suggest that KLF7 protein levels govern the adipogenic differentiation potential of preadipocyte cells, heightening our interest in determining whether phosphorylation of the KLF7 TPM enables the degradation of KLF7.

4.4.2 TAZ Governs Mesenchymal Stem Cell Differentiation

In an eloquent study conducted by Hong *et al.*, TAZ was identified as a critical transcriptional regulator of mesenchymal stem cell (MSC) differentiation. MSCs are capable of differentiating into several distinct cell types, including osteoblasts and adipocytes, whose formation is chiefly driven by the opposing activation of the transcription factors, Runx2 and peroxisome proliferator-activated receptor γ (PPARγ), respectively [45]. By modulating the expression of TAZ, in both model cell lines and in a more physiological context, TAZ was found to co-activate the transcription of Runx2-driven genes, while it repressed the expression of PPARγ-dependent genes. In

accordance with its aforementioned functions, TAZ over-expression was found to promote osteoblast formation, while simultaneously inhibiting the adipogenic differentiation program [45]. These findings were further supported through a series of knock-down experiments where the reductions in TAZ expression coincided with enhanced adipocyte levels and impaired osteogenic differentiation [45]. Thus, it appears that MSC fate determination is largely dependent upon the availability of transcriptionally active TAZ. As we have proposed that phosphorylation-induced activities at the TAZ TPM may contribute to the degradation of TAZ, we believe that in this way the TPM may influence the transcriptional abilities of TAZ in MSC differentiation.

Within the present study, we focused on the TAZ-mediated inhibition of the adipocyte differentiation program. We confirmed the finding published by Hong *et al.*, which revealed that the over-expression of TAZ results in a reduction of the adipogenic capacity of mouse 3T3-L1 cells (Figure 3.19). More importantly, we provide evidence that the TPM does indeed impact the TAZ-mediated inhibition of adipogenesis, as over-expression of the TAZ TPM mutant, TAZ SDM, reduced adipocyte differentiation to a degree far below that observed for wild-type TAZ. By correlating these results with our hypotheses of TPM-mediated TAZ degradation, we can contrive a possible model to explain the role of the TAZ TPM in its inhibition of adipogenesis. This proposition suggests that, in response to adipogenic stimuli, TAZ may be constitutively degraded in a manner dependent upon phosphorylation of its TPM; whereas TAZ stabilization, like that of β-catenin, may lead to its translocation into the nucleus, facilitating its repression of the adipogenic transcriptional program. In future studies, it will be interesting to determine whether the putatively more stable TAZ TPM mutant will exhibit predominant nuclear localization, as is observed for stabilized β-catenin [75]. Such a finding would further validate our hypothesis of TPM-dependent TAZ degradation and its contribution to the regulation of TAZ-mediated adipogenic inhibition.

Of course, we cannot dismiss the possibility that the effect of the TAZ TPM on adipogenesis may be related to its involvement in the interaction with 14-3-3. The transcriptional co-activation abilities of TAZ are known to be limited by its interaction with 14-3-3, as 14-3-3 binding results in the exclusion of TAZ from the nucleus [45]. Thus, our finding that, within 3T3-L1 preadipocyte cells, this interaction is reliant upon an intact TPM suggests a second possible model explaining the influence of the TAZ TPM on the inhibition of adipocyte differentiation, whereby the nuclear localization of TAZ dictates the progression of adipogenesis. Such a regulatory scheme suggests that reduced nuclear export of TAZ, as a result of a disruption of the TPM-dependent association between TAZ and 14-3-3, leads to the inhibition of adipogenic differentiation; whereas, adipocyte formation is favored by the TPM-mediated, 14-3-3-dependent cytoplasmic sequestration of TAZ. Lastly, it will be interesting to assess whether the TPM-afforded control of the transcriptional functions of both KLF7 and TAZ, observed within adipogenesis, will translate into other systems where the transcriptional influence of these proteins has been implicated. Such a feat would be possible through the employment of reporter assays, using the promoter regions of known KLF7 target genes, as well as those of genes bound by transcription factors that are mediated by TAZ. Such a study would allow us to determine the prevalence of TPM-mediated regulation in the control of TAZ and KLF7 transcriptional activities.

4.4.3 TPM-Mediated Inhibition of Adipocyte Differentiation by β-catenin, TAZ, and KFL7 Converges on PPARγ-Driven Gene Transcription

The transcriptional control of adipogenesis, afforded through the collaborative efforts of numerous transcriptional regulators, has been extensively studied. In brief, early adipogenic transcription factors, namely CCAAT/enhancer-binding protein (C/EBP) β and C/EBPδ, are induced, which relay the adipogenic signal through

activation of a second transcriptional regulator, peroxisome proliferator-activated receptor γ (PPARγ). PPARγ functions to induce the expression of yet another transcription factor, C/EBPα, which in turn serves to stimulate the transcription of PPARγ, initiating a mutual activation loop, where PPARγ and C/EBPα positively regulate the transcription of one another [76]. As we mentioned earlier, β-catenin, TAZ, and KLF7 have all been shown to inhibit the adipogenic differentiation program. Intriguingly, although they likely function within distinct signaling pathways, the contributions of these three TPM-containing transcriptional mediators to the inhibition of adipocyte differentiation converge on the same transcriptional regulator, PPARγ. Through studies in a human preadipocyte cell line, KLF7 was found to inhibit adipogenesis at a level downstream of C/EBPβ and C/EBPδ by reducing the expression of both PPARγ and C/EBPα [47]. β-catenin has also been shown to inhibit adipogenic differentiation through its interference of the activities of the master adipogenic regulators, PPARγ and C/EBPα [73]; whereas, through a direct interaction with PPARγ, TAZ was shown to repress PPARγ-driven gene transcription [45]. This mutual targeting of PPARγ by three distinct proteins looks to provide a high level of regulation dictating the progression of adipogenesis, with each leg of this regulatory team acting upon PPARγ in a different manner and in response to a different extracellular signal.

4.4.4 Aberrant Control of TPM-Dependent Inhibition of Adipogenesis May Contribute to Insulin Resistance

The possibility that β-catenin, TAZ, and KLF7 are all regulated by a similar mechanism centered upon their TPMs provides a common theme for these otherwise unrelated transcriptional regulators. The involvement of these three TPM-containing proteins in adipocyte differentiation has been shown to be influenced by their TPMs, suggesting a possible role for the TPM in this pathway and potentially implicating this

regulatory scheme in various obesity-related diseases, namely type 2 diabetes. The pathogenesis of type 2 diabetes is primarily characterized by the existence of insulin resistance in peripheral tissues. Thought to be a secondary effect of insulin resistance, an impairment of insulin biosynthesis and/or secretion is also often detected in patients with this metabolic disorder [46]. A definite relationship has been shown to exist between type 2 diabetes and obesity, revealing adipose tissue as an organ contributing to the onset and severity of this disease. One key function of mature adipocytes is their storage of fuel in the form of lipids, which protects non-adipose organs from the deleterious effects of lipid accumulation [77]. Extensive lipid deposition in non-adipose organs, namely the heart, liver, and pancreas, can disable and destroy the cells of these organs, eventually leading to their insulin resistance. Compromising adipogenic storage capacity through a disruption of adipogenesis increases the deleterious accumulation of lipids in non-adipose tissues [77]. In this manner, deregulated TPM-mediated inhibition of adipocyte differentiation may contribute to the development of peripheral tissue insulin resistance, as the stabilization of β-catenin and the proposed stabilization of TAZ and KLF7 would lead to a pronounced reduction in adipocyte differentiation, thereby effectively limiting the adipogenic capacity of adipose tissue.

A second means by which the TPM-mediated regulation of β-catenin, TAZ, and KLF7 may contribute to the pathogenesis of type 2 diabetes involves a potential impairment of adipocyte function. Adipose tissue secretes various hormones and cytokines that regulate metabolism in other tissues. Studies revealed that β-catenin stabilization, as well as KLF7 over-expression, inhibited the expression and secretion of adiponectin, an adipocyte-specific hormone that enhances insulin sensitivity and adipocyte differentiation of peripheral tissues [44,47,74]. KLF7 over-expression was also linked to the augmentation of interleukin-6 (IL-6) expression and excretion, an adipocytokine known to reduce insulin sensitivity [47]. As a result of its role in the regulation of adipogenesis, which is largely dependent on its protein levels, the targeting

of β-catenin signaling has been proposed as a potential therapy for obesity and its related disorders. Thus, it is possible that with further elucidation of the roles of the TPM in the regulation of TAZ and KLF7, specifically within the context of adipocyte differentiation, a better understanding of the biology and pathology of adipose tissue may be achieved, ultimately enabling the development of anti-obesity and anti-diabetes therapies that target TAZ and KLF7 through their TPM-dependent regulatory mechanisms.

PART II) A Comprehensive Analysis of TAZ Phosphorylation Sites

During the course of our study, anti-FLAG immunoblot analyses reproducibly revealed a slower migrating form of exogenous TAZ in response to phosphatase and/or proteasome inhibition (Figure 3.5, 3.7, 3.14). We show that this change in TAZ mobility is likely attributable to its phosphorylation, as alkaline phosphatase incubation nearly abolished the observed mobility shift of treated FLAG-TAZ (Figure 3.21). Since its discovery, TAZ has been routinely cited as a heavily phosphorylated protein [42,43,78]. However, very little information has actually been published corroborating this claim. To the best of our knowledge, only three TAZ phosphorylation sites have been identified: Ser89, Ser311, and Ser 314 of human TAZ [41-43]. Phosphorylation of TAZ at Ser89 is known to facilitate 14-3-3 binding, while the phosphorylation of both Ser311 and Ser314 mediates the binding of the TAZ C-terminal by the WD40-containing F-box protein, β-TrCP. Both Ser89 and Ser311 have been shown to be phosphorylated by the Lats tumor suppressor kinase, which functions within the Hippo pathway to govern cell proliferation and tumorigenesis [43].

Given the possibility that TAZ is a highly phosphorylated protein, it may be that the key to understanding the molecular details of TAZ regulation, which remain largely undetermined, lies within the identification and characterization of its multiple phosphorylation sites. Thus, with this in mind, we conducted a comprehensive analysis

of *in vivo* TAZ phosphorylation sites using mass spectrometry. Our efforts lead to the detection of 5 distinct phosphopeptides (Figure 3.22), on which, we identified 7 TAZ phosphorylation sites (Figures 3.23-3.29, Table 3.1). Mapping each of these phosphorylation sites to their location along TAZ roused our interest in two particular sites: Ser93 and Ser117 of human TAZ (Figure 3.30). The identification of Ser93 and Ser117 as TAZ phosphorylation sites intrigued us in light of their proximity to two critical TAZ regions, the 14-3-3 binding site and the TAZ WW domain, respectively.

4.5 TAZ Phosphorylation on Ser93 Affords a Means of Regulating 14-3-3 Binding

Earlier, we discussed the importance of 14-3-3 binding to the regulation of TAZ. Briefly, the phosphorylation-dependent binding of TAZ by 14-3-3, which requires the phosphorylation of TAZ on Ser89, results in the cytoplasmic retention of TAZ. Consequent to its nuclear exclusion, the ability of TAZ to co-activate transcription is hindered [42]. Owing to the critical nature of Ser89 phosphorylation to this interaction, our identification of Ser93 as a TAZ phosphorylation site piqued our interest, as the location of Ser93, immediately upstream of Ser89, suggested a putative relationship between these two TAZ phosphorylation sites. Thus, within this study, we initiated a functional analysis of Ser93 phosphorylation and provide evidence that this phosphorylation event does indeed influence the association between TAZ and 14-3-3. We show that substitution of Ser93 with an aspartic acid residue (TAZ S93D), which produces a TAZ mutant mimicking constitutive phosphorylation on Ser93, inhibits the binding of TAZ by 14-3-3; whereas, the alanine mutant of Ser93 (TAZ S93A) has no bearing on the interaction of TAZ and 14-3-3 (Figure 3.31). These findings illustrate that, in some manner, the phosphorylation of Ser93 blocks the phosphorylation-dependent recognition of TAZ by 14-3-3. This phosphorylation event may be a putative regulatory strategy, providing the cell with an additional means of governance over the

binding of TAZ by 14-3-3. Importantly, the amino acid sequence surrounding the 14-3-3 binding site of TAZ, including Ser93, is highly conserved throughout various TAZ orthologues (Figure 4.5). Moreover, equivalent phosphorylation sites to Ser93 are also found to be conserved within the human (Ser131), mouse (Ser116), and chicken (Ser130) orthologues of the TAZ paralogue, YAP. The highly conserved nature of Ser93 provides further evidence supporting the importance of this phosphorylation site to, not only the regulation of TAZ by 14-3-3, but also to the modulation of other 14-3-3 binding partners, such as YAP.

In the near future, we intend to confirm the Ser93 phosphorylation-dependent disruption of the association between TAZ and 14-3-3 through immunofluorescence. We expect the TAZ S93D mutant to exhibit a predominantly nuclear pattern of localization, akin to that observed for the TAZ S89A mutant, as both TAZ mutants resist 14-3-3 binding [42]. Since a potential means of governing the binding of TAZ by 14-3-3 is disrupted in the TAZ S93A mutant, we would expect this TAZ mutant to associate to a higher degree with 14-3-3, thereby promoting its sequestration in the cytoplasm. It will also be interesting to determine whether there exists a correlation between Ser93 phosphorylation and the ability of TAZ to influence adipocyte differentiation within 3T3-L1 cells. We hypothesize that, based upon its ability to escape 14-3-3 binding and localize to the nucleus, the TAZ S93D mutant would reduce adipocyte differentiation to a level below that of wild-type TAZ; whereas, the TAZ S93A mutant may not be able to inhibit adipogenesis as strongly as wild-type TAZ, as it is likely to be present primarily within the cytoplasm. Finally, it may also be of interest to assess whether this Ser93-depdendent regulation of 14-3-3 binding is functional within other systems in which TAZ has been implicated. Such analyses will likely rely on co-immunoprecipitation and immunofluorescence experiments in physiologically relevant cell lines, as well as the employment of luciferase reporter assays, wherein the transcriptional co-activity of TAZ

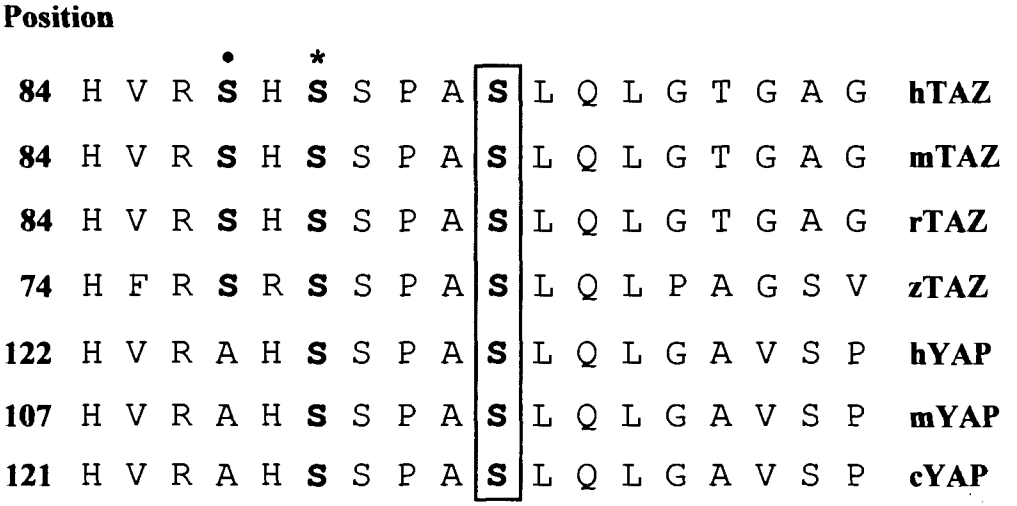

Figure 4.5- Sequence Alignment of Human TAZ with Orthologues of TAZ and YAP Illustrates the Conservation of Ser93. Ser93 of human TAZ and its equivalent serine residues are boxed. The serine residues responsible for the 14-3-3 binding of TAZ and YAP are highlighted with an asterisk (*). The serine residue located at the -2 position relative to the 14-3-3 binding site of TAZ is marked with a dot (•). The amino acid positions at which the alignments were initiated are indicated at left. (hTAZ, human TAZ; mTAZ, mouse TAZ; rTAZ, rat TAZ; zTAZ, zebrafish TAZ; hYAP, human YAP; mYAP, mouse YAP; cYAP, chicken YAP)

will be measured by its ability to promote the expression of luciferase driven by transcription factors known to interact with TAZ.

It may be possible to explain the inhibitory effect of Ser93 phosphorylation on the 14-3-3 binding of TAZ using a model whereby the phosphorylation of Ser93 antagonizes the successive phosphorylation of Ser89. Such a scenario has been shown to govern the activation of the cell cycle phosphatase, Cdc25C [79]. As outlined previously, Cdc25C functions to enable mitotic entry through activation of the mitosis-promoting kinase, Cdc2. Throughout interphase and in response to DNA damage, Cdc25C is maintained in an inactive state through phosphorylation on Ser216. This phosphorylation event affords the negative regulation of Cdc25C by facilitating its binding by 14-3-3. Within mitotic cells, however, the inhibitory phosphorylation of Cdc25C on Ser216 is prevented through its phosphorylation on Ser214. This dual phosphorylation mechanism provides a means to ensure that Cdc25C remains active during mitosis by eliminating the potential for Ser216 phosphorylation [79].

Based on the fact that, during our global analysis of TAZ phosphorylation sites, we detected the TAZ peptide ^{87}SHSSPASLQLGTGAGAAGSPAQQHAHLR^{114} in multiply phosphorylated forms (Figure 3.20, 3.26A), it may be more probable to hypothesize that both Ser89 and Ser93 can simultaneously exist in a phosphorylated form. Correlating this theory with our finding that Ser93 phosphorylation inhibits the binding of TAZ by 14-3-3 suggests that phosphorylated Ser93 conceals the 14-3-3 binding site centered at phosphorylated Ser89. In this instance, the dephosphorylation of Ser93 is thought to be a prerequisite for the binding of TAZ by 14-3-3, as it could alter the conformation of TAZ, unveiling the 14-3-3 binding site. Regulation of the activity of the tumor-suppressing transcription factor, p53, provides an example of the aforementioned mechanism [80]. Under normal cellular conditions, p53 is retained in a lowly active state through phosphorylation on both Ser376 and Ser378. In response to genotoxic stress, p53 is activated, facilitating the induction of cell cycle arrest or

apoptosis in the affected cells. The activation of p53 is partially driven by its association with 14-3-3, which serves to heighten the transcriptional activity of p53 by increasing its binding affinity for DNA. The binding of p53 by 14-3-3 must be preceded by the dephosphorylation of Ser376, as the removal of this phosphate group unmasks a 14-3-3 consensus binding sequence comprised of phosphorylated Ser376 and its surrounding residues. The dependence of the interaction between 14-3-3 and p53 on a preceding dephosphorylation event imparts an additional layer of control to the activation of p53 [80].

In future studies, it will be important to assess the validity of the model depicting Ser93 dephosphorylation as a prerequisite for the binding of TAZ by 14-3-3. In order to prove the existence of this regulatory scheme, we must ascertain whether the second phosphorylation site on the doubly phosphorylated form of the TAZ peptide spanning amino acids 87 to 114 (2857.77 m/z) can be mapped to Ser89. Interestingly, we also detected a triply phosphorylated version of this TAZ peptide (2937.28 m/z). Since TAZ, like both Cdc25C and p53, also features a serine residue at the –2 position (Ser87) relative to its 14-3-3 binding site (Ser89), we intend to determine whether the third phosphorylation site of this peptide can be located to Ser87. A successful identification of Ser87 as a novel TAZ phosphorylation site would suggest the potential for yet another mechanism of regulating the interaction between TAZ and 14-3-3.

4.6 Ser117 Phosphorylation of TAZ May Influence Its Ability to Bind (L/P)PXY-Containing Transcription Factors

The transcriptional co-activation function of TAZ is thought to be, in part, mediated by a centrally located WW domain [42]. WW domains, named for their typical inclusion of two signature tryptophan residues, recognize and bind short proline-rich sequence motifs within their target ligands [81]. Studies have also shown WW domains

capable of associating with phosphoserine/phosphothreonine residues immediately N-terminal to a proline residue [81]. An oriented peptide library screening revealed the TAZ WW domain to optimally bind peptides adhering to the sequence, Leu/Pro-Pro-Xxx-Tyr (L/PPXY) [42]. Interestingly, sequences of this form have been identified in the transcriptional activation domains of a number of TAZ-mediated transcription factors, most notably within Runx2 and PPARγ, the master transcriptional regulators of osteoblast and adipocyte differentiation, respectively [45,48]. Both the physical interaction of TAZ with these transcription factors, as well as the co-activation/repressive influences of TAZ on Runx2- and PPARγ-driven gene transcription, respectively, were shown to be dependent upon the recognition of the (L/P)PXY motifs within Runx2 and PPARγ by the WW domain of TAZ [45].

Our identification of Ser117 as a novel TAZ phosphorylation site is an intriguing discovery in light of these findings that illustrate the criticality of the TAZ WW domain to the transcriptional regulation of both Runx2 and PPARγ, as Ser117 of human TAZ flanks the N-terminal of the TAZ WW domain (amino acids 124-157) [42]. The highly conserved nature of Ser117 was shown through amino acid sequence alignment of human, mouse, rat, and zebrafish TAZ, suggesting the potential significance of this newly identified TAZ phosphorylation site (Figure 4.6). Moreover, equivalents of Ser117 of human TAZ were also found to be conserved within the human (Ser164), mouse (Ser149), and chicken (Ser162) orthologues of the TAZ paralogue, YAP. Consequent to its location and conservation, we hypothesized that the phosphorylation of Ser117 might influence the WW domain-dependent binding of Runx2 and PPARγ, as well as that of other (L/P)PXY-containing transcription factors, by TAZ. In order to determine whether Ser117 phosphorylation did indeed provide a means by which to regulate the interactions of the WW domain, we examined the functional consequence of this phosphorylation event on the progression of adipocyte differentiation in 3T3-L1 preadipocytes.

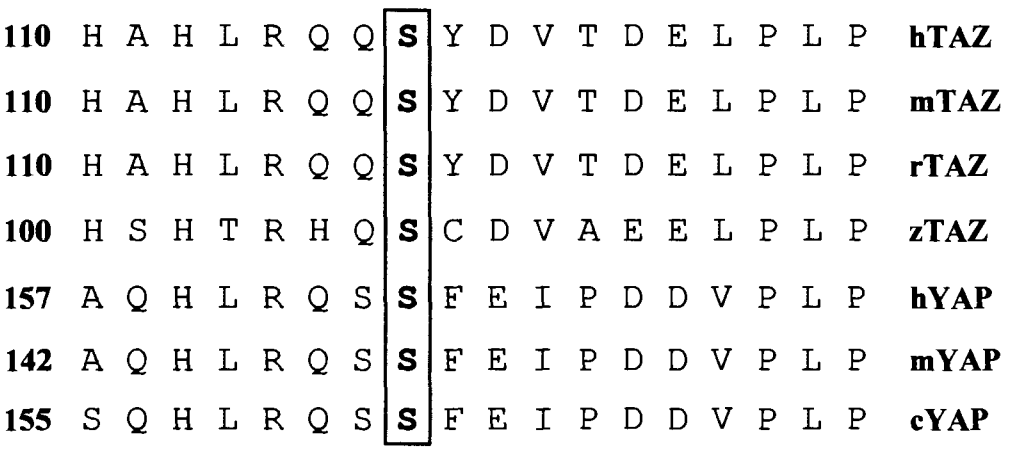

Figure 4.6- Sequence Alignment of Human TAZ with Orthologues of TAZ and YAP Demonstrates the Conservation of Ser117. Ser117 of human TAZ and its equivalent serine residues are boxed. The amino acid positions at which the alignments were initiated are indicated at left. (hTAZ, human TAZ; mTAZ, mouse TAZ; rTAZ, rat TAZ; zTAZ, zebrafish TAZ; hYAP, human YAP; mYAP, mouse YAP; cYAP, chicken YAP)

We provide preliminary evidence suggesting that the phosphorylation of TAZ on Ser117 may negatively regulate interaction of TAZ and PPARγ. We show that over-expression of TAZ S117A, a phosphorylation-defective mutant of TAZ containing an alanine substitution at Ser117, reduces the degree of adipocyte differentiation in 3T3-L1 cells to a level below that observed for wild-type TAZ (Figure 3.32). The heightened inhibitory capacity of TAZ S117A in the context of adipogenesis indicates that the absence of this putative regulatory phosphorylation site at Ser117 might enhance the TAZ-mediated inhibition of PPARγ activity. Accordingly, 3T3-L1 cells over-expressing a mutant of TAZ that is thought to behave as if it is phosphorylated at Ser117 (TAZ S117D) appeared to differentiate to a level comparable to, if not slightly higher than, wild-type TAZ over-expressing 3T3-L1 cells. This putative increase in adipocyte differentiation accompanying TAZ S117D over-expression insinuates that Ser117 phosphorylation of TAZ hinders the ability of TAZ to repress PPARγ-driven gene transcription. Taken together, our findings suggest that the phosphorylation of TAZ on Ser117 disrupts the WW domain-mediated binding of TAZ to the PPXY-motif within PPARγ, which provides a potential explanation for our adipogenesis data. Since TAZ S117A cannot undergo phosphorylation at Ser117, its over-expression presumably increases the stoichiometry of TAZ-bound, transcriptionally repressed PPARγ; whereas, over-expression of TAZ S117D, which mimics a mutant of TAZ that is constitutively phosphorylated on Ser117, likely results in an increase of unbound, transcriptionally active PPARγ. Hence, it appears that the reversible phosphorylation of TAZ on Ser117 may afford a means by which the WW domain-mediated binding of TAZ to, not only PPARγ, but also to other (L/P)PXY-containing transcription factors, can be regulated, ultimately governing the transcriptional co-activation/repression of such transcription factors by TAZ.

Interestingly, there have been studies citing the significance of regions surrounding the WW domain, which lends credence to our hypothesis that the

phosphorylation of TAZ on Ser117 plays a regulatory role in the WW domain-mediated binding of (L/P)PXY-transcription factors by TAZ. It is proposed that critical amino acid residues, lying adjacent to WW domains, may engage in interactions that either stabilize the fold of the WW domain or enhance the binding affinity of the WW domain for target ligands [81]. Thus, it is possible that the phosphorylation of such an amino acid residue (i.e. Ser117 of TAZ) could disrupt the aforementioned interactions, potentially leading to an unfavorable change in the conformation of the WW domain or the elimination of additional binding co-operativity, ultimately hindering the binding of the WW domain to its target ligand.

In the near future, we intend to directly assess the influence of Ser117 TAZ phosphorylation on the WW domain-mediated binding of PPARγ by TAZ. Co-immunoprecipitation analysis of PPARγ with the Ser117 phosphorylation variants of TAZ will allow us to determine whether this phosphorylation event does indeed antagonize the association of the TAZ WW domain and the PPXY motif of PPARγ. Our investigation of the functional consequence of Ser117 phosphorylation on the transcriptional repression activity of TAZ on PPARγ will likely benefit from the employment of reporter assays, wherein the ability of the Ser117 TAZ variants to repress PPARγ can be measured through the expression of a luciferase gene fused to the promoter region of a PPARγ target gene. Moreover, it will be interesting to determine whether Ser117 phosphorylation of TAZ will also inhibit the binding of TAZ to Runx2, a master transcriptional regulator of osteogenesis, as this interaction has also been shown to be WW domain dependent [45]. Analyzing the effect of Ser117 phosphorylation of TAZ on the WW domain-mediated binding of Runx2 and PPARγ will allow us to comment on the prevalence of this phosphorylation event as a putative regulatory strategy governing the transcriptional co-activation/repression functions of TAZ.

During our comprehensive analysis of TAZ phosphorylation, we were unable to unambiguously identify all of the phosphorylation sites on the TAZ phosphopeptides that

were detected. In future studies dedicated to further elucidating novel TAZ phosphorylation sites, we intend to employ separation techniques, such as immobilized metal affinity chromatography (IMAC) and/or high performance liquid chromatography (HPLC), to facilitate the separation of TAZ phosphopeptides from those that are not phosphorylated. If necessary, we can also utilize chemically assisted fragmentation (CAF) techniques, which enhance the fragmentation of peptide ions during PSD through the derivatization of tryptic peptides with sulfonic acid. As CAF derivatization promotes the exclusive detection of y-ions, it can reduce the complexity of the resultant MS/MS spectra, potentially simplifying both peptide sequencing and the mapping of phosphorylation sites.

4.7 Concluding Remarks

The work described in this thesis focuses on a specific phosphomotif that has been shown to regulate protein degradation. To date, the TPM has solely been implicated as a regulatory strategy in the maintenance of β-catenin protein levels [16]. However, based upon the level of sophistication within this mechanism and its fundamentality to the modulation of β-catenin activity, we hypothesized that this strategy might be a widespread regulatory scheme. Indeed, within this study, we revealed a number of putative TPM proteins through their ability to react with a novel phosphorylation-specific TPM antibody, as well as by their responsiveness to phosphatase and proteasome inhibition. Specifically, we identified two transcriptional mediators, TAZ and KLF7, as novel TPM proteins. Using mass spectrometry, we have provided convincing evidence to support the presence of the TPM within TAZ.

With regard to the biochemical characterization of the KLF7 and TAZ TPMs, our hypothesis was that TPM phosphorylation would drive their ubiquitin-dependent proteasomal degradation. This rationale was based upon the role of the β-catenin TPM, wherein it has been well-established that phosphorylation of the TPM facilitates its recognition by β-TrCP, which initiates the ubiquitination and subsequent degradation of β-catenin by the proteasome [16-21]. In accordance with this premise, we uncovered a novel interaction between KLF7 and β-TrCP and also provide evidence that KLF7 is subject to ubiquitination. Importantly, both the β-TrCP recognition and ubiquitination of KLF7 were found to be entirely dependent upon the KLF7 TPM. Although our preliminary attempts at linking these TPM-dependent activities to the potential degradation of KLF7 were inconclusive, the existing parallel between β-catenin and KLF7, in that each protein contains an N-terminal TPM that mediates its association with β-TrCP and its ubiquitination, sustains our belief that KLF7, like β-catenin, will be degraded in a manner dependent upon the TPM.

Within our investigation of the TAZ TPM, we compiled evidence indicating that the function of the TAZ TPM is likely much more complex than our original hypothesis suggested. In line with our hypothesis, we were able to demonstrate that TAZ likely undergoes ubiquitination in a manner reliant upon TPM phosphorylation. However, unlike that of β-catenin and KLF7, this ubiquitination event is not consistent with our initial hypothesis, as an interaction between β-TrCP and the consensus sequence within the TAZ TPM could not be detected, both in our study and in a previously published study [41]. Interestingly, β-TrCP does associate with TAZ through its binding to an atypical site within the TAZ C-terminal; however, this interaction, which highlights the role of TAZ as an E3 adapter protein, was shown to facilitate the proteasomal degradation of a TAZ binding partner (PC2) [41]. Despite its function as an E3 adapter and our inability to illustrate the turnover of TAZ, there does exist evidence suggesting that TAZ may also be regulated by degradation. Hence, we proposed that the inclusion of TAZ in a degradation complex might, in the context of a negative feedback loop, lead to its demise via the ubiquitin-proteasome pathway in a manner dependent upon both the TAZ C-terminal and its TPM.

Here, we also revealed the likelihood that the TAZ TPM influences the critical regulatory interaction between TAZ and 14-3-3, as this association was observed to depend upon the TAZ TPM. We suggested that this TPM-dependency of 14-3-3 binding was likely due to phosphorylation of the TPM, which could potentially promote the phosphorylation of Ser89 or antagonize the phosphorylation of other residues in the vicinity, such as that of Ser93, that could negatively regulate 14-3-3 binding. Since both the ubiquitination of TAZ and its association with 14-3-3 were found to be reliant upon its TPM, we hinted at the possibility that there may exist a direct link between these two events. Our proposed model portrayed TPM phosphorylation as a nuclear occurrence required to initiate the 14-3-3-mediated nuclear export of TAZ, which enables the ubiquitination and subsequent proteasomal degradation of TAZ within the cytoplasm.

We also discussed the possibility that 14-3-3 binding and ubiquitination of TAZ may be isolated situations, providing the cell with multiple means by which to regulate TAZ. Interestingly, the effect of the TPM on the binding of TAZ by 14-3-3 appeared to be cell-type specific, for within 3T3-L1 cells, a TAZ TPM mutant could not interact with 14-3-3, whereas, within HEK 293 cells, the same mutant retained its capacity to bind 14-3-3.

In previous studies, β-catenin, TAZ, and KLF7 have all been identified as negative regulators of adipocyte differentiation [44-47,73]. The existence of this functional parallel incited our functional characterization of the KLF7 and TAZ TPMs, in terms of their influence on the progression of adipogenesis within 3T3-L1 preadipocyte cells, as we considered the possibility that the inhibitory capacity of these three TPM proteins may be afforded by phosphorylation-induced activities at their TPMs. Our results revealed that serine/threonine to alanine substitutions of the critical TPM residues within the KLF7 and TAZ TPMs increased the ability of both TAZ and KLF7 to inhibit adipogenesis. Correlating these findings with our original hypotheses concerning the role of the TPMs in regulating the stability of TAZ and KLF7, we proposed that the effect of the TPMs on adipogenesis might be related to their ability to dictate the steady state levels of TAZ and KLF7, which agrees with studies that presented the role of KLF7 in adipogenesis, as well as with the working model of TAZ-mediated MSC differentiation [45-47]. The discovery that the TAZ TPM mutant resists 14-3-3 binding leaves open the possibility that the enhanced inhibitory influence of this TAZ mutant on adipogenesis could be a direct result of its ability to escape 14-3-3-mediated cytoplasmic sequestration.

The second part of this thesis describes an analytical project involving the identification of TAZ phosphorylation sites using mass spectrometry. The results of previously published studies, as well as those presented within this work, indicated the likelihood that TAZ is highly phosphorylated [42,43,78]. Since it is likely that the key to understanding the regulation of TAZ functions is encoded within its multiple phosphorylation sites, we believed the identification and characterization of these sites to

be of the utmost importance. In total, our efforts lead to the detection of 6 distinct TAZ phosphopeptides, including that which contained the TAZ TPM. Through MS/MS analysis, we successfully identified 10 TAZ phosphorylation sites, of which 7 were mapped to regions outside of the TPM. We demonstrated that two of the identified TAZ phosphorylation sites, Ser93 and Ser117, are located in the vicinity of two critical TAZ regulatory regions, the 14-3-3 binding site and the WW domain, respectively. In light of their intriguing locale, we performed preliminary functional analyses of both Ser93 and Ser117. We provide evidence highlighting the negative regulatory effect of Ser93 phosphorylation on the binding of TAZ by 14-3-3. Since TAZ S93D could not interact with 14-3-3, we hypothesized that this phosphorylation event may antagonize the subsequent phosphorylation of Ser89. We also described the possibility of a second model, whereby Ser89 and Ser93 are simultaneously phosphorylated and the binding of TAZ by 14-3-3 must be preceded by the dephosphorylation of Ser93.

Our functional characterization of Ser117 phosphorylation revealed a putative link between this phosphorylation event and the ability of TAZ to bind to the (L/P)PXY motif of specific transcription factors through its WW domain. Since the TAZ-induced transcriptional repression of PPARγ-driven gene expression is dependent upon the binding of the TAZ WW domain to the PPXY motif present within the transcriptional activation domain of PPARγ [45], we hypothesized that the phosphorylation of TAZ at Ser117 might disrupt the interaction between TAZ and PPARγ. We indirectly illustrated that this is likely the outcome of phosphorylation at Ser117, as we showed that the phosphorylation-defective TAZ mutant, TAZ S117A, exhibited an enhanced capacity to inhibit adipocyte differentiation within 3T3-L1 cells. Our findings suggest a negative regulatory role for the phosphorylation of Ser117 on the WW domain-mediated interaction of TAZ with not only PPARγ, but also with other (L/P)PXY motif-containing transcription factors.

Presently, relatively little experimental data has been published regarding the intricate molecular details of TAZ and KLF7 regulation. Here, we introduced the possibility that both TAZ and KLF7 might be regulated in a manner dependent upon a phosphomotif that was first shown to govern the protein levels of β-catenin. A better understanding of the course of events occurring at the TAZ and KLF7 TPMs will likely enhance our understanding of the mechanisms regulating these critical transcriptional mediators, potentially providing insights into their putative contributions to the pathogenesis of obesity-related disorders, such as type 2 diabetes. We also reported the identification of a number of *in vivo* TAZ phosphorylation sites, whose functional characterization will likely provide invaluable information concerning the regulation of TAZ function. Importantly, we provided the first indication of mechanisms governing the release of TAZ from 14-3-3. In closing, the findings presented within this thesis will provide a strong foundation for future studies focused on elucidating the mechanisms responsible for the tight regulation of the activities of the TPM-containing transcriptional mediators, TAZ and KLF7.

Gene	Amino Acid Position	TPM Sequence
CAD22	583-596	D S G P P T L S S T G T L T
BSN	682-695	D T G Y S S D G I S S S Q S
F135B	685-698	D S G I E S E P S S V A W S
VGFR2	392-405	D T G N Y T V I L T N P I S
KIF1C	675-688	D S G D D S D K R S C E E S
SYNM	78-91	D S G L D S R E L T F G S S
DLL1	693-706	D S G C S T S K D T K Y Q S
CTNB1	32-45	D S G I H S G A T T T A P S
ZBT20	376-389	D S G V S S S I G T E P D S
YM018	936-949	D S G N K T D K D T P G I T
H2B1A	53-66	D T G I S S K A M S I M N S
KLF7	18-31	D T G Y F S A L P S L E E T
MKKS	254-267	D T G E G T V V V S Y G V S
SI1L3	1308-1321	D S G I D T T L Y T S S P S
PLAK	23-36	D S G I H S G A N T C V P S
BAZ2B	52-65	D S G T S S D T S S E G I S
CASZ1	159-172	D S G P S T R Q A S G E A S
PRP16	219-232	D S G Y G S S R R S Q W E S
AKP13	390-403	D S G T V S D Q D S C L Q S
FLT3	324-337	D T G Y Y T C S S S K H P S
MLL5	1280-1293	D S G G E S P C V S C S P S
UTP20	1746-1759	D S G G T S A K E S E C I T
S45A3	417-430	D T G G A S S E D S L M T S
CEA21	116-129	D T G Y Y T L Q V T Y R N S
DMKN	299-312	D S G S E S S W G S S T G S
WWTR1	57-70	D S G S H S R Q S S T D S S
AKA11	443-456	D S G L F S P I R S S A F S
WNK2	617-630	D S G Q G S T V Y S D S Q S
DMRT1	331-344	D S G L V S L S S S S P I S
CADH7	566-579	D S G S P S L S S T S T L T
CHD1	23-36	D S G S A S G S G S G S S S
ZEP1	672-685	D S G Y F S R S E S A D Q T
DOK7	337-350	D S G I A T G S H S S Y S S

Appendix 1- Compilation of Putative TPM-Containing Proteins. Analysis of the human SwissProt database with an ambiguous form of the TPM sequence (DS/TGXXS/TXXXS/TXXXS/T) was conducted using the Pattern Search command of the My Hits web-based tool (myhits.isb-sib.ch/cgi-bin/pattern_search; Swiss Institute of Bioinformatics). The genes encoding the TPM-containing proteins identified are listed and the amino acid positions of their TPMs are indicated. The Ser/Thr residues constituting the putative TPMs are highlighted, as are the residues comprising the β-TrCP consensus sequence (DSGXXS). The genes encoding β-catenin (*CTNB1*), KLF7 (*KLF7*), and TAZ (*WWTR1*) are boxed.

References

[1] Nelson, D.L. and Cox, M.M. (2000) Lehninger Principles of Biochemistry: Third Edition. New York: Worth Publishers.

[2] Graves, D.J., Martin, B.L., and Wang, J.H. (1994) Co- and Post-Translational Modification of Proteins: Chemical Principles and Biological Effects. New York: Oxford University Press, Inc..

[3] Raggiaschi, R., Gotta, S., and Terstappen, G.C. (2005) *Bioscience Reports.* **25**, 33-44.

[4] Hunter, T. (1998) *Philos. Trans. R. Soc., London B-Biol.* **353**, 583-605.

[5] Sickmann, A. and Meyer, H.E. (2001) *Proteomics* **1**, 200-206.

[6] Zolnierowicz, S. and Bollen, M. (2000) *EMBO J.* **19**, 483-488.

[7] Paradela, A. and Albar, J.P. (2008) *J. Proteome Res.* **7**, 1809-1818.

[8] Reinders, J. and Sickmann, A. (2005) *Proteomics* **5**, 4052-4061.

[9] Noble, M.E.M, Endicott, J.A., and Johnson, L.N. (2004) *Science* **303**, 1800-1805.

[10] Kalume, D.E., Molina, H., and Pandey, A. (2003) *Curr. Opin. Chem. Biol.* **7**, 64-69.

[11] Cohen, P. (2000) *Trends Biochem. Sci.* **25**, 596-601.

[12] Gingras, A.C., Raught, B., Gygi, S.P., Niedzwiecka, A., Miron, M., Burley, S.K., Polakiewicz, R.D., Wyslouch-Cieszynska, A., Aebersold, R., and Sonenberg, N. (2001) *Genes Dev.* **15**, 2852-2864.

[13] Deshaies, R.J. and Ferrell Jr., J.E. (2001) *Cell* **107**, 819-822.

[14] Kühl, M. (2003) Wnt Signaling in Development. New York: Kluwer Academic/Plenum Publishers.

[15] Kikuchi, A., Kishida, S., and Yamamoto, H. (2006) *Exp. Med. Mol.* **38**, 1-10.

[16] Liu, C., Li, Y., Semenov, M., Han, C., Baeg, G., Tan, Y., Zhang, Z., Lin, X., and He, X. (2002) *Cell* **108**, 837-847.

[17] Amit, S., Hatzubai, A., Birman, Y., Andersen, J.S., Ben-Shushan, E., Mann, M., Ben-Neriah, Y., and Alkalay, I. (2002) *Genes Dev.* **16**, 1066-1076.

[18] Aberle, H., Bauer, A., Stappert, J., Kispert, A., and Kemler, R. (1997) *EMBO J.* **16**, 3797-3804.

[19] Winston, J.T., Strack, P., Beer-Romero, P., Chu, C.Y., Elledge, S.J., and Harper, J.W. (1999) *Genes Dev.* **13**, 270-283.

[20] Wu, G., Xu, G., Schulman, B.A., Jeffrey, P.D., Harper, J.W., and Pavletich, N.P. (2003) *Mol. Cell.* **11**, 1445-1456.

[21] Winer, I.S., Bommer, G.T., Gonik, N., and Fearon, E.R. (2006) *J. Biol. Chem.* **281**, 26181-26187.

[22] Nandi, D., Tahiliani, P., Kumar, A., and Chandu, D. (2006) *J. Biosci.* **31**, 137-155.

[23] Ciechanover, A. and Schwartz, A.L. (1998) *Proc. Natl. Acad. Sci. USA* **95**, 2727-2730.

[24] Myung, J., Kim, K.B., and Crews, C.M. (2001) *Med. Res. Rev.* **21**, 245-273.

[25] Reboud-Ravaux, M. (2002) Protein Degradation in Heath and Disease. Progress in Molecular and Subcellular Biology. **29,** New York: Springer.

[26] Waltzer, L. and Bienz, M. (1999) *Cancer Metastasis Rev.* **18**, 231-246.

[27] Gronborg, M., Kristiansen, T.Z., Stensballe, A., Andersen, J.S., Ohara, O., Mann, M., Jensen, O.N., and Pandey, A. (2002) *Mol. Cell. Proteomics* **1**, 517-527.

[28] Mann, M., Ong, S., Gronborg, M., Steen, H., Jensen, O.N., and Pandey, A. (2002) *Trends Biotech.* **20**, 261-268.

[29] Pandey, A., Podtelejnikov, A.V., Blagoev, B., Bustelo, X.R., Mann, M., and Lodish, H.F. (2000) *Proc. Natl. Acad. Sci. USA* **97**, 179-184.

[30] Rush, J., Moritz, A., Lee, K.A., Guo, A., Goss, V.L., Spek, E.J., Zhang, H., Zha, X., Polakiewicz, R.D., and Comb, M.J. (2004) *Nat. Biotechnol.* **23**, 94-101.

[31] Zhang, H., Zha, Z., Tan, Y., Hornbeck, P.V., Mastrangelo, A.J., Alessi, D.R., Polakiewicz, R.D., and Comb, M.J. (2002) *J. Biol. Chem.* **277**, 39379-39387.

[32] Kane, S., Sano, H., Liu, S.C.H., Asara, J.M., Lane, W.S., Garner, C.C., Lienhard, G.E. (2002) *J. Biol. Chem.* **277**, 22115-22118.

[33] Chavez, J.A., Gridley, S., Sano, H., Lane, W.S., and Lienhard, G.E. (2006) *Biochem. Biophys. Res. Commun.* **342**, 1218-1222.

[34] Gridley, S., Chavez, J.A., Lane, W.S., and Lienhard, G.E. (2006) *Cell Signal.* **18**, 1626-1632.

[35] Matsuoka, S., Ballif, B.A., Smogorzewska, A., McDonald III, E.R., Hurov, K.E., Luo, J., Bakalarski, C.E., Zhao, Z., Solimini, N., Lerenthal, Y., Shiloh, Y., Gygi, S.P., and Elledge, S.J. (2007) *Science* **316**, 1160-1166.

[36] Kinter, M. and Sherman, N.E. (2000) Protein Sequencing and Identification Using Tandem Mass Spectrometry. Toronto: John Wiley & Sons, Inc..

[37] Laugesen, S., Bergoin, A., and Rossignol, M. (2004) *Plant Physiol. Biochem.* **42**, 929-936.

[38] Suckau, D., Resemann, A., Schuerenberg, M., Hufnagel, P., Franzen, J., and Holle A. (2003) *Anal. Bioanal. Chem.* **376**, 952-965.

[39] Collins, M.O., Yu, L., and Choudhary, J.S. (2007) *Proteomics* **7**, 2751-2768.

[40] Jordan, M., Schallhorn, A., and Wulm, F.M. (1996) *Nucleic Acids Res.* **24**, 596-601.

[41] Tian, Y., Kolb, R., Hong, J., Carroll, J., Li, D., You, J., Bronson, R., Yaffe, M.B., Zhou, J., and Benjamin, T. (2007) *Mol. Cell Biol.* **27**, 6383-6395.

[42] Kanai, F., Marignani, P.A., Sarbassova, D., Yagi, R., Hall, R.H., Donowitz, M., Hisaminato, A., Fujiwara, T., Ito, Y., Cantley, L.C., and Yaffe, M.B. (2000) *EMBO J.* **19**, 6778-6791.

[43] Lei, Q., Zhang, H., Zhao, B., Zha, Z., Bai, F., Pei, X., Zhao, S., Xiong, Y., Guan, K. (2008) *Mol. Cell Biol.* **28**, 2426-2436.

[44] Liu, J. and Farmer, S.R. (2004) *J. Biol. Chem.* **279**, 45020-45027.

[45] Hong, J., Hwang, E.S., McManus, M.T., Amsterdam, A., Tian, Y., Kalmukova, R., Mueller, E., Benjamin, T., Spiegelman, B.M., Sharp, P.A., Hopkins, N., and Yaffe, M.B. (2005) *Science* **309**, 1074-1078.

[46] Kanazawa, A., Kawamura, Y., Sekine, A., Iida, A., Tsunoda, T., Kashiwagi, A., Tanaka, Y., Babazono, T., Matsuda, M., Kawai, K., Iiizumi, T., Fujioka, T., Imanishi, M., Kaku, K., Iwamoto, Y., Kawamori, R., Kikkawa, R., Nakamura, Y., and Maeda, S. (2005) *Diabetologia* **48**, 1315-1322.

[47] Kawamura, Y., Tanaka, Y., Kawamori, R., and Maeda, S. (2006) *Mol. Endocrinol.* **20**, 844-856.

[48] Cui, C.B., Cooper, L.F., Yang, X., Karsenty, G., and Aukhil, I. (2003) *Mol. Cell Biol.* **23**, 1004-1013.

[49] Park, K., Whitsett, J.A., Di Palma, T., Hong, J., Yaffe, M.B., and Mariastella, Z. (2004) *J. Biol. Chem.* **279**, 17384-17390.

[50] Murakami, M., Tominaga, J., Makita, R., Uchijima, Y., Kurihara, Y., Nakagawa, O., Asano, T., and Kurihara, H. (2006) *Biochem. Biophys. Res. Commun.* **339**, 533-539.

[51] Di Palma, T., D'Andrea, B., Liguori, G.L., Liguoro, A., de Cristofaro, T., Del Prete, D., Pappalardo, A., Mascia, A., and Zannini, M. (2009) *Exp. Cell Res.* **315**, 162-175.

[52] Mahoney, Jr., W.M., Hong, J., Yaffe, M.B., and Farrance, I.K. (2005) *Biochem. J.* **388**, 217-225.

[53] Murakami, M., Nakagawa, M., Olson, E.N., and Nakagawa, O. (2005) *Proc. Natl. Acad. Sci. U.S.A.* **102**, 18034-18039.

[54] Hossain, Z., Ali, S.M., Ko, H.L., Xu, J., Ng, C.P., Guo, K., Qi, Z., Ponniah, S., Hong. W., and Hunziker, W. (2007) *Proc. Natl. Acad. Sci. U.S.A.* **104**, 1631-1636.

[55] Varelas, X., Sakuma, R., Samavarchi-Tehrani, P., Peerani, R., Rao, B.M., Dembowy, J., Yaffe, M.B., Zandstra, P.W., and Wrana, J.L. (2008) *Nat. Cell. Biol.* **10**, 837-848.

[56] Matsumoto, N., Laub, F., Aldabe, R., Zhang, W., Ramirez, F., Yoshida, T., and Terada, M. (1998) *J. Biol. Chem.* **273**, 28229-28237.

[57] Lei, L., Ma, L., Nef, S., Thai, T., and Parada, L.F. (2001) *Development* **128**, 1147-1158.

[58] Laub, F., Aldabe, R., Friedrich, Jr., V., Ohnishi, S., Yoshida, T., and Ramirez, F. (2001) *Dev. Biol.* **233**, 305-318.

[59] Lei, L., Laub, F., Lush, M., Romero, M., Zhou, J., Luikart, B., Klesse, L., Ramirez, F., and Parada, L.F. (2005) *Genes Dev.* **19**, 1354-1364.

[60] Laub, F., Lei, L., Sumiyoshi, H., Kajimura, D., Dragomir, C., Smaldone, S., Puche, A.J., Petros, T.J., Mason, C., Parada, L.F., and Ramirez, F. (2005) *Mol. Cell Biol.* **25**, 5699-5711.

[61] Laub, F., Dragomir, C., and Ramirez, F. (2006) *Brain Res.* **1103**, 108-113.

[62] Lei, L., Zhou, J., Lin, L., and Parada, L.F. (2006) *Dev. Biol.* **300**, 758-769.

[63] Kajimura, D., Dragomir, C., Ramirez, F., and Laub, F. (2007) *Gene* **388**, 34-42.

[64] Kingsbury, T.J. and Krueger, B.K. (2007) *Mol. Cell. Neurosci.* **35**, 447-455.

[65] Yook, J.I., Li, X., Ota, I., Fearon, E.R., and Weiss, S.J. (2005) *J. Biol. Chem.* **280**, 11740-11748.

[66] Belaïdouni, N., Marchal, C., Benarous, R., and Besnard-Guérin, C. (2007) *Biochem. Biophys. Res. Commun.* **357**, 688-693.

[67] Latres, E., Chiaur, D.S., and Pagano, M. (1999) *Oncogene* **18**, 849-854.

[68] Pham, N. and Rotin, D. (2001) *J. Biol. Chem.* **50**, 46995-47003.

[69] Darling, D.L., Yingling, J., and Wynshaw-Boris, A. (2005) *Curr. Topics Devel. Biol.* **68**, 281-315.

[70] Vogt, P.K., Jiang, H., and Aoki, M. (2005) *Cell Cycle* **4**, 908-913.

[71] Eymin, B., Claverie, P., Salon, C., Brambilla, C., Brambilla, E., and Gazzeri, S. (2006) *Cell Cycle* **5**, 759-765.

[72] Prestwich, T.C. and MacDougald, O.A. (2007) *Curr. Opin. Cell Biol.* **19**, 612-617.

[73] Li, H., Luo, X., Liu, R., Yang, Y., and Yang, G. (2008) *Mol. Cell Endocrinol.* **291**, 116-124.

[74] Cho, S.Y., Park, P.J., Shin, H.J., Kim, Y., Shin, D.W., Shin, E.S., Lee, H.H., Lee, B.G., Baik, J., and Lee T.R. (2007) *Am. J. Physiol. Endocrinol. Metab.* **292**, 1166-1172.

[75] Sadot, E., Conacci-Sorrell, M., Zhurinsky, J., Shnizer, D., Lando, Z., Zharhary, D., Kam, Z., Ben-Ze'ev, A., and Geiger, B. (2002) *J. Cell Sci.* **115**, 2771-2780.

[76] Kawai, M., Mushiake, S., Bessho, K., Murakami, M., Namba, N., Kokubu, C., Michigami, T., and Ozono, K. (2007) *Biochem. Biophys. Res. Commun.* **363**, 276-282.

[77] Wang, M., Grayburn, P., Chen, S., Ravazzola, M., Orci, L., and Unger, R.H. (2008) *Proc. Natl. Acad. Sci. U.S.A.* **105**, 6139-6144.

[78] Hong, J. and Yaffe, M. (2006) *Cell Cycle* **5**, 176-179.

[79] Bulavin, D.V., Higashimoto, Y., Demidenko, Z.N., Meek, S., Graves, P., Phillips, C., Zhao, H., Moody, S.A., Appella, E., Piwnica-Worms, H., Fornace Jr., A.J. (2003) *Nat. Cell. Biol.* **5**, 545-551.

[80] Waterman, M.J.F., Stavridi, E.S., Waterman, J.L.F., and Halazonetis, T.D. (1998) *Nat. Genet.* **19**, 175-178.

[81] Macias, M.J., Wiesner, S., Sudol, M. (2002) *FEBS Lett.* **513**, 30-37.

Vita Auctoris

Name: Catherine Sykes

Place of Birth: Oldcastle, Ontario, CA

Year of Birth: 1983

Education: St. Thomas of Villanova Secondary School, Lasalle, Ontario, CA
1997-2002

University of Windsor, Windsor, Ontario, CA
2002-2006 B.Sc., Honours Chemistry

University of Windsor, Windsor, Ontario, CA
2006-Present M.Sc, Candidate in Biochemistry

Conferences: Sykes, C.E. and Vacratsis, P.O. (2006) Phosphoproteomic Analysis of a Dual Kinase Mechanism. *Poster Presentation.* Progress in Systems Biology Symposium, Ottawa Institute of Systems Biology, Ottawa, Ontario, CA.

Sykes, C.E. and Vacratsis P.O. (2008) Phosphoproteomic Analysis of a Tetra-Phosphorylation Motif. Poster Presentation. Protein Phosphatases. FASEB. Snowmass, CO, USA.

Papers: Sykes, C.E. and Vacratsis, P.O. (2006) Phospho-Specific Antibodies: A Versatile Tool for Phosphoproteomic Studies. *Current Proteomics* **3**(2), 113-117.